INFORMATION TO USERS

This manuscript has been reproduced from the microfilm master. UMI films the text directly from the original or copy submitted. Thus, some thesis and dissertation copies are in typewriter face, while others may be from any type of computer printer.

The quality of this reproduction is dependent upon the quality of the copy submitted. Broken or indistinct print, colored or poor quality illustrations and photographs, print bleedthrough, substandard margins, and improper alignment can adversely affect reproduction.

In the unlikely event that the author did not send UMI a complete manuscript and there are missing pages, these will be noted. Also, if unauthorized copyright material had to be removed, a note will indicate the deletion.

Oversize materials (e.g., maps, drawings, charts) are reproduced by sectioning the original, beginning at the upper left-hand corner and continuing from left to right in equal sections with small overlaps.

Photographs included in the original manuscript have been reproduced xerographically in this copy. Higher quality 6" x 9" black and white photographic prints are available for any photographs or illustrations appearing in this copy for an additional charge. Contact UMI directly to order.

ProQuest Information and Learning
300 North Zeeb Road, Ann Arbor, MI 48106-1346 USA
800-521-0600

UMI®

HETEROCOAGULATION OF SULPHIDE MINERALS

Anthony DiFeo

Department of Mining and Metallurgical Engineering
McGill University
Montreal, Quebec

A thesis submitted to the Faculty of Graduate Studies and Research in partial fulfillment of the requirements for the degree of Doctor of Philosophy

November, 1999

National Library of Canada
Acquisitions and Bibliographic Services
395 Wellington Street
Ottawa ON K1A 0N4
Canada

Bibliothèque nationale du Canada
Acquisitions et services bibliographiques
395, rue Wellington
Ottawa ON K1A 0N4
Canada

Your file Votre référence

Our file Notre référence

0-612-64547-9

Canada

Knowledge is similar to the universe, it has an endless frontier

To my wife Maria and
my children Vanessa and
Gian Marco and my nephews
Francis Camille and David
Joshua

ABSTRACT

Interactions among sulphide minerals (sphalerite, galena and pyrite) and sphalerite and silica were studied using electrophoresis, an automated settling apparatus and, in the sphalerite/silica case, atomic force microscopy (AFM).

Significant changes in zeta-potential were observed in some cases as a result of contact (conditioning) with a second mineral. As a function of pH when sphalerite was conditioned with pyrite, the zeta-potential increased to ca. pH 9 and decreased above this pH. For sphalerite conditioned with galena, the zeta-potential decreased below pH 5, increased between pH 5 to 9 and decreased above pH 9. Galena conditioned with sphalerite and pyrite resulted in a decrease in zeta-potential below pH 5 and an increase above this pH. The results are interpreted on the basis of galvanic interactions. The mineral with the lower rest potential preferentially oxidizes and the ions released migrate and influence the zeta-potential. Measurements made in solutions of various suspected released ions generally supported the galvanic model. The zeta-potential results for mixed sulphide minerals were correlated with settling velocity. For the pyrite/galena, sphalerite/pyrite and sphalerite/galena systems, the pH of maximum settling rate corresponded to the zeta-potential of both minerals approaching zero. When the minerals were oppositely charged the conditions remained (relatively) dispersing. In the case of silica and sphalerite/silica at around pH 2 and 8.5 sphalerite homocoagulated and some silica was dispersed; from ca. pH 3 to 7, the system heterocoagulated; and above pH 9.5 the suspension was dispersed. This behavior did not correlate with the behaviour of the minerals alone. In the presence of calcium ions, from ca. pH 2 to 7, the sphalerite homocoagulated and the silica was dispersed while above pH 7 heterocoagulation was observed. This behavior did correlate more closely with that of minerals alone. The zeta-potential measurements provided only a partial interpretation: a force of attraction between sphalerite and silica appears to exist at moderately alkaline pH. An electrostatic origin to the attractive force due to the large difference in zeta-potential for sphalerite and silica is discussed.

The settling results for the sphalerite/silica system were correlated with AFM measurements. For silica alone, the interaction was repulsive at pH 6.2 and 8.3. This behavior did correlate with the settling tests. In the presence of calcium ions, the interaction was repulsive at pH 6.1 and 9.6 and was attractive at pH 11.4. This behavior also correlated with the settling data. For the mixed system, the interaction was repulsive at pH 7.2, 8.4 and 10.6 and was attractive at pH 9.6. The behavior at pH 8.4 and 10.6 correlated with the settling tests but not at pH 7.2 and 9.6. The lack of correlation is discussed.

RESUME

Les intéractions entre les minéraux sulfurés et la silice ont été étudier en utilisant les propriétés interfaciales comme la charge de surface et la microscopie de force atomique (MFA) et la vélocité de sédimentation.

Dans certains cas, à cause de la présence d'un deuxième minérale, des changement siginificant du potentiel-zéta ont été observer. Quand la sphalérite a été conditioné avec la pyrite le potentiel-zéta a augmenteé jusqu'a environ pH 9 et a diminué au-dessus de ce pH. Pour la sphalérite conditioné avec la galène, le potentiel-zéta a diminué au-dessous de pH 5, a augmenté entre pH 5 et 9 et a diminué au-dessus de pH 9. Quand la galène conditioné avec la sphalérite et la pyrite, le potentiel-zéta a diminué, au-dessous de pH 5 et une augmentation au-dessus de ce pH. Les résultats on été interprétés sur la base des intéractions galvanique. Les ions formés à cause des intéractions galvanique ont influencé le potentiel-zéta. La quantité des ions formés à cause des intéractions galvanique ont supportés le modèle galvanique. Les résultats du potentiel-zéta pour les minéraux en paires ont éts comparés avec la vélocité de sédimentation. Pour les paires pyrite/galène, sphalérite/pyrite et sphalérite/galène, le pH correspondant à la vélocité de sédimentation maximale correspond à le potentiel-zéta des deux minéraux approchent zero. Quand les minéraux avaient une charge opposée, les conditions étaient relativement dispersées. Les potentiel-zéta de la silice et sphalérite ont étés comparés avec les vélocités de sédimentation. Environ pH 2 et 8.5, la sphalérite a homocoagulée et une portion de la silice a été dispersée, de environ pH 3 à 7, le système a hétérocoagulé et au-dessus de pH 9.5 la suspension était dispersée. Ces résultats n'avaient pas une bonne corrélation avec les résultats du potentiel-zéta des minéraux isolés. Dans la présence des ions de calcium, d'environ pH 2 à 7, la sphalérite a homocoagulée et la silice était dispersée tendit au-dessus pH 7 la hétérocoagulation a été observé. Ces résultats avient une bonne corrélation avec les minéraux isolés. La magnitude du potentiel-zéta ont donnés une interpretation partielle: une interaction électrostatique peut existé à cause de la grande différence dans le potentiel-zéta des deux minéraux.

Les expériences de sé dimentation de la silice et le système sphalérite-silice ont étés correlées avec les expériences de la microscopie de force atomique (MFA). Pour la silice dans la présence des ions de calcium, les intéractions étaient répulsives à pH 6.2 et 8.3. Ce phénomène avait une bonne corrélation avec les testes de sédimentation. Dans la présence des ions de calcium, l’intéraction était répulsive à pH 6.1 et 9.6 et attractive à pH 11.4. Ce phénomène avait une bonne corrélation avec les testes de sédimentation. Pour le système sphalerite-silice, l’intvraction était répulsive à pH 7.2, 8.4 et 10.6 était attractive à pH 9. Ce phénomène à pH 8.4 et 10.6 avait une bonne corrélation avec les testes de sédimentation mais pas à pH 7.2 et 9.6. La cause de mauvaise corrélation est discustée.

ACKNOWLEDGEMENTS

I would like to express my appreciation to Dr. J. A. Finch for his guidance and wisdom throughout this research.

I want to greatly thank my wife Maria for her love, support and encouragement throughout my studies, without her patience it could not have been possible. I also want to thank my parents - in - law, Camillo & Teresina Vitulano for babysitting my children and their love and support throughout my studies. These people really made a difference and their help is greatly appreciated.

I express my gratitude to both my supervisors (Drs Finch & Xu) for their financial assistance.

I want to thank Dr. A. Vreughdenhil and Dr. S. R. Rao for some interesting discussions regarding mineral chemistry. Also I am grateful to Dr. T.G.M. van de Ven for his help regarding colloid chemistry.

Appreciation is expressed toward Mr. R. Langlois, Mr. M. Leroux and Ms. Monique Riendeau for their expertise in the laboratory.

I thank all the people in the mineral processing group for the valuable discussions and their friendship.

Lastly, I thank Noranda, Inco, Cominco, Falconbridge, Teck, Hudson Bay Mining & Smelting and the Natural Sciences and Engineering Research Council of Canada for research funding.

TABLE OF CONTENTS

CHAPTER 1

INTRODUCTION

CHAPTER 2

THEORETICAL CONSIDERATIONS

CHAPTER 3

SURFACE ANALYSIS AND SURFACE FORCES

CHAPTER 4

EXPERIMENTAL PROCEDURES

CHAPTER 5

ELECTROKINETIC AND SETTLING STUDY OF MIXED SULPHIDE MINERALS

CHAPTER 6

INTERACTIONS IN THE SPHALERITE/SILICA SYSTEM

CHAPTER 7

ATOMIC FORCE MICROSCOPY

CHAPTER 8

CONCLUSIONS, CONTRIBUTIONS, AND FUTURE WORK

APPENDIX A

LIST OF TABLES

LIST OF FIGURES

CHAPTER 1

INTRODUCTION

1.1 Problems Encountered in Processing Complex Sulphide Ores

Complex sulphide ores are characterized by a fine dissemination of several sulphide minerals such as galena, sphalerite, copper sulphides, often hosted in massive pyrite. The grain size is frequently <50 µm demanding fine grinding and multiple stages of flotation. A method common of processing these ores is to first recover Cu-sulphides and galena as a bulk concentrate at alkaline conditions, while sphalerite and pyrite are depressed with the addition of sulphur dioxide, cyanide or zinc sulphate. Afterwards sphalerite is activated with copper sulphate in an alkaline pulp regulated with lime and floated with xanthate. This process does not always yield satisfactory results due to one or a combination of the following four factors: inadequate liberation (or locking), mechanical entrainment, accidental activation and lastly, the topic addressed in this thesis, entrapment/ agglomeration effects. The four factors are briefly described.

1.2 Locking

The composition of individual particles (or liberation) is the ultimate determinant of the physical separation of minerals. The objective of size reduction (comminution) is to achieve sufficient liberation of minerals so that the target mineral can be separated from the others. Insufficient comminution results in production of locked (composite) particles which yield an incomplete separation. A high level of comminution can increase liberation, but the increased production of fine particles (slimes) may give a mixture that proves difficult to separate.

1.3 Entrainment

This is the phenomenon where fine particles (<20 μm) are carried in the wake of an air bubble rising in slurry. The recovery of fine particles due to entrainment increases with decreasing particle size [1]. Entrainment is directly related to water recovery to the concentrate except where froth washing is employed and using a more dilute pulp increases the water recovery so there is not normally a net benefit from simple dilution.

1.4 Accidental Activation to Flotation

Mineral surfaces become cross-contaminated by metallic and sulphoxy species derived from superficial oxidation of the minerals in the ore. Some contaminant species, notably metallic ions and elemental sulphur, can promote (activate) flotation.

Oxidation and surface contamination have been extensively studied in flotation of sulphide minerals. Sulphide minerals can sustain galvanic interactions which enhance the oxidation of the anodic mineral, therefore promoting its dissolution and release of metal ions [2-4]. The most common cathodic mineral is pyrite, another is chalcopyrite, while galena and sphalerite are usually the anodic minerals. Metal ions generated on one mineral migrate to others potentially affecting the surface properties of all minerals. For example, Guy and Trahar [5] reported that the surface of chalcopyrite became like galena through transfer of lead ions, whereas the surface of galena was modified towards chalcopyrite by copper ions.

1.5 Entrapment/Agglomeration

The decreasing grain size typically associated with increasingly complex ores, demands fine grinding. In consequence particle size is progressively becoming finer and mineral processing is becoming more and more an applied colloid chemistry discipline.

The particle size at which separation problems become significant depends on the flotation system, but in general particles below 20 μm are potentially troublesome. For fine particle systems, the characteristics of the suspension, such as stability, settling rate, and viscosity, depend less on particle bulk properties compared to particle surface properties.

The presence of fine particles is often responsible for poor metallurgy [6]. Slime coatings - fines of one mineral coating larger particles of another - is one well known problem [7]. Another problem may be that agglomerates physically entrap particles of another mineral leading to misplacement. In some situations desliming is carried out prior to flotation, especially when processing non-sulphide ores [6].

One cause of agglomeration derives from the surface charge that all particles develop in water. Another cause of agglomeration derives from hydrophobic surface species. Agglomeration resulting from surface charge and hydrophobic effects are referred to as coagulation. There are two forms of coagulation: homo- and heterocoagulation. For example, when the zeta-potential is brought to near zero the force of repulsion is lost and particles may coagulate. This usually applies (but not exclusively) to particles of one mineral type, hence the term homocoagulation. If two particles have opposite charge there is a positive force of attraction. In this case the particles are composed of different minerals, hence the description heterocoagulation.

1.6 Objectives of Thesis

The general objective is to study the impact of agglomeration on sulphide mineral separation by flotation.

Two specific objectives are:

a) To evaluate the correlation between zeta-potential and settling rate (used as a measure of agglomeration) for sphalerite, pyrite and galena in single and mixed systems.

b) To investigate and interpret homo- and heterocoagulation characteristics of silica and sphalerite determined by settling rate and the relation to surface charge and surface forces.

1.7 References

1. Trahar, W. J., A rational Interpretation of the Role of Particle Size in Flotation, International Journal of Mineral Processing, 8, 1981, pp289-327.
2. van Meersbergen, M. T., Loregen, L., and van Deventer, J. S. J., The Electrochemical Dissolution of Gold in Bromine Medium, Minerals Engineering, 6(8-10), 1993, pp1067-1079.
3. Rao, S. R., and Finch, J. A., Galvanic Interactions Studies on Sulphide Minerals, Canadian Metallurgical Quarterly, 27(4), 1988, pp253-259.
4. Majima, H., How Oxidation Affects Selective Flotation of Complex Sulphide Ores, Canadian Metallurgy Quarterly, 8(3), 1969, pp269-273.
5. Guy, P. J. and Trahar, W. J., The Effects of Oxidation and Mineral Interaction on Sulphide Flotation, Flotation of Sulphide Minerals (Editor, Forssberg, K. S. E.), 1985, pp91-110.
6. Parsonage, P. G., Effects of Slime and Colloidal Particles in the Flotation of Galena, Flotation of Sulphide Minerals (Editor, Forssberg, K. S. E), 1985, pp111-139.
7. Gaudin, A. M., Fuerstenau, D. W., and Miaw, H. L., Slime Coatings in Galena Flotation, The Canadian and Metallurgical Bulletin, December 1960, pp960-963.

CHAPTER 2

THEORETICAL CONSIDERATIONS

2.1 Electrical Double Layer

Particle surfaces exposed to water develop an electrical charge due to ionization of surface groups or adsorption of ions from solution. Electrical neutrality is maintained by a screening of surface charge by a cloud of oppositely charged counter ions. Together, these oppositely charged regions are referred to collectively as the electrical double layer. Models have been developed to explain the structure and properties of the double layer [1].

2.1.1 The Poisson-Boltzmann Equation

The electrostatic potential, ψ (mV), anywhere near the surface is related to the volume charge density, ρ (C/m^3), the net excess of positive over negative ions or vice versa.

The relationship between ψ and ρ is described by the Poisson equation, which for a flat surface is as follows: [1]

$$\frac{d^2\psi}{dx^2} = -\frac{\rho}{\epsilon_w} = -\frac{\rho}{\epsilon_o\epsilon_r} \qquad (2.1)$$

where ϵ_w is the permittivity of water, ϵ_r $(=\epsilon_w/\epsilon_o)$ is the relative permittivity and ϵ_o the permittivity of a vacuum.

The derivation of equation (2.1) assumes that the potential in planes parallel to the surface is constant and the distance x is at right angles to the surface (Figure 2.1).

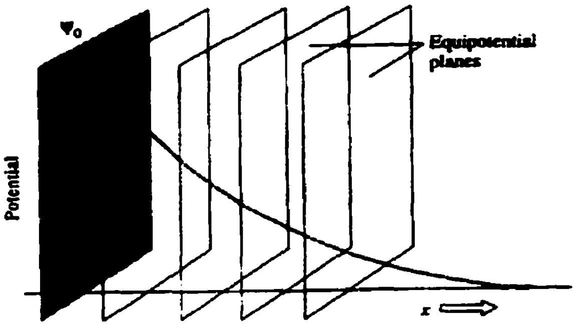

Figure 2.1. Electrostatic Potential Decays with Distance from a Surface [2].

The quantity of ions of each type, n_i, is given by: [1]

$$n_i = n_i^o \exp\frac{-z_i e \psi}{kT} \tag{2.2}$$

where n_i^o (m^{-3}) is the number of ions of type i per unit volume in the bulk solution far from the surface, k is the Boltzmann constant (1.38 X 10^{-23} J/K), T is the temperature (K), z_i is the valence carried by ion i, and ψ is the potential (mV). The volume density of charge, ρ, is calculated by summing all the ions of either sign in a unit volume of the electrolyte solution in the neighbourhood of the point in question: [1]

$$\rho = \Sigma n_i z_i e = \Sigma n_i^o e z_i \exp\frac{-z_i e \psi}{kT} \tag{2.3}$$

$$\frac{d^2\psi}{dx^2} = -\frac{1}{\epsilon_o\epsilon_r}\Sigma n_i^o e z_i \exp\frac{-z_i e\psi}{kT} \tag{2.4}$$

where e (Coulombs) is the electronic charge.

2.1.2 Solution of the Complete Poisson-Boltzmann Equation

In many cases, the assumption $|ze\psi|<kT$ does not hold. To simplify let $z_i=z_+=-z_-=z$ so that the

$$\frac{d^2\psi}{dx^2} = \frac{2n^o ze}{\epsilon_o\epsilon_r}\sinh\frac{ze\psi}{kT} \tag{2.5}$$

solution is limited to symmetrical z:z valent electrolytes. Equation (2.4) can be written as follows:

$$\frac{d\psi}{dx} = -\frac{2\kappa kT}{ze}\sinh\frac{ze\psi}{2kT} \tag{2.6}$$

The negative sign ensures that $|\psi|$ always decreases towards the bulk solution and becomes zero far from the surface. Integrating equation (2.6) from the bulk solution up to a point a small distance, y, from the surface results in : [1]

$$\tanh\frac{ze\psi}{4kT} = \tanh\left(\frac{ze\psi_y}{4kT}\right)\exp[-\kappa(x-y)] \tag{2.7}$$

For very low potentials the substitution $\tanh x \approx x$ can be made so equation (2.7) becomes, [1]

$$\psi = \psi_y \exp[-\kappa(x-y)] \tag{2.8}$$

which is the solution of the linear equation (2.10), referred to as the Debye-Hückel approximation. The ions in the solution have a finite size and cannot get closer than a certain distance to a surface. Consequently there is a charge-free region near the surface, that has to be treated differently from the rest of the double layer. The potential at point d is ψ_y, that is why equations (2.7) and (2.8) have this term.

2.1.3 The Debye - Hückel Approximation

If the electrical energy is small compared to the thermal energy of the ions then equation (2.4) is as follows: [1]

$$\frac{d^2\psi}{dx^2} = -\frac{1}{\epsilon_o\epsilon_r}(\Sigma z_i e n_i^o - \Sigma z_i^2 e^2 n_i^o \psi/kT) \tag{2.9}$$

The first summation has to be zero in order to maintain electroneutrality in the bulk solution, therefore, [1]

$$\frac{d^2\psi}{dx^2} = \frac{\Sigma z_i^2 e^2 n_i^o}{\epsilon_o\epsilon_r kT}\psi = \kappa^2\psi \tag{2.10}$$

The quantity κ (nm^{-1}) is referred to the Debye - Hückel parameter. The reciprocal, $1/\kappa$ is referred to as the "thickness of the double layer" [2].

$$\kappa = \left(\frac{e^2\Sigma n_i^o z_i^2}{\epsilon_o\epsilon_r kT}\right)^{1/2} \tag{2.11}$$

The curves in Figure 2.2 are marked (with a dot) at the x value that corresponds to κ^{-1} (nm). The thickness of the double layer varies inversely with z and inversely with $M^{1/2}$ (M is the electrolyte concentration) for a symmetrical z:z electrolyte. So κ^{-1} equals 1.0 nm for a 0.01 M solution of a 3:3

electrolyte and is approximately 10 nm for a 0.001 M solution of a 1:1 electrolyte.

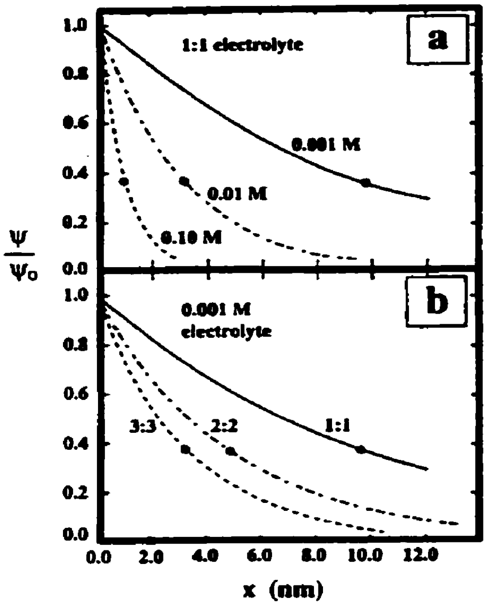

Figure 2.2. Fraction of Double-Layer Potential versus Distance from a SurfaceAccording to the Debye-Hückel Approximation. a) curves for 1:1 electrolyte at three concentrations and b) curves drawn for 0.001 M symmetrical electrolytes of three different valence types [2].

2.1.4 The Electrical Double Layer: Gouy-Chapman Theory

Around 1910 a model was proposed by Gouy and a similar treatment was developed independently a few years later by Chapman [1]. Today the model is referred to as the Gouy-Chapman model. It assumes that the electrical charge on the surface influences the distribution of ions in the electrolyte, so that an excess of ions of opposite sign is established in the layers of solution close to the surface [1].

Returning to the Poisson-Boltzmann equation as it applies to a planar interface, equation (2.4) to develop the Gouy-Chapman result [2]. If both sides of equation (2.4) are multiplied by $2d\psi/dx$, we obtain,

$$2(d\psi/dx)(\frac{d^2\psi}{dx^2}) = 2(\frac{d\psi}{dx})\{(\frac{e}{(\epsilon_o\epsilon_r)}\Sigma_i z_i n_i^o \exp(-z_i e\psi/kT)\} \qquad (2.12)$$

The left-hand side of this equation is the derivative of $(d\psi/dx)^2$ so,

$$(\frac{d\psi}{dx})^2 = (\frac{2kT}{\epsilon_o\epsilon_r})\Sigma_i n_i^o \exp(\frac{-z_i e\psi}{kT}) + const \qquad (2.13)$$

The integration constant in the equation above can be easily evaluated if the potential is defined in the solution at $x=\infty$ to be zero. At the same limit, $d\psi/dx$ also equals zero. Equation (2.13) becomes

$$(\frac{d\psi}{dx})^2 = (\frac{2kT}{\epsilon_o\epsilon_r})\Sigma_i n_i^o[\exp(\frac{-z_i e\psi}{kT}) - 1] \qquad (2.14)$$

This result can be integrated further if we restrict the electrolyte in solution to the symmetrical z:z type. In that case, equation (2.7) can be written as,

$$(\frac{d\psi}{dx})^2 = (\frac{2kTn^o}{\epsilon_o\epsilon_r})[\exp(\frac{-ze\psi}{kT}) + \exp(\frac{ze\psi}{kT}) - 2] \qquad (2.15)$$

in which z is the absolute value of the valence number. The bracketed term (in equation (2.15)) is equal to $[\exp(-ze\psi/2k\,T)-\exp(ze\psi/2k\,T)]^2$; therefore equation (2.15) can be written as

$$(\frac{d\psi}{dx})^2 = (\frac{2kTn^o}{\epsilon_o\epsilon_r})[\exp(\frac{-ze\psi}{2kT}) - \exp(\frac{ze\psi}{2kT})]^2 \qquad (2.16)$$

Identifying $(ze\psi/k_BT)$ as y permits the simplification of notation to

$$\left(\frac{d\psi}{dx}\right) = \left(\frac{2e^2z^2n^o}{\epsilon_o\epsilon_r kT}\right)^{1/2}\left[\exp\left(\frac{-y}{2}\right) - \exp\left(\frac{y}{2}\right)\right] \tag{2.17}$$

$$\left(\frac{d\psi}{dx}\right) = \kappa\left[\exp\left(\frac{-y}{2}\right) - \exp\left(\frac{y}{2}\right)\right] \tag{2.18}$$

with some mathematical analysis (not shown here), equation (2.18) becomes,

$$\frac{\left[\exp\left(\frac{ze\psi}{2kT}\right) - 1\right]}{\left[\exp\left(\frac{ze\psi}{2kT}\right) + 1\right]} = \frac{\left[\exp\left(\frac{ze\psi_o}{2kT}\right) - 1\right]}{\left[\exp\left(\frac{ze\psi_o}{2kT}\right) + 1\right]}\exp(-\kappa x) \tag{2.19}$$

Equation (2.19) is the Gouy-Chapman expression for the variation of potential within the double layer. For simplicity, equation (2.19) n be written

$$\Upsilon = \Upsilon_o\exp(-\kappa x) \tag{2.20}$$

where Υ_o is defined by the relationship,

$$\Upsilon = \frac{\left[\exp\left(\frac{ze\psi}{2kT}\right) - 1\right]}{\left[\exp\left(\frac{ze\psi}{2kT}\right) + 1\right]} \tag{2.21}$$

and Υ_o is equal to Υ evaluated with $\psi=\psi_o$.

Another situation of interest in which equation (2.19) simplifies considerably is the case of large values of x at which ψ has fallen to a small value regardless of its initial value. Under these conditions the exponentials of the left-hand side are expanded to give,

$$\frac{ze\psi}{4kT} = \Upsilon_o \exp(-\kappa x) \tag{2.22}$$

$$\psi = \left(\frac{4kT}{ze}\right)\Upsilon_o \exp(-\kappa x) \tag{2.23}$$

For large values of ψ_o, $\Upsilon_o \to 1$. In this case, equation (2.23) becomes,

$$\psi = \left(\frac{4kT}{ze}\right)\exp(-\kappa x) \tag{2.24}$$

which shows that the potential in the outer portion of the diffuse double layer is independent of the potential at the wall for larger potentials.

2.1.5 The Diffuse Layer Charge

The total charge, per unit area of surface, in the diffuse layer (Figure 2.3) can be obtained by adding the volume charge density through the whole region distance d to ∞: [1]

$$\sigma_d = \int_d^\infty e\,dx \tag{2.25}$$

Substituting equation (2.1): [1]

$$\sigma_d = \int_\infty^d \epsilon \frac{d^2\psi}{dx^2}dx = \epsilon\left(\frac{d\psi}{dx}\right)_\infty^d \tag{2.26}$$

As $x \to \infty$ $(d\psi/dx)=0$ so $\sigma_d=\epsilon(d\psi/dx)$ $x=d$ and using equation (2.6): [1]

$$\sigma_d = -\frac{2\kappa kT\epsilon}{ze}\sinh\frac{ze\psi_d}{2kT} = -\frac{4n^o ze}{\kappa}\sinh\frac{ze\psi_d}{2kT} \tag{2.27}$$

2.1.6 Zeta-Potential

The assumption that ions have no volume is acceptable for the bulk region of dilute solutions; however, ions do have a finite radius.

One method of taking this into account, included in the Stern model, is to divide the aqueous part of the double layer by a boundary known as the Stern surface. The Stern surface is located at a distance δ from the actual surface. Figure 2.3 shows the way this surface intersects the double layer potential and how it divides the charge density of the double layer.

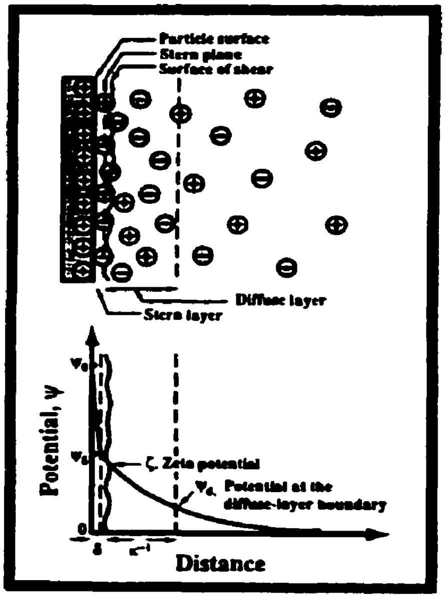

Figure 2.3. Variation of Potential with Distance from a Charged Surface in the Presence of a Stern Layer [2].

When a particle migrates in an electric field, the layer of liquid immediately adjacent to the particle moves with the same velocity as the particle. The actual distance from the surface at which the relative motion sets in between the stationary layer and the mobile fluid is not known. This boundary is referred to as the surface of shear.

The surface of shear occurs within the double layer, at a location usually taken as equivalent to the Stern surface. Instead of identifying the Stern surface as the surface of shear, however, the potential at the surface of shear is defined as the zeta-potential, ζ (mV). It is presumed to be close to the Stern potential ψ_δ in magnitude and it is, of course, lower than the potential at the surface ψ_o.

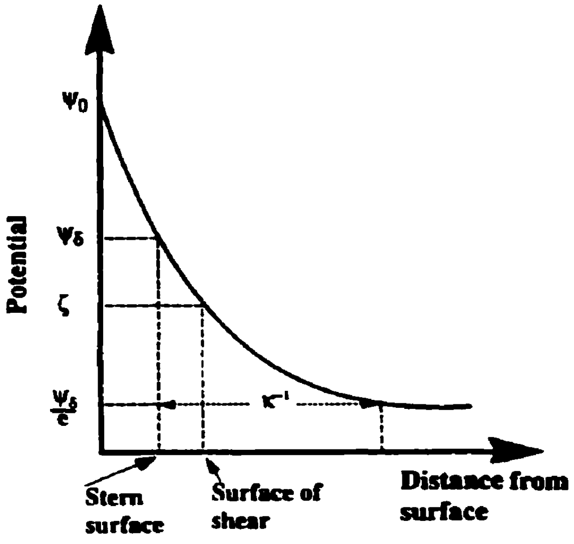

Figure 2.4. The Relative Magnitudes of Various Double Layer Potentials [2].

2.1.7 Types of Ions

Three types of ions exist, based on their ability to modulate the electrical properties of the solid-liquid interface.

Potential determining ions: Ionic species that adsorb on the surface and control the surface charge. A variation in concentration of potential determining ions causes a change in the surface potential.

Indifferent ions: Ionic species that do not affect the surface but control the double layer thickness. These ions interact with the surface by electrostatic force only and lower the zeta-potential asymptotically to zero.

Specifically adsorbing ions: Any ion whose adsorption at the surface is influenced by other forces in addition to the electrostatic force could be considered as a specifically adsorbing ion. The additional forces could be chemical in nature or physical. Specifically adsorbing ions can be recognized by their ability to reverse the sign of the zeta-potential.

2.1.8 Point of Zero Charge (p.z.c) and Iso-electric Point (i.e.p)

The point of zero charge (p.z.c) refers to the pH where the surface charge density (σ_o, Coulomb/m^2)

$$\sigma_o = F(\Gamma_{H^+} - \Gamma_{OH^-}) = 0 \tag{2.28}$$

is zero, [1] (equation 2.28, where Γ_{H^+}, Γ_{OH^-} represent the surface excess (mol/m^2) for H^+ and OH^- ions and F represents the Faraday constant (Coulomb/mol)). The surface charge can be determined by potentiometric titration [1].

The iso-electric point (i.e.p) refers to the pH where the zeta-potential is zero. The p.z.c and the i.e.p of a solid are the same only in the absence of specifically adsorbing ions.

2.2 Colloid Stability

The stability of a colloid suspension, according to the DLVO (Derjaguin, Landau, Verwey and Overbeek) theory [3,4], is established by the balance between the attractive and repulsive forces experienced by the particles as they come close together.

2.2.1 Total Potential Energy of Interaction

The total potential energy of interaction between surfaces is given by the following equation: [1]

$$V_T = V_A + V_R \tag{2.29}$$

where V_A and V_R are the van der Waals attractive energy and repulsive energy respectively. The van der Waals attraction always dominates at both large and small separations. At small separations, V_R has to approach a finite value, whereas $|V_A|$ increases markedly and is expected to pull the surfaces into a deep attractive well referred to as the primary minimum. This well is not indefinitely deep because of a very large, short-range repulsion between the atoms on each surface (Figure 2.5).

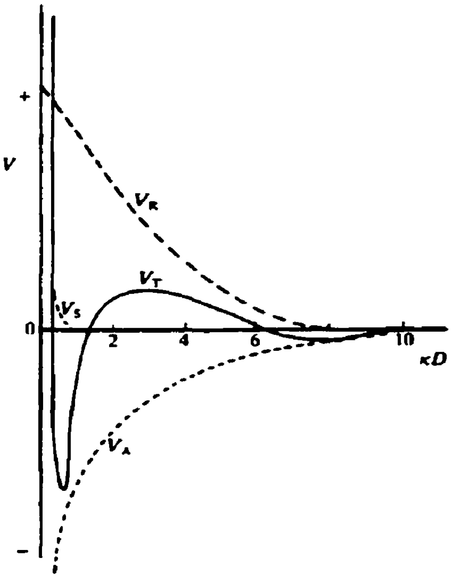

Figure 2.5. Total Potential Energy of Interaction $V_T=V_S+V_R+V_A$, where V_S is the Potential Energy of Repulsion due to the Structural Layers (hydration forces). V_S is assumed to be negligible until D<~10 nm (D is the distance between surfaces). [2]

The classical DLVO theory predicts the stability of lyophobic colloidal suspensions based on the balance between electrical repulsion and attraction. However, the theory fails with very hydrophobic and very hydrophilic colloidal suspensions and needs to be extended by incorporating the appropriate structural force term [5].

These terms have to be considered because of the influence of a surface on adjacent solvent layers. Depending on the type of surface this can give rise to either repulsive or attractive forces.

2.2.1.1 *Electrostatic Energy (Hogg et al. Model)*

This force is based on the charge of the particles, caused by surface dissociation or preferential adsorption of ions. In order to conserve electro neutrality, the charges on particles are surrounded by a diffuse atmosphere of counter ions which forms the electric double layer (Figure 2.3).
The energy of repulsion between two particles carrying double layers decays approximately as exp(-κH) (H is the distance between the particles) and can be written as: [6]

$$V_E = \frac{\varepsilon a_1 a_2 (\Psi_1^2 + \Psi_2^2)}{4(a_1 + a_2)} \left[\frac{(2\Psi_1\Psi_2)}{(\Psi_1^2 + \Psi_2^2)} \ln\frac{(1+\exp(-\kappa H))}{(1-\exp(-\kappa H))} + \ln(1-\exp(-2\kappa H)) \right] \quad (2.30)$$

Where ϵ is equal to $4\pi\epsilon_o\epsilon_r$, and ϵ_o is the permittivity of free space ($8.82 \text{ X } 10^{-12}$ C/(m*V)), ϵ_r is the relative dielectric constant of the medium, a_1 is the radius of solid 1, a_2 is the radius of solid 2, ψ_1 is the potential of solid 1, ψ_2 is the potential of solid 2, κ is the Debye-Hückel parameter and H is the distance between the surfaces of two particles.

The term $((2\Psi_1\Psi_2)/(\Psi_1^2 + \Psi_2^2))*\ln((1 + \exp(-\kappa H))/(1- \exp(-\kappa H)))$ represents the electrostatic interaction between the electrical double layers and $\ln(1- \exp(-2\kappa H))$ is called the symmetry term.

Equation (2.30) applies for Ψ_1 and/or Ψ_2 of less than 60 mV and for solution conditions such that the double layer thickness is small compared to the particle size. Verwey and Overbeek [4] have shown the Derjaguin's method gives a good approximation for the interaction provided the product $\kappa a > 10$.

2.2.1.2 *van der Waals Energy*

These forces arise from the interaction of atomic and molecular dipoles. There are three types of interactions [7]:

(I) A permanent molecular dipole which creates an electric field that orients other permanent dipoles so they are attracted to the first one. This interaction is referred to as the Keesom interaction.

(ii) A permanent dipole induces a dipole in a polarizable atom, molecule or medium which results in attraction. This is referred to as the Debye interaction.

(iii) An instantaneous dipole, arising from a fluctuation in the distribution of electronic charge, induces dipoles in the surrounding atoms and molecules. Again, the induced dipoles are attracted to the inducing one. This is referred to as the London or dispersion force.

The van der Waals energy of interaction between two spherical particles when a_1, a_2 >> H is: [1]

$$V_A = -\frac{A_{312}}{6H}\left(\frac{a_1 a_2}{a_1 + a_2}\right) \qquad (2.31)$$

where A is the Hamaker constant (Joules) which depends on the nature of the particles and the medium, a_1 is the radius of solid 1 (m), a_2 is the radius of solid 2 (m) H is the distance between the particles (m).

The Hamaker constant for two interacting bodies can be approximated from the following equation: [8]

$$A_{131} = \frac{[\sqrt{A_{11}} - \sqrt{A_{33}}]^2}{(1-2.5X10^{18}\sqrt{A_{11}A_{33}})} \qquad (2.32)$$

where the parameters A_{11} and A_{33} are the Hamaker constants of the solid and the medium, in vacuum respectively, and A_{131} is the Hamaker constant for the solid-medium-solid.

These two Hamaker constants can be determined by [9]:

$$A_{ii} = 6\pi r_{ii}^2 \gamma_s^d \tag{2.33}$$

where r_{ii} is the intermolecular distance within the interacting body of the solid and γ_s^d refers to the dispersion component of the surface free energy of the solid (N/m).

The Hamaker constant for two materials interacting across water was calculated from Lifshitz theory by the following approximation: [10]

$$A_{312} = A_{\nu=0} + A_{\nu>0} \approx$$

$$\approx \frac{3}{4}kT\left(\frac{\epsilon_1-\epsilon_3}{\epsilon_1+\epsilon_3}\right)\left(\frac{\epsilon_2-\epsilon_3}{\epsilon_2+\epsilon_3}\right) + \frac{3h\nu}{8(2)^{1/2}}\frac{(n_1^2 - n_3^2)(n_2^2 - n_3^2)}{(n_1^2 + n_3^2)^{1/2}(n_2^2 + n_3^2)^{1/2}\ X\ ((n_1^2 + n_3^2)^{1/2} + (n_2^2 + n_3^2)^{1/2})} \tag{2.34}$$

where n_i are the refractive indices, ϵ_i the dielectric constants for the respective media and ν_e a common adsorption frequency ($3 \text{ X } 10^{15}\ s^{-1}$).

2.2.1.3 *Repulsive Hydration Force*

At long-range in addition to the attractive van der Waals forces there are repulsive electrostatic "double layer" forces. The van der Waals force is always expected to ultimately win out at small surface separations. However, certain surfaces (usually oxide or hydroxide surfaces such as clays and silica) swell spontaneously or repel each other in aqueous solutions even in very high salt solutions. Between hydrophilic surfaces there is a short range repulsive force commonly referred to as the hydration or structural force. Repulsive hydration forces arise from strongly H-bonding surface groups, like hydrated ions or hydroxyl (-OH) groups which modify the H-bonding network of water molecules adjacent to them [11].

2.2.1.4 *Attractive Hydrophobic Force*

Between hydrophobic surfaces the force is attractive. A hydrophobic surface is defined as being inert to water meaning that it cannot bind to water molecules via ionic or hydrogen bonds. Hydrocarbons are hydrophobic, for example. The hydrophobic force can be far stronger than the van der Waals attraction especially between hydrocarbon surfaces for which the Hamaker constant is small. The magnitude of the hydrophobic attraction decreases with decreasing hydrophobicity (increasing hydrophilicity) of a surface.

Hydrophobic forces were first measured by Israelachvili and Pashley [12] with mica surfaces in equilibrium with cetyltrimethylammonium bromide (CTAB) solution. They were relatively short-range and decayed exponentially in the range of 0-10 nm, [5]

$$\frac{F}{R} = C\,exp(-\frac{H}{D_o}) \tag{2.35}$$

in which R is the radius of particle (μm), D_o the decay length (nm), H the separation distance (nm) and C the pre-exponential parameter which is negative for hydrophobic interaction. Later investigations illustrated the existence of long-range hydrophobic forces which are best described by a double-exponential function where the first term represents the "short-range" hydrophobic force and the second term the "long-range" hydrophobic force [5].

$$\frac{F}{R} = C_1\exp(-\frac{H}{D_1}) + C_2\exp(-\frac{H}{D_2}) \tag{2.36}$$

2.2.1.5 *Coagulation*

Particles with either a positive or negative charge repel each other (electrostatic repulsion), however, when the zeta-potential approaches zero coagulation occurs. This is because the electrostatic repulsive force is lowered and the van der Waals attractive force becomes proportionally larger in magnitude. Also particles with a zeta-potential of opposite sign can agglomerate through electrostatic attraction. If particles of the same material agglomerate, coagulation is referred to as homocoagulation and it is referred to as hetrocoagulation if the materials are different.

For very hydrophobic and very hydrophilic colloidal suspensions, the appropriate structural force term has to be considered (section 2.2.1).

2.3 Measuring Stability

The state of agglomeration of slurries has a dramatic influence on their processing. In addition to controlling the transport of slurries, the state of agglomeration has a controlling influence on solid-solid (e.g flotation) and solid-liquid (e.g dewatering) separations. From a diagnostic point of view, the state of agglomeration of slurries is indicative of the level of inter-particle interaction in a pulp [13].

Two methods used to investigate the state of agglomeration of a slurry are rheology and settling characteristics.

2.3.1 Rheology

Rheology is a fundamental interdisciplinary-science which is concerned with the study of the internal response of materials to stress.

Rheology has been extensively used to investigate particle-particle interactions in slurries of oxide minerals [14,15], clays [16] and coal [17], providing information on the state of aggregation induced through changes in pH, electrolyte concentration, and the addition of various reagents [13].

A characteristic of fluids is that, if an external stress is applied, they deform and continue to deform as long as the stress is present. Moreover, removal of the stress will not always result in a return of the fluid to the undeformed state. This is called a viscous response [18].

The fluid deforms under an external stress, because of the great mobility of the molecules, but internal frictional forces retard the rate of deformation and create an equilibrium condition in which a constant external stress results in a constant rate of deformation [18].

In the simplest case there is a direct proportionality between the stress and the rate of deformation. The rheological properties of such a fluid may be described by Newton's law: according to this the stress is directly proportional to the rate of deformation and does not depend on the deformation itself. There are viscous fluids, however, that do not obey Newton's law and exhibit a non-linear dependence between the stress and rate of deformation. Such fluids are termed non-Newtonian [18].

For Newtonian fluids (<15% solids), the viscosity (η Ns/m^2) is independent of the shear rate (D), thus equation (2.37) can be applied [13]:

$$\tau = \eta D \tag{2.37}$$

where τ is the shear stress.

Flow curves of slurries at high solids content ($\geq 15\%$ solids) show non-Newtonian behaviour; yield values are observed and in some cases, shear thinning is evident. These flow curves are better described by the Bingham model: [13]

$$\tau = \tau^o + \eta_{pl} D \tag{2.38}$$

where τ^o is the Bingham (or extrapolated) yield value and η_{pl} is the plastic viscosity. Alternately, at the highest solids content (>45%), the Herschel Bulkley model: [13]

$$\tau = \tau^o + K D^n \tag{2.39}$$

gives the best fit, where n and K are constants.

Shear stress (τ) or the Bingham yield value (τ^o) can be used as a measure of the extent of aggregation of a slurry. As a slurry becomes more dispersed, the shear stress and Bingham yield value decrease, however, if the slurry becomes more agglomerated, these values increase.

2.3.2 Settling

The state of dispersion of a slurry can be determined by its settling velocity. If the particle-particle interaction is attractive, the particles will agglomerate, effectively giving a greater diameter and increasing the settling velocity as inferred from Stokes law: [19]

$$v = \frac{d^2 g(D_s - D_f)}{18\eta} \tag{2.40}$$

where v is the terminal velocity of the particle (m/sec), d is the particle diameter (m), g is the acceleration due to gravity (m/sec^2), η is the fluid viscosity (Ns/m^2). It is important to note that equation (2.40) does not take into account hindered settling.

2.4 Sulphide Minerals

2.4.1 Oxidation/Hydrolysis

Compared to nonsulphide minerals, sulphides are chemically reactive with water and dissolved oxygen. This is due to the relative instability of sulphide sulphur. Oxidation occurs by the transfer of electrons from sulphur to oxygen, a charge transfer mechanism. The initial oxidation reaction for a sulphide mineral can be written: [20]

$$MS + xH_2O = M(H_2O)_x^{2+} + S^- + e \tag{2.41}$$

where M is a bivalent ion and S^- an intermediate product. The metal ions formed can hydrolyse and/or oxidize: [20]

$$M(H_2O)_x^{2+} = M(OH)(H_2O)_y^+ + H^+ + (x-y-1)H_2O \tag{2.42}$$

$$M(OH)(H_2O)_y^+ = M(OH)_2\, z(H_2O) + H^+ + (x-z-1)H_2O \tag{2.43}$$

The. hydrolysis products can play a role in flotation.

The sulphur intermediate S^- can oxidize through a series of reactions to form, eventually, SO_4^{2-}. The first step of the oxidation process is the formation of elemental sulphur:

$$S^- = S^o + e \tag{2.44}$$

Subsequent steps involve various sulphoxyl species, $S_xO_y^{2-}$.

2.4.2 Galvanic Interactions

When two sulphide minerals are in contact, galvanic interactions can occur where electrons transfer from one to the other. Galvanic interactions derive from the different electro-chemical reactivities of the sulphide minerals as indicated by their rest potential. Rest potentials for a number of sulphide minerals have been determined by Rao and Finch [21], Nowak et al [22] and Majima [23] as shown in Table 2.1.

Table 2.1. The Rest Potential of Minerals in Distilled Water in the Presence of Oxygen.

Mineral	Rest Potential (V vs SHE)			
	pH 2	pH 4	pH 6	pH 9.2
Pyrite	0.61	0.66	0.42	0.34
Chalcopyrite	0.51	0.56	0.36	0.29
Chalcocite	0.35			
Sphalerite		0.46	0.19	0.19
Galena	0.33	0.40	0.23	0.23

The general electrode reactions for this two mineral system are [24]:

Anodic reaction:

$$MS + H_2O = M(H_2O)^{2+} + S^{O} + 2e \tag{2.45}$$

Cathodic reduction of oxygen (as the cathodic mineral):

at higher pH solution:

$$\tfrac{1}{2}O_2 + H_2O + 2e = 2OH^- \tag{2.46}$$

at low pH solution:

$$\tfrac{1}{2}O_2 + 2H^+ + 2e = H_2O \tag{2.47}$$

The overall reaction under neutral or basic conditions (most relevant to flotation) is:

$$MS + \frac{1}{2}O_2 + 2H_2O = M(H_2O)^{2-} + 2OH^- + S^O \qquad (2.48)$$

Consider pyrite in contact with another sulphide mineral. Because of its high rest potential pyrite acts as a cathode drawing electrons from the second sulphide mineral, giving rise to a galvanic current. Pyrite is susceptible to the formation of hydroxide on its surface as the electrons are taken up by dissolved oxygen to form OH^- ions.

Figure 2.6 illustrates the mixed potential model of the sphalerite pyrite galvanic couple: Sphalerite oxidizes releasing Zn^{2+}in solution and OH^- is formed on the pyrite surface. Rao and Finch [21] showed that the pyrite-sphalerite combination potential is intermediate between the rest potential of pyrite and sphalerite.

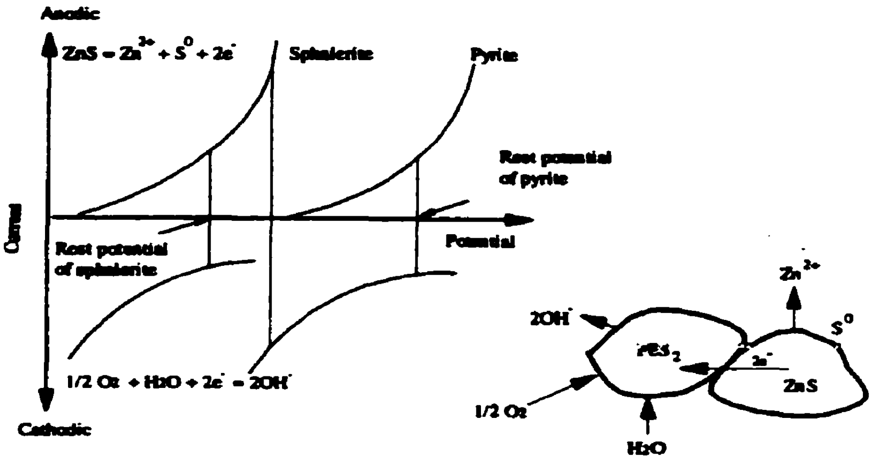

Figure 2.6. Mechanism of Sphalerite Oxidation and Pyrite Reduction in Galvanic Couple.

Galvanic interaction is affected by variables such as pH, rate of mixing and aeration. The influence of dissolved oxygen and pH on galvanic interaction is linked to the fact that oxygen reduction is the most common reduction process with OH^- as the reaction product and consequently the rest potential of minerals varies with solution pH and dissolved oxygen content. Figure 2.7 shows that as the dissolved oxygen content increases, the rest potential of a mineral also increases.

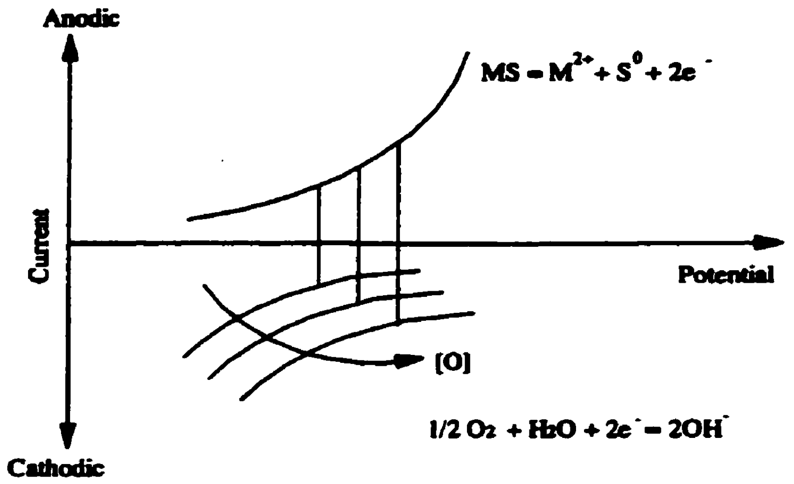

Figure 2.7. The Effect of Concentration of Dissolved Oxygen on Rest Potential.

2.5 References

1. Hunter, R. J., Foundations of Colloid Science, Volume 1, 1987.
2. Hiemenz, P. C., and Rajagopalan, R., Principles of Colloid and Surface Chemistry, 3rd Edition, 1997, pp499-574.
3. Derjaguin, B. V. and Landau, L., Acta Physicochimica, U.S.S.R., 1941, p63.
4. Verwey, E.J.W. and Overbeek, J. Th. G., Theory of the Stability of Luphobic Colloids, Elsevier, Amsterdam, 1948, pp135-182.
5. Yoon, R. H., and Ravishankar, S. A., Application of Extended DLVO Theory, Journal of Colloid and Interface Science, 166, 1994, pp215-224.
6. Hogg, R., Healy, T. W., and Fuerstenau, D. W., Mutual Coagulation of Colloid Dispersions, Transactions of the Faraday Society, 62, 1966, pp1638-1651.
7 Horn, G. R., Surface Forces and Their Action in Ceramic Materials, Journal of the American Ceramic Society, 73(5), 1990, pp1117-1135.
8. Hamaker, H. C., Physica, 1937, p1058.

9 Fowkes, F. M., Attractive Forces at Interfaces, Industrial and Engineering Chemistry, 56(12), 1964, p40.

10. Israelachvili, J. N., Intermolecular and Surface Forces, 2nd edition, Academic Press, London, 1992.

11. Israelachvili, J. N., Surface Science Reports, 14(3), 1992, pp109-159.

12. Israelachvili, J. N., and Pashley, R. M., Journal of Colloid and Interface Science, 98(2), 1984, pp500-514.

13. Muster, T. H., and Prestidge, C. A., Rheological Investigations of Sulphide Mineral Slurries, Minerals Engineering, 8(12), 1995, pp1541-1555.

14. Rao, A. S., Rheology of Aqueous Dispersions of Alumina, Titania and Mixture of Alumina and Titania Powders, Journal of Dispersion Science and Technology, 8(5 & 6), 1987, pp457-476.

15. Leong, Y. K., and Boger, D. V., Surface Chemistry and Rheological Properties of Zirconia Suspensions, Journal of Rheology, 35(1), 1990, pp149-165.

16. Heath, D., and Tadros, Th. F., Influence of pH, Electrolyte and Poly(vinyl alcohol) Addition on the Rheological Characteristics of aqueous Dispersions of Sodium Martmorillonite, Journal of Colloid and Interface Science, 93(2), 1983, pp307-319.

17. Lai, R. W., McMahan, L. G., Richardson, A. G., and Chiang, S. H., Size Reduction and Selective Agglomeration of Coal: Technical Feasibility of Cleaning Pittsburgh Seam Coal with Isooctane, Advances in Coal and Mineral Processing Using Flotation, Littleton, Colorado, Society for Mining, Metallurgy and Exploration Inc., 1989, pp120-129.

18. Ferguson, J., and Kembłowski, Z., Applied Fluid Rheology, Elsevier Applied Science, 1991, pp3-46.

19. Wills, B. A., Mineral Processing Technology, 4th edition, Pergamon Press, 1988, p337.

20. Chander, S., Electrochemistry of Sulphide Mineral Flotation, Mineral and Metallurgical Processing, 5, 1988, pp104-114.

21. Rao, S. R., and Finch, J. A., Galvanic Interaction Studies on Sulphide Minerals,

Canadian Metallurgical Quarterly, 27(4), 1988, pp253-259.

22. Nowak, P., Krauss, E. and Pomianowski, A., The Electrochemical Characteristics of the Galvanic Corrosion of Sulphide Minerals in Short Circuited Model Galvanic Cells, Hydrometallurgy, 12, 1984, pp95-110.

23. Majima, H., How Oxidation Affects Selective Flotation of Complex Sulphide Ores, Canadian Metallurgical Quarterly, 8(3), 1969, pp269-273.

24. Kocabag, D., and Smith, M. R., the Effect of Grinding Media and Galvanic Interactions upon the Flotation of Sulphide minerals, in complex Sulphides, processing of Ores, concentrates and By-products (Editors, Zunkel, A. D., Boorman, R. S., Morris, A. E. and Wesely, R. J.), 1985, pp55-81.

CHAPTER 3

SURFACE ANALYSIS AND INSTRUMENTATION

3.1 Introduction

Interfacial science plays an important role in mineral processing, and many industries involving solid/liquid suspensions. Interfacial science helps interpret and predict the behaviour of suspensions under given physicochemical conditions, for example, whether particles tend to agglomerate or disperse.

Various instruments are used to provide the fundamental measurements. The instruments used in this work are the atomic force microscope (measurement of surface forces), zeta-potential meter (measurement of surface charge), and an automated settling apparatus (measurement of agglomeration).

3.2 Atomic Force Microscopy

In the last 20 years new devices for measuring surface and intermolecular forces have been developed. The surface forces apparatus of Israelachvili and Adams [1,2] has permitted accurate measurement of surface forces and has led to improved understanding of these forces and their implications in wetting, lubrication, and colloid stability.

Developments in the field of control, manipulation and measurement at the nano scale led to the development of the scanning tunnelling microscope by Binnig and Rohrer [3] in 1982 and the atomic force microscope (AFM) [4]. The AFM allows molecular and surface forces to be measured on a near molecular scale for the first time, both in air [5,6] and in water [7,8]. In those early studies, the force was measured between a sharp tip and a flat surface. Unfortunately, because the geometry of a tip is not simple, comparisons with theory proved difficult. Materials of a variety of compositions and geometries can now be studied.

The forces between colloidal particles dominate the behaviour of a great variety of systems including minerals, paints, paper, soil, clays and biological cells [9]. With the invention of the atomic force microscope (AFM) surface forces between small particles (down to 1 μm in diameter) and a flat surface can be measured.

3.2.1 Hardware

In this section, the AFM hardware is discussed. The AFM consists of seven major components: scanning probe microscope (SPM), controller, computer, keyboard, mouse, display monitor and control monitor.

3.2.2 Atomic Force Microscope

The main component of the system is the AFM (Figure 3.1).

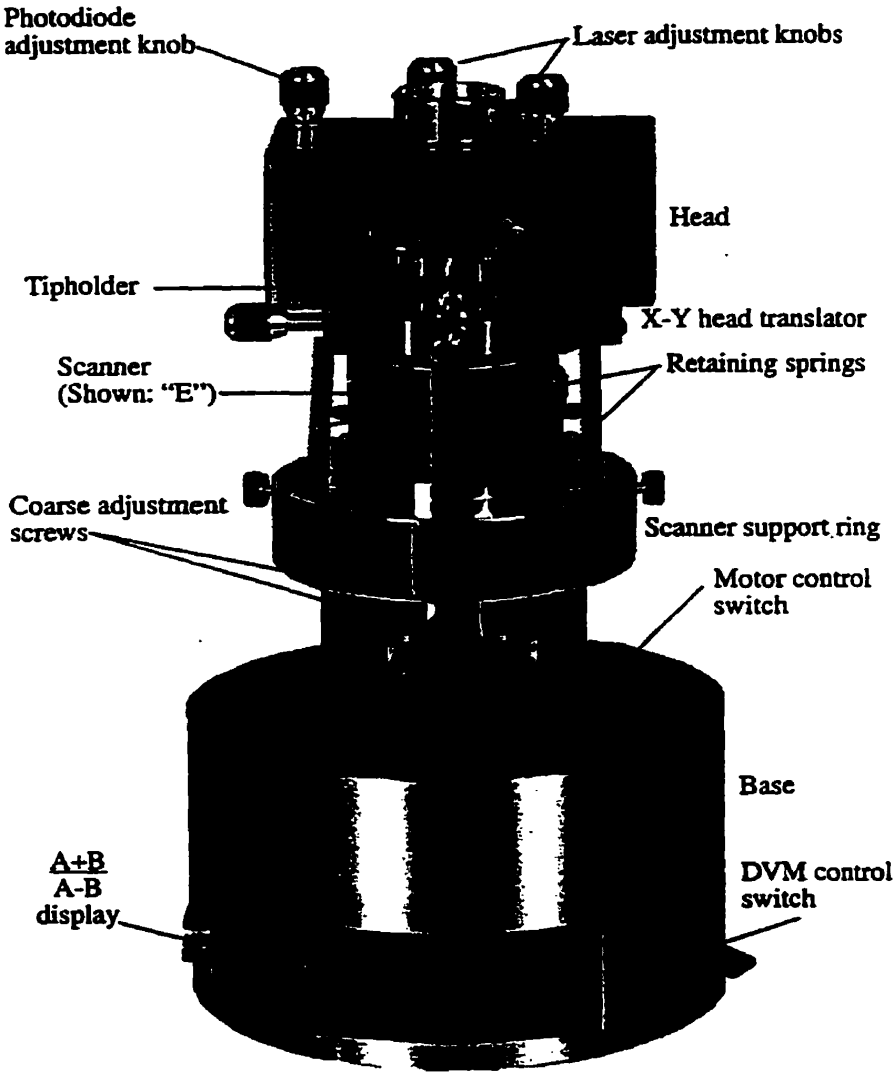

Figure 3.1. Atomic Force Microscope

3.2.3 Atomic Force Microscope Head

Figure 3.2 illustrates an AFM head. The head and attached X-Y stage are kinematically mated to the scanner via three contact points. Two retaining springs restrain the head, allowing it to be raised and lowered using adjustment screws threaded through the scanner body.

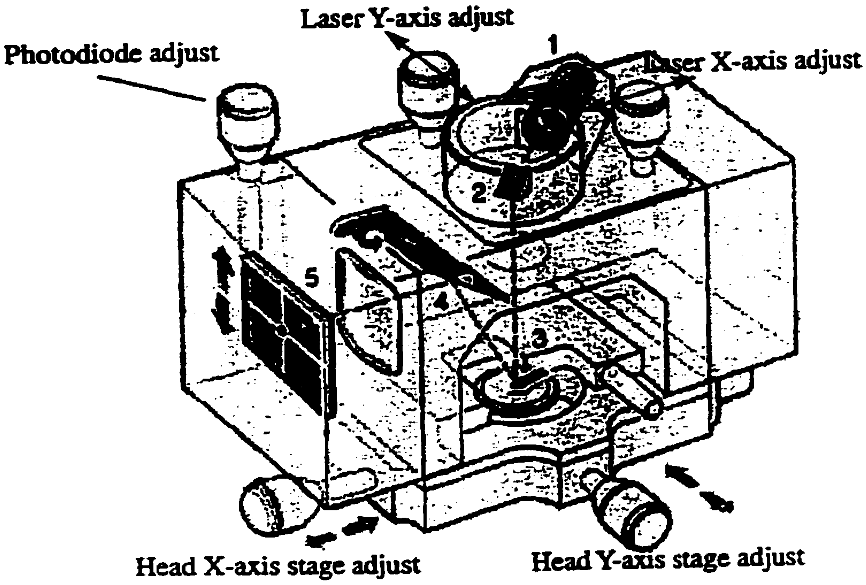

Figure 3.2. AFM Head and Major Components: Laser (1); Mirror (2); Cantilever (3); Tilt Mirror (4); Photodiode (5).

Photodiode array - The four elements of the quad photodiode (position sensitive detector) are combined to provide different information depending on the operating mode. In all modes the four elements combine to form the SUM signal. The amplified differential signal between the top two elements and the two bottom elements provides a measure of the deflection of the cantilever. This differential signal is used directly in contact AFM. Figure 3.3 illustrates the arrangement of the photodiode elements in the AFM head.

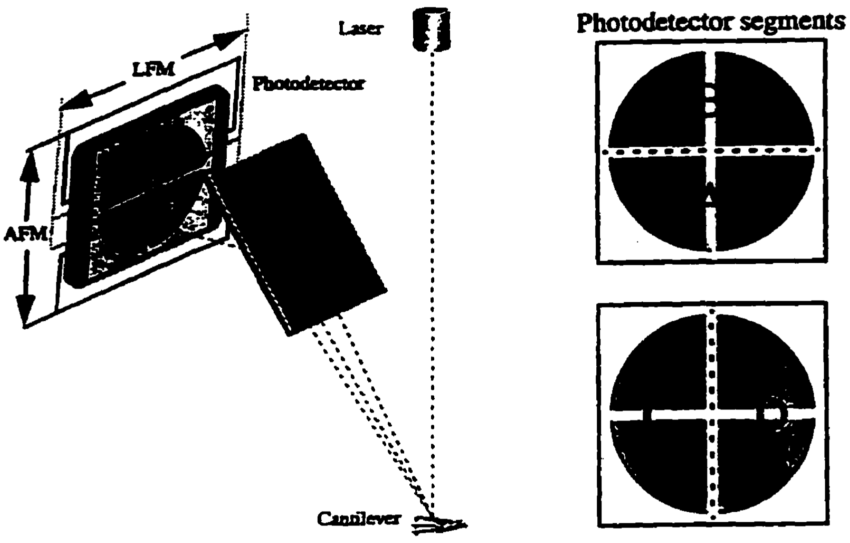

Figure 3.3. **Quad Photodetector Arrangement Different Segments of the Photodetector are used for Generating AFM.**

3.2.4 Scanners

Figure 3.4 shows the electrode configuration used in one type of scanner piezo tube. Electrodes are oriented as shown when the AFM is viewed from the front. With the scan angle parameter in the control panel set to 0.00, the fast-scan direction is in the direction of the x-axis.

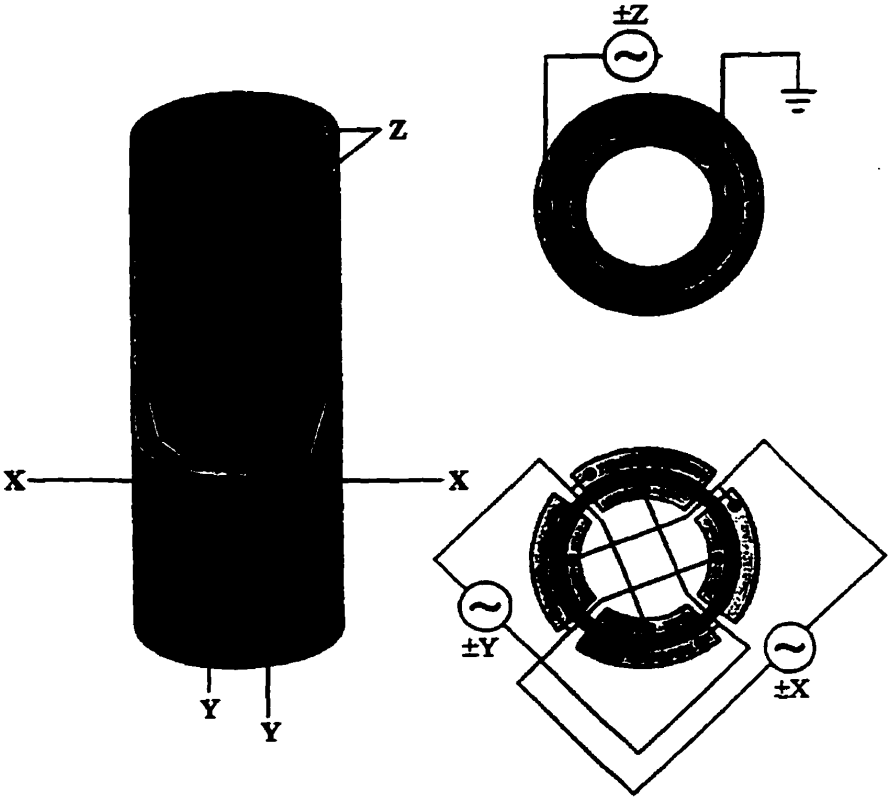

Figure 3.4. Typical Scanner Piezo Tube and X-Y-Z Electrical Configurations. AC Signals Applied to Conductive Areas of the Tube Create Piezo Movement along the Three Major Axes.

AC voltages applied to the scanner crystal's X-Y axes produce a raster-type scan motion as shown in Figure 3.5. The horizontal axis presented on the display monitor is referred to as the "fast axis" (in the example, the x-axis) and scans at a scan rate entered by the user. The orthogonal axis is known as the "slow axis" (in this example, the Y axis).

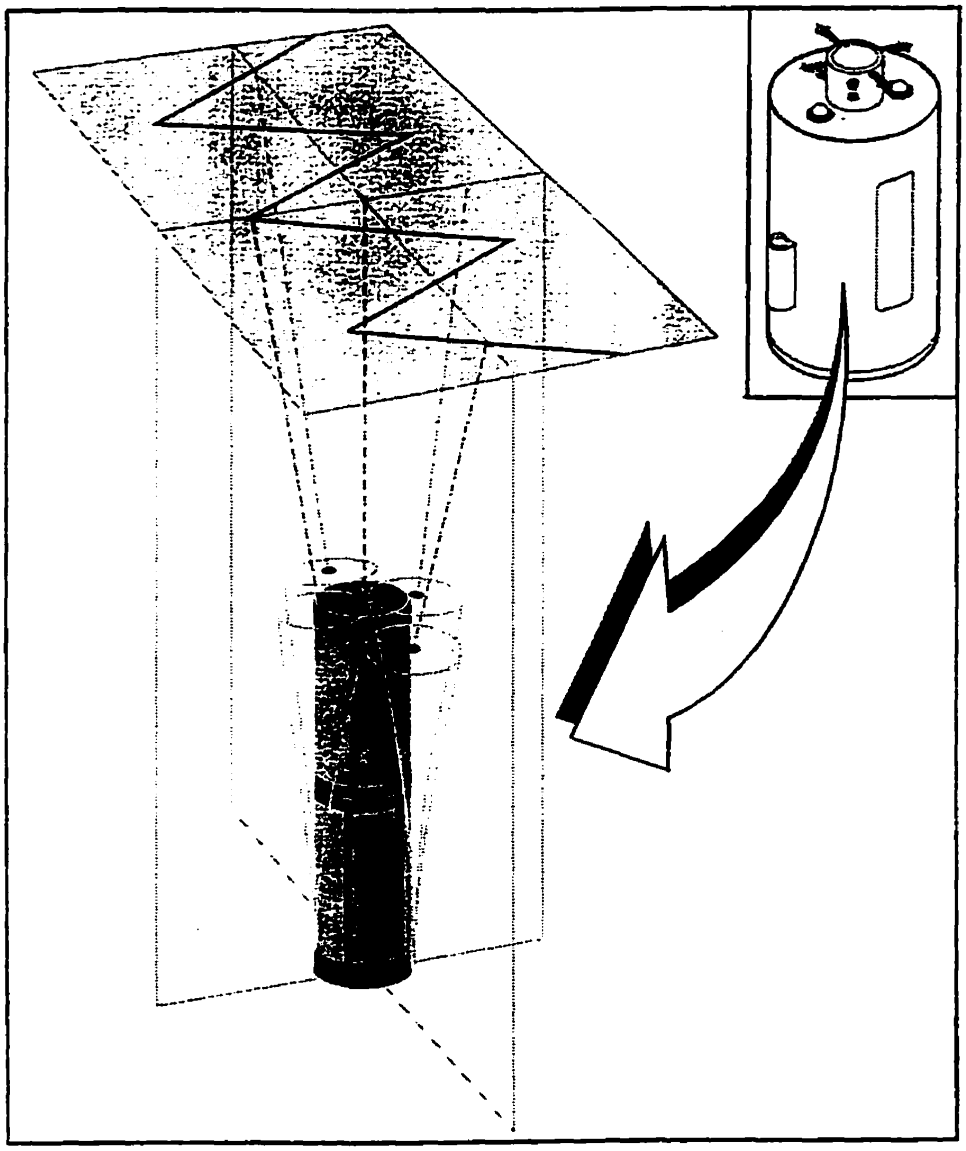

Figure 3.5. Voltages Applied to the X and Y axes Produce a Raster Scan Pattern. Any Angle may be Designated as the "fast axis" using the Scan Angle Parameter.

3.2.5 Cantilevered Probes - Silicon Nitride

Most scanning probe microscope work is performed using cantilevered probes. These are flexible cantilevers extending from a rigid substrate, to which a tip is attached. In atomic force microscopy

(AFM), the cantilever acts as a spring, allowing the tip to measure surface forces.

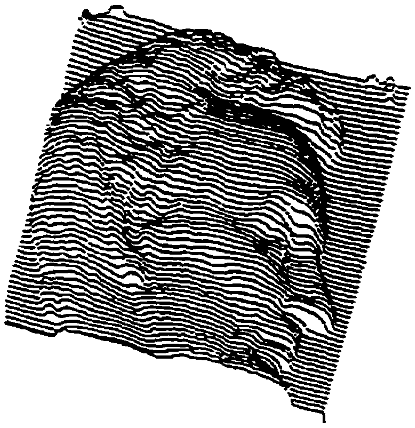

Figure 3.6. Face on a Coin.

The figure above illustrates how an adjacent, lagging scan line can be used to determine local scan lines on regular surfaces. For example, on the forehead (Figure 3.6) each scan line changes little from the line adjacent. In some local areas (such as under the nose) there are small, sudden changes; however, these are relatively isolated. In contrast, a similar trace of an irregular, random surface would reveal that each scan line bears little resemblance to its neighbour line.

The entire purpose of Look ahead gain is to take full advantage of regular features by using every line to anticipate the next one. Although Look ahead gain is relatively useless for random surfaces, it is a tremendous help on regular surfaces.

3.2.6 General Operating Concepts For Imaging of Surfaces

The AFM system comprises two main components: the scanner and the AFM detection system. The scanner houses the piezo electric element. The piezo element physically moves the sample in the X, Y, Z direction. The detection system consists of a laser which generates a spot of light that is reflected off a microfabricated cantilever onto a mirror and finally into a photodetector (Figure 3.7).

The position of the spot is determined by circuitry which generates a voltage from the difference between the photodiode segments (A-B). The circuit output, a voltage ranging from +10 V to -10V, depends on the position of the spot on the two photodiodes.

The AFM system maintains the tip at the end of the cantilever in contact with the sample surface. The sample is scanned under the tip in the X, Y plane. Features on the sample surface deflect the cantilever, which in turn changes the position of the laser spot on the photodiodes. This position change is read by the feedback loop. The feedback loop moves the sample in Z to restore the spot to its original position (Figure 3.7). The sequence A to E in Figure 3.7 is:

Figure 3.7.A. A flat portion of the sample surface is scanned beneath the tip left-to-right, maintaining the laser beam at the centre of the photodiode array.

Figure 3.7.B. As the tip encounters a raised feature, the cantilever is pushed up, deflecting the laser beam upward onto the "A" portion of the array. With the "A" photodiode receiving an increased portion of the laser light, its voltage increases while portion "B's" decreases (A>B).

Figure 3.7.C. The vertical deflection (A-B) voltage differential is sensed by the feedback electronics, causing a dropped voltage to the Z piezo crystal, the piezo retracts. As the Z piezo retracts, the cantilever recentres the laser beam onto the photodiode array (A=B).

Figure 3.7.D. As the tip encounters a decline in the sample topology, the tip drops. This directs more of the beam onto the "B" portion of the photodiode receiving an increased portion of the laser light, its voltage increases while portion "A's" decreases (A<B).

Figure 3.7.E. The vertical deflection (A-B) voltage differential is sensed by the feedback electronics, increasing voltage to the Z piezo crystal, the piezo extends. As the Z piezo extends, the tip is pushed down until the laser beam recentres on the photodiode array (A=B).

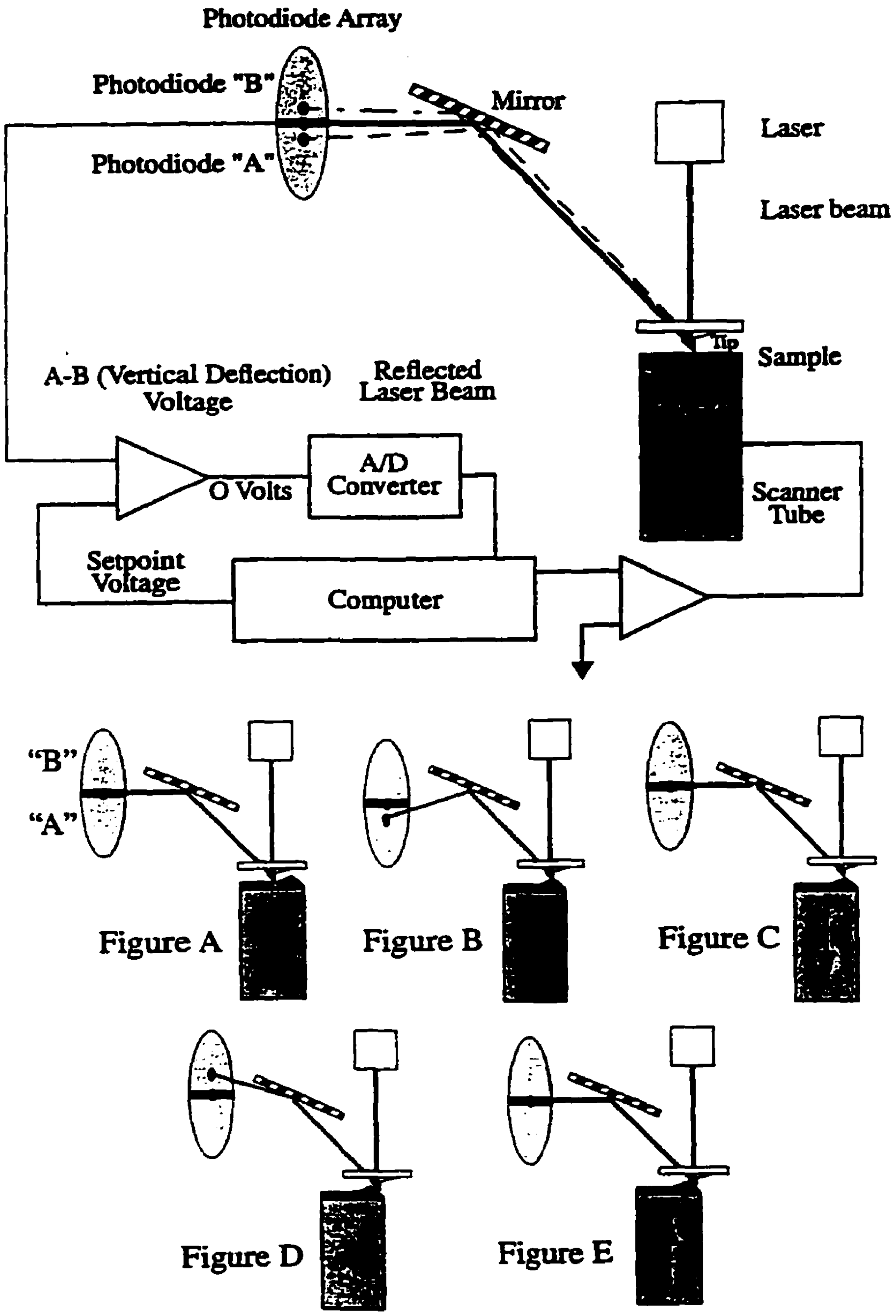

Figure 3.7. Contact AFM Concepts.

3.2.6.1 *Feedback Gains*

The feedback system used to control tip-sample interactions and render images has to be optimized for every fresh sample. This can be accomplished by adjusting various gains in the SPM's feedback circuit. This section discusses gains and how they are used to obtain images.

Setpoint: The setpoint controls the amount of cantilever flexion, as the setpoint increases the cantilever flexes more and tip-sample forces increase.

Proportional Gain: Proportional gain means that something is done proportionally in response to something else. In atomic force microscopy this implies that the scanner piezo tube moves relative to the topography of the sample. For example, when the surface of a sample rises, the scanner piezo tube moves downward and vice versa.

Integral Gain: Integral gain is used to correct the cumulative error between a system and its target state. There would be a constant error around the setpoint if the system relied on proportional gain alone. Also it is very important to consider whether the total error of the setpoint is increasing or decreasing over some interval of time. To correct for cumulative error, integral gain can be used.

Look Ahead Gain: Look ahead gain allows the atomic force microscope to better anticipate the rise and fall of a sample. Similarly, the feedback controller relies upon data from the previous (immediately adjacent) scan line to anticipate local features. It is easier to image samples which contain regular, periodic features since scan lines change relatively little from scan to scan. Consider, for example, scan lines tracing the surface shown below (Figure 3.6).

3.2.7 General Operating Concepts For Force Measurements

In AFM the force between a sample and a tip (a spherical particle may be glued to the tip) is measured as a function of the displacement of the sample. Sample displacement is achieved using a piezoelectric crystal or scanner. The force on a tip is obtained from the deflection of the microfabricated cantilever (0.1-0.2 mm in length) to which the tip is attached. A laser beam reflected from the back of the cantilever falls onto a photodiode which detects small changes in deflection, Figures 3.3 and 3.8 [10].

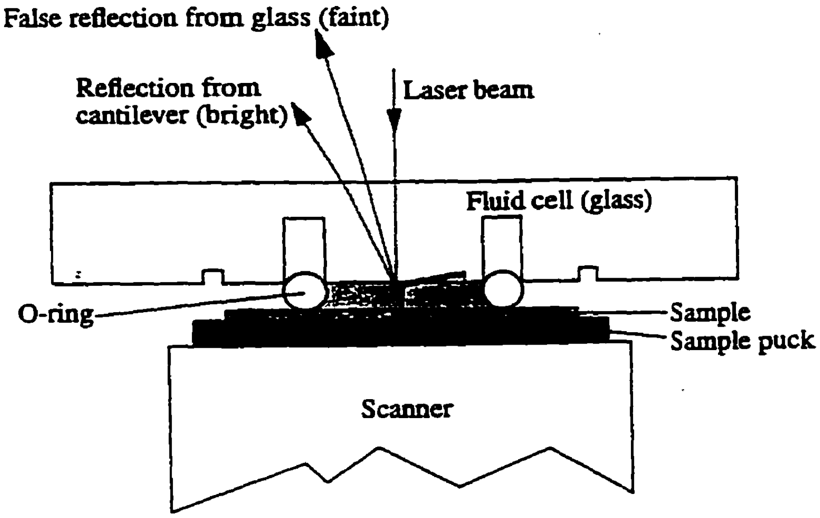

Figure 3.8. Fluid Glass Assembly.

The software provided with the AFM produces a screen file which records the change in photodiode output (which is proportional to spring deflection) as a function of sample displacement [10].

3.3 Zeta-Potential Meter

A Laser Zee meter (Model 501, PenKem Inc) was used to measure zeta-potentials of particles suspended in an electrolyte. This instrument determines the migration rate of particles in a known electric field. The technique is referred to as electrophoresis.

The suspension to be measured is placed in a chamber. This chamber consists of three parts:

a) Measurement compartment, which is a sandwich of three optically polished fused silica plates, permanently fused together to form a precise rectangular compartment.

b) Two electrodes in the compartment, a molybdenum anode, and a palladium cathode.

c) A rugged support base, on which the chamber is positioned.

3.3.1 Electrophoresis

A voltage is applied between the two electrodes. The applied voltage produces a uniform electric field in the connecting chamber and the charged particles respond by moving toward one electrode. The direction of movement is determined by the sign of the charge: positively charged particles move towards the cathode (negative electrode) and the negatively charged particles move towards the anode (positive electrode). The migrating speed of the particles is directly proportional to the magnitude of the surface charge or, more precisely, zeta-potential of the particles.

The sign and magnitude of surface charge are determined by, respectively, observing the direction and measuring the velocity of the particle moving under the influence of the applied electrical field. There are some complications. The wall of the measurement chamber carries a surface charge inducing an associated double layer. The electric field causes the counter-ions near the wall to move towards the electrode of opposite polarity. The counter-ions in turn drag fluid along causing an electroosmotic flow. In a closed chamber this action at the wall is compensated by a reverse flow at the centre, such that the average flow along the axis is zero. In the measuring chamber, there are two parallel locations or layers where the fluid flow is zero. These layers are called the stationary layers.

The observed velocity of a particle is the sum of the electrophoretic and electroosmotic component. To measure the desired electrophoretic component, only the particles in the stationary layer should be followed, which is accomplished by focussing the microscope at this layer.

3.3.2 The Optics

The chamber slides into position on a specially designed microscope stage. Before conducting any experiments, the microscope has to be focussed on the stationary layer. This is done by using the fine focus control and a manufacturer-supplied calibration constant.

Special cylindrical optics compress the collimated laser beam into a thin horizontal sheet of laser light. A vertical adjustment is provided to align the position of this illumination to coincide with the focal plane of the microscope.

3.3.3 The Electronics

A cube prism inside the microscope causes the viewed image to appear to move at a rate proportional to the prism's speed of rotation. To make a zeta-potential measurement, the operator applies a potential across the chamber by closing switch S.

The resultant electric field causes the particles to move at an electrophoretic velocity proportional to the mobility u and the applied voltage V. Adjustment of potentiometer P1 causes the prism to rotate at a rate proportional to the potentiometer voltage U times voltage V.

The user adjusts the potentiometer to control the rotational velocity of the prism top to be equal in magnitude but opposite in direction to the mean electrophoretic velocity of the particles, so that the cloud of particles appears stationary. The voltage U is therefore proportional to the mean particle mobility u. In the instrument the mobility value is multiplied by an appropriate constant and the resultant zeta-potential value is shown on a display.

3.4 Automated Settling Apparatus

One method to measure suspension settling velocity v is to fill a cylinder with slurry and visually measure the time, (t_2-t_1), for the settling of the solid-liquid interface, over a distance h. Hence:

$$v = \frac{h}{t_2 - t_1} \tag{3.1}$$

This technique has two major drawbacks:

1) Visual location of the solid-liquid interface is not always possible or precise.

2) It is tedious and consequently subject to operator error.

To automate measurement of (t_2-t_1), a cylinder was equipped with two ring electrodes mounted flush to the inside cylinder wall separated 8.3 cm. The electrodes were connected to a conductivity meter which was interfaced with a computer.

The cylinder, made of plexiglass, was 3.8 cm in diameter and 29 cm in height. The bottom stands on a plastic base and the open top is covered with a rubber stopper after filling with slurry. Through the stopper various probes, e.g. for pH, can be inserted and brought into contact with the slurry. The general setup is given in Figure 3.9.

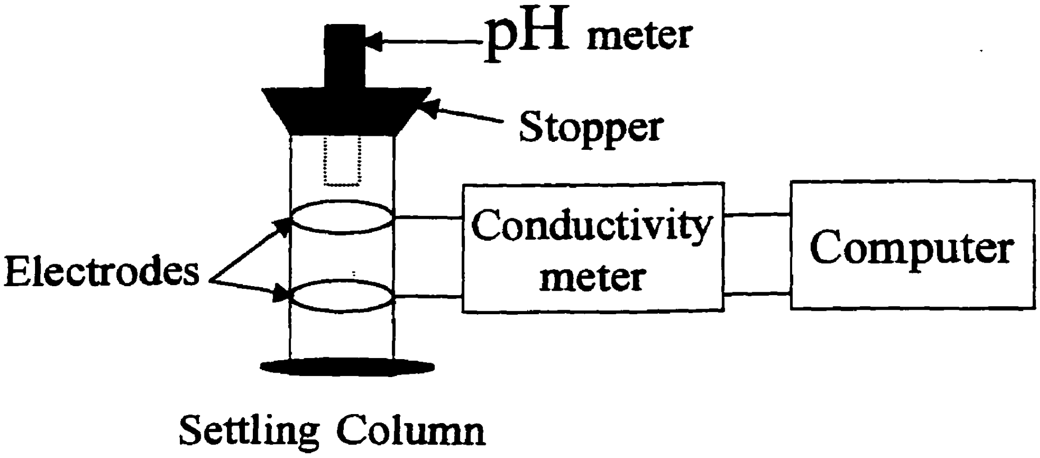

Figure 3.9. Experimental Setup to Automate Measurement of Settling Rate.

A computer program was written to record the conductivity as a function of time. Measurements were made every 1 s and the conductance vs time was plotted directly on the computer monitor during the course of settling.

The solids were suspended by subjecting the column to a rhythmic end-over-end rotation. After a homogeneous dispersion had been obtained, judged by a constant conductance, the column is stood vertically to allow the solids to settle and the data are recorded.

3.4.1 Data Analysis

The data was analysed using a program called "Tablecurve". As shown in Figure 3.10, three stages of settling are evident. Stage A represents the initial well dispersed system. Stage B represents the settling of solids between the two electrodes; as the solid-liquid interface moves between the two ring electrodes the conductance increases (most solids of interest are essentially non-conducting relative to the liquid). Stage C represents the clear liquid with the solid-liquid interface below the bottom ring. Linear regression is used to fit the data in the three stages. From the interception of A & B and B & C (t_2-t_1) is obtained. The settling velocity is then calculated by dividing the distance between the electrodes (8.3 cm) by the time.

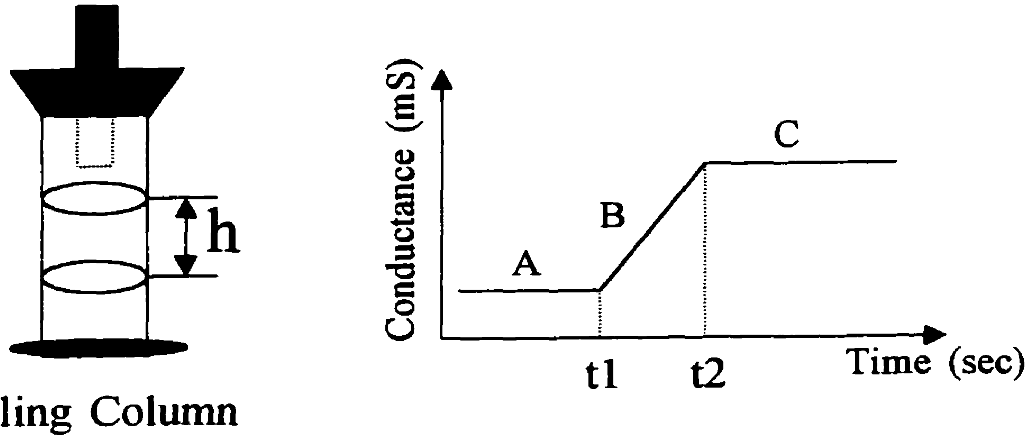

Figure 3.10. Data readout from Settling Experiment.

3.5 References

1. Israelachvili, J. N., Adams, G. E., Measurement of Forces between Two Mica Surfaces in Aqueous Electrolyte Solutions in the Range 0-100 nm, Journal of the Chemical Society, Faraday Transactions I, 74, 1978, pp975-1001.
2. Parker, J. L., Christenson, H. K., Ninham, B. W., Device for Measuring the Force and Separation between Two Surfaces Down to Molecular Separations, Review of Scientific Instruments, 60, 1989, pp3135-3138.
3. Binnig, G., Rohrer, H., Scanning Tunnelling Microscopy, Helvetica Physica Acta, 1982, 55, pp726-735.
4. Binnig, G., Quate, C., Gerber, G., Atomic Force Microscope, Physical Review Letters, 1986,

56, pp930-933.

5. Martin, Y., Williams, C., Wickramasinghe, H. K, Atomic Force Microscope - Force mapping and Profiling on a Sub 100 - AA Scale, Journal of Applied Physics, 61, 1987, pp4723-4729.
6. Burnham, N. A., Dominguez, D. D., Mowery, R. L., Colton, R. J., Probing the Surface Forces of Monolayer Films with an Atomic Force Microscope, Physical Review Letters, 64, 1990, pp1931-1934.
7. Weisenhorn, A. L., Hansma, P. K., Albrecht, T. R., Quate, C. F., Forces in Atomic Force Microscopy in Air and Water, Applied Physics Letters, 54, 1989, pp2651-2653.
8. Butt, H., Measuring Electrostatic, van der Waals, and Hydration Forces in Electrolyte Solutions with an Atomic Force Microscope, Biophysical Journal, 60, 1991, pp1438-1444.
9. Ducker, W. A., Senden, T. J., and Pashley, R. M., Nature, Direct Measurement of Colloidal Forces using an Atomic Force Microscope, 353, 1991, pp239-241.
10. Ducker, W. A., Senden, T. J., and Pashley, R. M., Measurement of Forces in Liquids Using a Force Microscope, Langmuir, 8, 1992, pp1831-1836.

CHAPTER 4

EXPERIMENTAL PROCEDURES

4.1 Chemical Composition of Minerals

The chemical composition of the minerals was determined using atomic adsorption spectrophotometry (AA).

Table 4.1 - Chemical Composition of Minerals used in Experiments

Mineral	% Wt. of element			
	Fe	Cu	Pb	Zn
Sphalerite, Sp*	0.22	0	0.08	63
Sphalerite, Sp	0.18	0.05	0.04	64
Pyrite, Py	45.64	0.04	0.01	0.01
Galena, Ga	0	0	85.60	0.03

*Used for atomic force microscopy work.

4.2 Size Distribution of Minerals

The size distribution of sphalerite and silica were determined using a particle size analyser (Micromeritics Instrument Corporation, model 5000D). The results are shown in appendix A.

4.3 Electrokinetic and Settling Study of Mixed Sulphide Minerals

4.3.1 Sample Preparation

Samples of pyrite, galena and sphalerite were purchased from Ward's Natural Science Establishment. The minerals were dry-pulverized and screened to obtain -38 and +106-150 µm size fractions which were stored in a freezer at -4 °C until needed.

4.3.2 Zeta-Potential

When two minerals were mixed different sizes were used to facilitate subsequent separation for analysis. Prior to mixing the coarse was ultrasonicated in distilled water to remove any adhering fines which may otherwise interfere with the measurements. The procedure involved mixing coarse and fine particles (using a mixer with a teflon coated impeller) for five minutes at a given set of conditions (pH etc). The suspension was allowed to settle and a sample of the remaining suspension of fine mineral (25 mL) was taken using a syringe for zeta-potential measurements (measured using the Laser-Zee meter). Settling was for 5 minutes except in the case of fine galena with coarse sphalerite or pyrite, when only 15 seconds was used because galena settled quickly. Blank tests indicated that few particles of the coarse mineral remained in the suspension after settling. The experimental conditions are summarized in Table 2.

In order to investigate which ions were responsible for the changes in zeta-potential of the fine mineral in the presence of the coarse mineral, the fine mineral was conditioned singly in the presence of the ions which were thought to cause the change in zeta-potential. Zinc(II) ($ZnCl_2$), Pb^{2-} ($PbCl_2$) and SO_4^{2-} (Na_2SO_4) ions were added to the single mineral suspensions and the same conditions as in Table 2 were used.

Table 4.2 - Mineral Mixing Conditions.

Minerals Mixed in 500 mL 1 X 10^{-3} M KCl		Conditioning Time (minutes)	Settling Time (minutes)
Fine (-38 µm)	Coarse (+106-150 µm)		
Pyrite, 0.75g	Sphalerite, 2.0 g	5	5
Pyrite, 0.75g	Galena, 2.0 g	5	5
Sphalerite, 0.75 g	Pyrite, 2.0 g	5	5
Sphalerite, 5.0 g	Galena, 6.0 g	5	5
Galena, 5.0 g	Pyrite, 6.0 g	5	1/4
Galena, 5.0 g	Sphalerite, 6.0 g	5	1/4

The suspensions were prepared using Millipore water and all the measurements were conducted at room temperature (ca. 25 °C) and typically took approximately one minute. The pH of the suspension was adjusted using dilute HCl and NaOH solutions. Repeat tests showed a precision of ±3 mV, and the results reported in this thesis are the average of the readings from at least two independent experiments.

To explore mineral interactions and to try to distinguish between contaminants transferred via solution from those transferred by direct contact, two further experiments were conducted. In the first, coarse pyrite (+106-150 µm) was conditioned with fine silica (<10 µm) for 5 minutes and then after 5 minutes of settling, the zeta-potential of silica was measured. In the second, two grams of coarse galena (+106-150 µm) was mixed in 500 mL 10^{-3} M KCl solution for 5 minutes at pH 9.5, the supernatant was removed and 0.75 grams of fine pyrite (-38 µm) was conditioned in this supernatant for 5 minutes at the same pH.

4.3.3 Settling

In the settling experiments for the mixed minerals (pyrite-sphalerite, pyrite-galena, sphalerite-galena), the solids content was 2% v/v for all experiments. The solids were suspended by a rhythmic, end-over-end rotation of the cylinder. After complete mixing had been obtained as judged from a constant conductance of the slurry, the cylinder was placed vertically to allow the solids to settle and data acquisition was started. Data were saved for later analysis [1,2].

4.4 Experimental Procedures for Sphalerite-Silica System

4.4.1 Sample Preparation

Samples of sphalerite were purchased from Ward's Natural Science Establishment (same as section 4.3.1). The minerals were dry-pulverized and screened to obtain -38 μm size fraction. Fine silica (<30 μm) was purchased from U. S. Silica. Coarse silica was purchased from Daubois Inc. (+75-106 μm) and was prepared by dry screening and leaching in warm 23 % nitric acid solution for one hour. The silica was then washed with distilled water till the pH of the solution approached natural pH.

4.4.2 Zeta-Potential

The zeta-potential of silica and sphalerite were measured individually. Silica (0.25 g) (<30 μm) was conditioned in 350 ml 1 x 10^{-3} M KCL and 0.5 g of sphalerite in 500 ml 1 x 10^{-3} M KCl and the zeta-potential was measured as a of pH using the Lazer-Zee Meter.

In the presence of Ca^{2+} (0.05 g Ca^{2+}/g solids), minerals of different size were mixed to facilitate subsequent separation. Prior to mixing, the coarse sphalerite was ultrasonicated in 100 % ethanol to remove any adhering fines. The procedure involved mixing coarse and fine particles for five minutes (using a mixer with a teflon coated impeller) at a given pH.

The suspension was allowed to settle for 5 minutes and a sample of the remaining suspension of fine mineral (25 ml) was taken using a syringe for zeta-potential measurements. Blank tests indicated that few particles of the coarse mineral remained in the suspension after settling. The zeta-potential (at the conditioning pH) was measured using the Lazer-Zee Meter. The experimental conditions are summarized in Table 4.3.

Table 4.3 - Mineral Mixing Conditions for the Sphalerite-Silica System in the Presence of Calcium Ions

Minerals Mixed in 500 ml 1 X 10^{-3} M KCL			Conditioning Time (minutes)	Settling Time (minutes)
Fine (-30 μm)	Fine (-38 μm)	Coarse (+75-106 μm)		
Silica, 0.25 g		Sp, 5 g	5	5
	Sp, 0.4 g	Silica, 5 g	5	5

The suspensions were prepared using Millipore water and all the measurements were conducted at room temperature (ca. 25 °C). The pH of the suspension was adjusted using dilute HCl and NaOH solutions. Repeat tests showed a precision of ±3 mV, and the results reported in this communication are the average of the readings from at least two independent experiments.

To explore mineral interaction and to try to distinguish if contaminants are transferred via solution or by direct contact, two further experiments were conducted. In the first, 5 grams of coarse sphalerite (+75 - 106 μm) was conditioned with 0.25 grams of fine silica (<30 μm) for 5 minutes and, after 1 minute of settling, the zeta-potential of silica was measured. In the second, 10 grams of coarse sphalerite (+106 - 150 μm) was conditioned with two grams of fine silica (<30 μm) for 5 minutes. Then, after 5 minutes of settling, the remaining silica slurry was decanted and allowed to settle for two days, the remaining clear water was decanted and the silica was allowed to dry. X-ray Photoelectron Spectroscopy (XPS) analysis was performed on the silica.

4.4.3 Settling

For the settling experiments on sphalerite, silica and sphalerite-silica slurries, 2.5% v/v, 3.0% v/v and 4.5% v/v solids were used, respectively (chapter 6). In the automated settling apparatus, in order to detect the change in conductivity with precision, a minimum of 2 %v/v was required. In a slurry of two components, at least 2 %v/v of each component has to be used if the settling of the one in the background of the other is to be detected. The conditioning procedure is the same as for the mixed minerals (section 4.3.3).

4.4.4 Atomic Force Microscopy

4.4.4.1 *Chemicals*

Sodium hydroxide ($NaOH*H_2O$) 99.996% pure was used to modify the pH. Calcium Chloride ($CaCl_2*5H_2O$), was 99.9965% pure (used for silica-silica-calcium interactions). Potassium chloride, ultra dry, (oxygen<300 ppm) 99.998% (metal basis) was used as supporting electrolyte.

4.4.4.2 *Sample Preparation*

Flat silica surfaces were prepared from polished silicon wafers. These wafers were oxidized at 920 °C in purified oxygen to produce SiO_2 [3].

For silica-silica interactions, a silica plate (approximately 1 cm x 1 cm) was attached to a steel disk with an epoxy resin. The steel disk was placed on a heating stage at a temperature above the melting point of the glue, then the epoxy resin was placed on the disk (was allowed to melt) followed by the silica plate. The glue solidified upon removal from the hot plate. For sphalerite-silica interactions, mica was glued on the disk plate using the epoxy resin and sphalerite was glued on the mica using a Master Bond Polymer EP2LV glue.

To avoid particulate contamination, surfaces were handled and loaded into the AFM in a laminar flow cabinet. The equipment in contact with solutions was washed with distilled ethanol and blown dry with ultra high pure nitrogen (99.99999% pure).

4.4.4.3 *Cleaning Procedures*

All glassware was soaked in a mixture containing 10% NaOH (approximately 95% pure), water (10-15 megaohm-cm, <30 ppm dissolved organics) and 100% pure ethanol for about 20 minutes. Then the glassware was washed thoroughly with water (10-15 megaohm-cm, <30 ppm dissolved organics) and Millipore water (18 megaohm-cm). The fluid cell and tweezers were soaked in chloroform and dried using ultra high pure nitrogen (99.99999%) prior to use.

4.4.4.4 *Colloid Probe Preparation*

The colloid probes were prepared by attaching a silica sphere to a microfabricated AFM cantilever. The cantilevers were standard V-shaped AFM single cantilever springs manufactured by Digital Instruments (Santa Barbara, CA).

The colloid particles were attached to the cantilevers with a Master Bond Polymer System EP2LV glue. A thin carbon fibre attached to a three-dimensional translation stage was used to position the resin near the apex of the cantilever. Care was taken to avoid coating the reflective gold side of the cantilever. Another clean wire was used to position a colloid particle on the cantilever, then the glue was allowed to dry for at least 24 hours.

Prior to each experiment, the colloid probe was rinsed with ethanol (100% pure) then blown dried with ultra high pure nitrogen and was placed under a UV lamp for approximately one hour.

Figure 4.1 shows SEM images of the silica sphere.

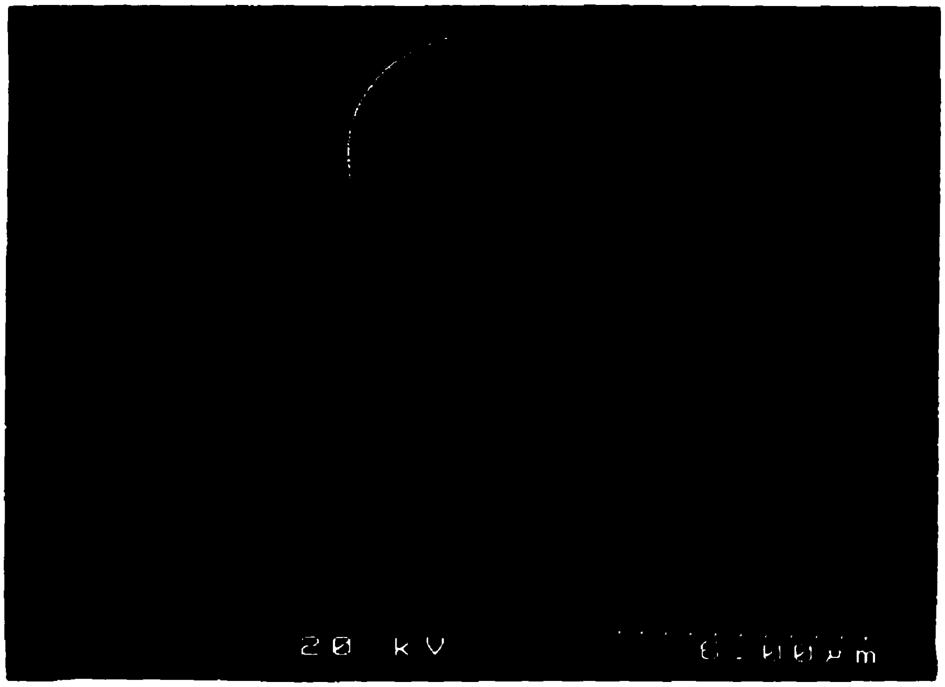

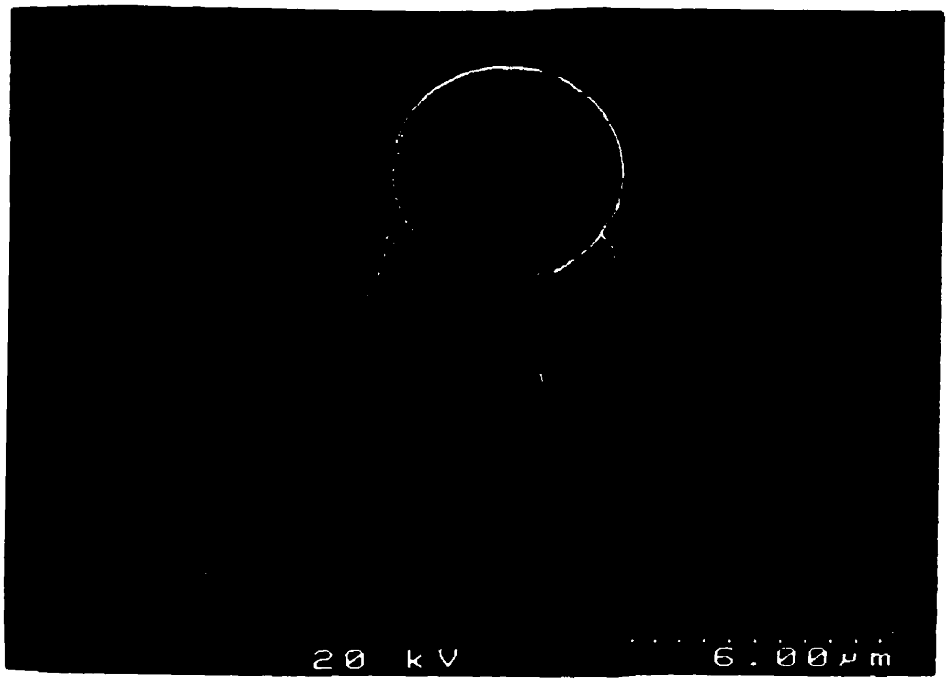

Figure 4.1. SEM Image of a Silica Sphere (Top) used in Silica-Silica Interactions, (Bottom) used in Sphalerite-Silica Interactions.

4.5 Colour Analysis

Images of the settling cylinder contents, taken with a 35 mm Canon T70 camera or Kodak DC40 digital camera, were scanned (Microtek ScanMaker) and processed using Photoimpact SE software. The colour intensity (red, blue, green) was measured at the top, middle and bottom of the cell (Figure 4.2) using Paint Shop Pro 4.

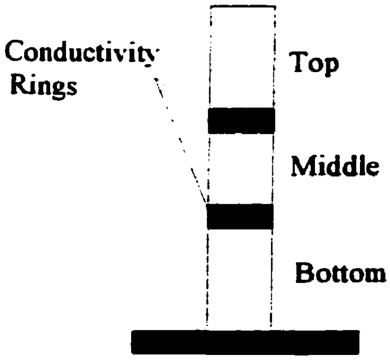

Figure 4.2. Settling Cylinder

4.6 References

1. Vergouw, J. M., DiFeo, A., and Finch, J. A., An Agglomeration Study of Sulphide Minerals Using Zeta-Potential and Settling Rate. Part I: Pyrite and Galena, Minerals Engineering, 11(2), 1998, pp159-169.
2. Vergouw, J. M., DiFeo, A., and Finch, J. A., An Agglomeration Study of Sulphide Minerals Using Zeta-Potential and Settling Rate. Part II: Sphalerite/Pyrite and Sphalerite/Galena, Minerals Engineering, 11(7), 1998, pp605-614.
3. Ducker, W. A., Senden, T. J., and Pashley, R. M., Measurement of Forces in Liquids Using a Force Microscope, Langmuir, 8, 1992, pp1831-1836.

CHAPTER 5

ELECTROKINETIC AND SETTLING STUDY OF MIXED SULPHIDE MINERALS

5.1 Electrokinetic Study of Mixed Mineral Systems

Pyrite: The zeta-potential of pyrite as a function of pH is shown in Figure 5.1a. An isoelectric point (i.e.p.) of ca. pH 6 (i.e.,$pH_{i.e.p.}$ 6) was obtained for pyrite alone. A similar i.e.p. value, pH 6.2-6.4, was reported by Fuerstenau et al. [1] and by Gaudin and Sun [2], although Fornasiero et al. [3] reported a significantly lower value (ca. pH 1.2). The latter attributed the variations in i.e.p. among researchers to different degrees of mineral oxidation: the more oxidized the pyrite, the higher the i.e.p.. The pyrite used in this study appears to be oxidized to a moderate degree.

Figure 5.1a shows that contact with sphalerite and galena had a minor effect on pyrite zeta-potential except above pH 6-8, where an increase in (i.e., less negative) zeta-potential was apparent. In galena supernatant, no significant effect was found at pH 9.5 (Figure 5.1a).

The zeta-potential of pyrite was measured in the presence of Zn ions and/or SO_4^{2-} ions. The effect was minor at 3 ppm Zn^{2+} with or without 4 ppm SO_4^{2-} (Figure 5.1b) although the zeta-potential generally increased above pH 6-8. However, with 95 ppm SO_4^{2-} below pH 8 the zeta-potential decreased (was less positive) significantly (from +10 mV to -10 mV at pH 4, for example). This suggests specific adsorption of SO_4^{2-} ions.

The pyrite-sphalerite results in Figure 5.1a, by reference to the results in Figure 5.1b, appear to indicate a modest contamination by predominantly cationic Zn species compared to anionic sulphoxy species. The presence of significant levels of SO_4^{2-} apparently can be identified by a decrease in zeta-potential below pH 8.

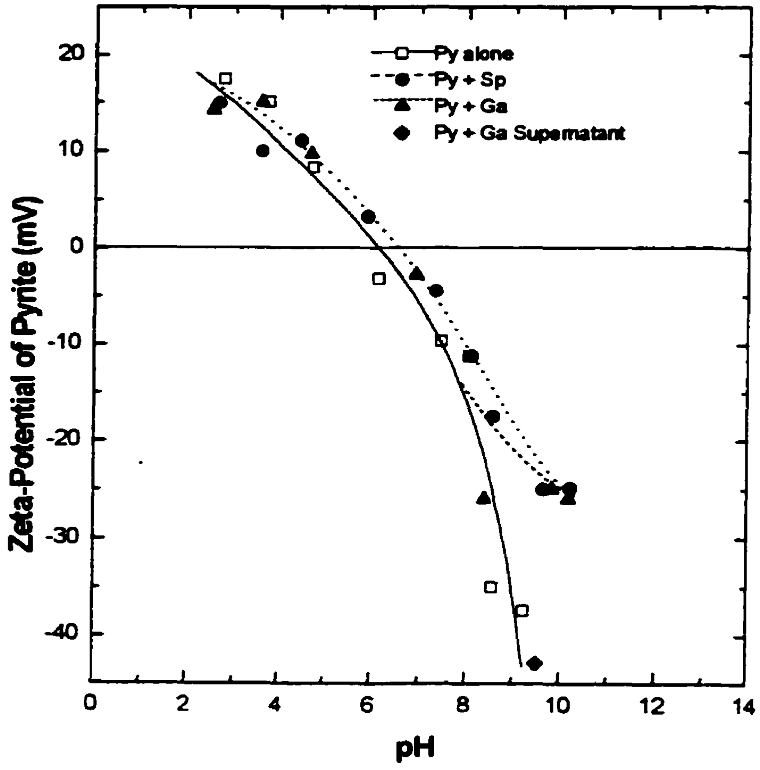

Figure 5.1a. Zeta-potential of Pyrite as a Function of pH: Alone, after mixing with sphalerite, and with Galena.

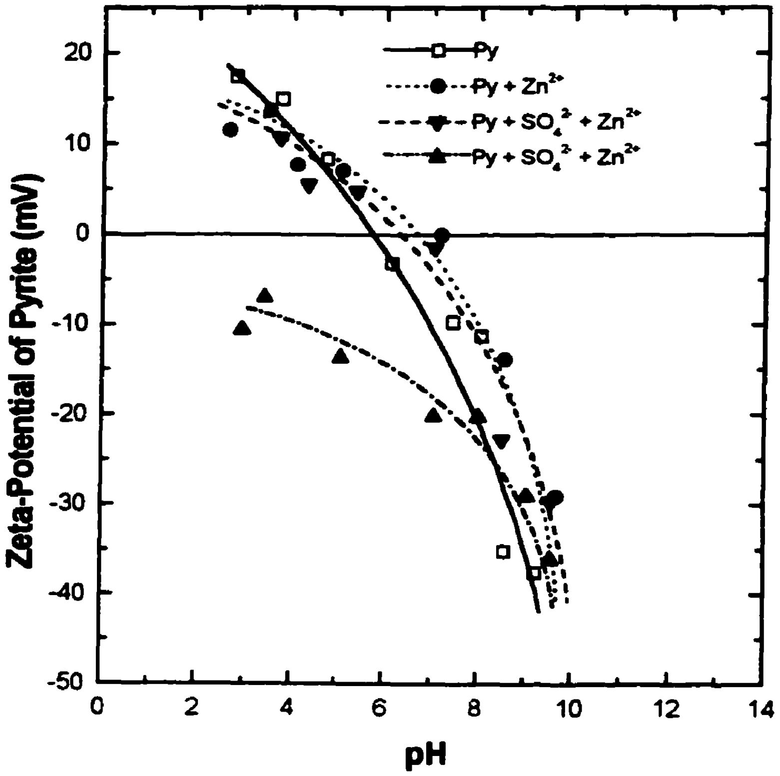

Figure 5.1b. Zeta-Potential of Pyrite as a Function of pH: Alone, in the Presence of 3 ppm Zn^{2+}, 4 ppm SO^{2-}_4 and 3 ppm Zn^{2-}, 95 ppm SO^{2-}_4 and 3 ppm Zn^{2-}.

The zeta-potential decreased slightly below pH 8. This may indicate a predominance of SO_4^{2-} over Pb^{2-} ions on the pyrite surface at acidic pH (Figure 5.1c).

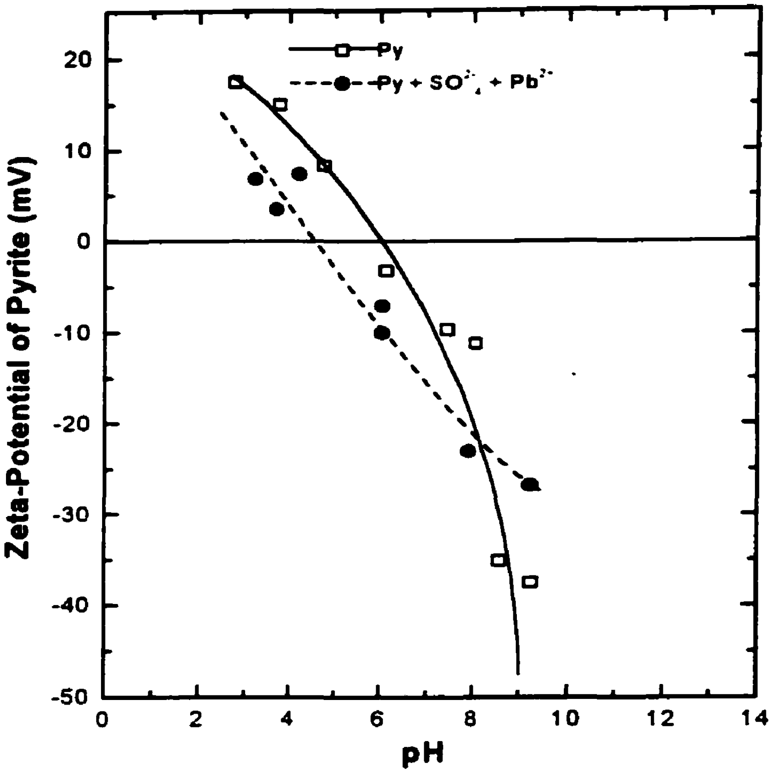

Figure 5.1c. Zeta-Potential of Pyrite as a Function of pH: Alone, in the Presence of 4 ppm SO^{2-}_4 and 9 ppm Pb^{2+}.

Sphalerite: The iso-electric point ($pH_{i.e.p.}$) of sphalerite alone was between 2 and 3 (Figure 5.2a). This value agrees with that reported by Gaudin and Sun [2] and Zhang et al. [4]. An effect of conditioning with pyrite and galena is evident. With pyrite, above pH 8 the zeta-potential decreased (became more negative) while below this pH, it increased. The decrease in zeta-potential above pH 8 correlates with the increase in pyrite zeta-potential after mixing with sphalerite (Figure 5.1a). This tends to support a mechanism of transfer of cationic Zn species from sphalerite to pyrite.

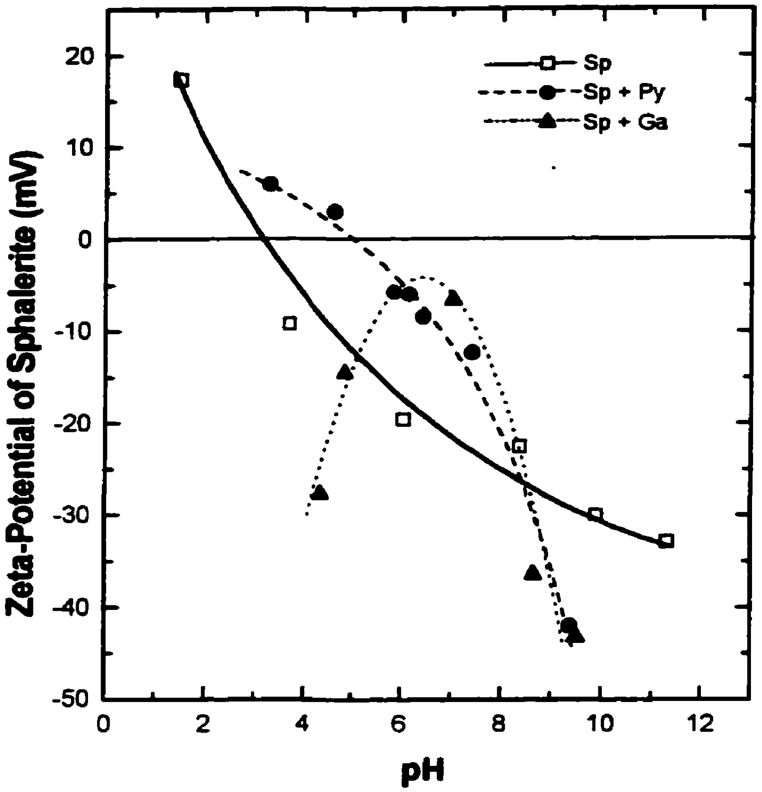

Figure 5.2a. Zeta-Potential of sphalerite (Sp) as a Function of pH: Alone, after mixing with Pyrite (Py), and Galena (Ga).

Conditioning sphalerite with galena above ca. pH 5 showed a similar effect as for conditioning with pyrite. Below pH 5, however, the zeta-potential in the presence of galena reduced significantly. The zeta-potential was similar for sphalerite in the presence of SO_4^{2-} and Pb^{2+} (and Zn^{2+}) ions (Figure 5.2b) suggesting these are the species responsible for the changes. The reduction in zeta-potential below that of sphalerite alone at <pH 5 suggests specific adsorption of sulphoxy species (like SO_4^{2-}), as noted in relation to pyrite.

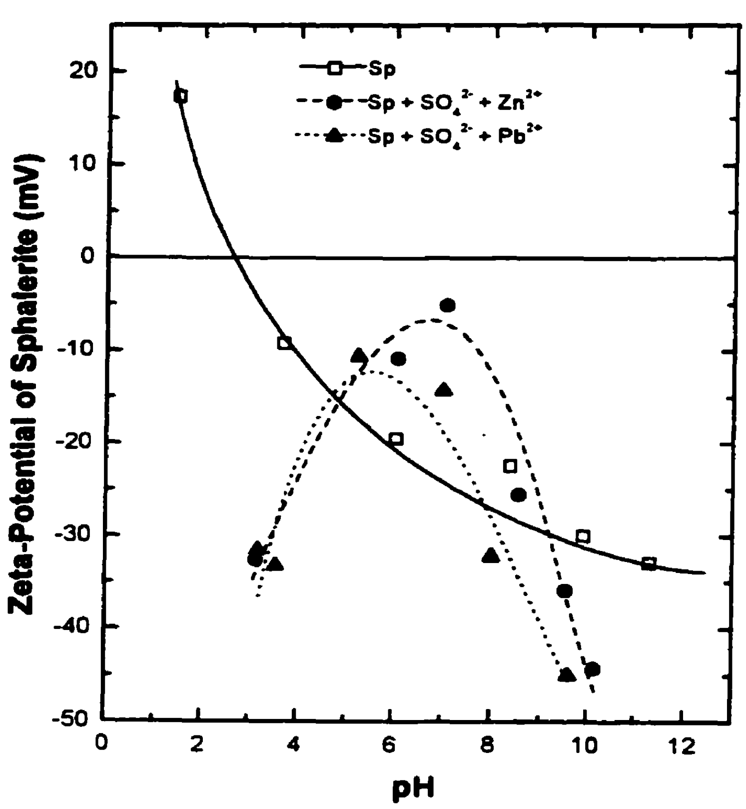

Figure 5.2b. Zeta-Potential vs pH for Sphalerite: Alone, in the Presence of 4 ppm SO^{2-}_4 and 3 ppm Zn^{2+}, 4 ppm SO^{2-}_4 and 9 ppm Pb^{2+}.

Galena: For galena alone the i.e.p. was ca. pH 3 (Figure 5.3a). This value agrees with reported values, for example, Bull et al. [5] determined $pH_{i.e.p.}$ 2.4 and Gaudin and Sun [2] $pH_{i.e.p}$ 3. The study by Neville and Hunter [6], like that of Fornasiero et al [8] for pyrite, demonstrated an effect of aging (essentially oxidation).

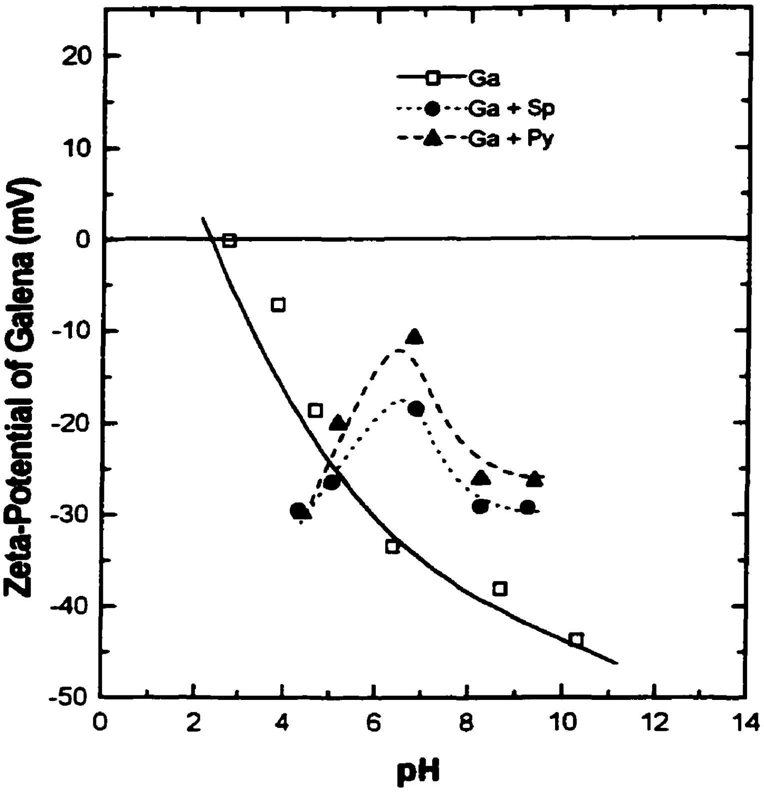

Figure 5.3a. Zeta-Potential of Galena as a Function of pH: Alone, after mixing with Sphalerite, and Pyrite.

Figure 5.3a shows the effect of mixing with pyrite and sphalerite. Below pH 5, a significant decrease in zeta-potential occurred while a substantial increase was observed above pH 5. To elucidate the effect of possible ionic species derived from sphalerite, measurements were conducted in the presence of 3 ppm Zn^{2+} (low enough to avoid zinc precipitation) and 4 ppm SO_4^{2-} (same amount as zinc on a mole basis). As shown (Figure 5.3b), the electrokinetics were similar to conditioning with sphalerite.

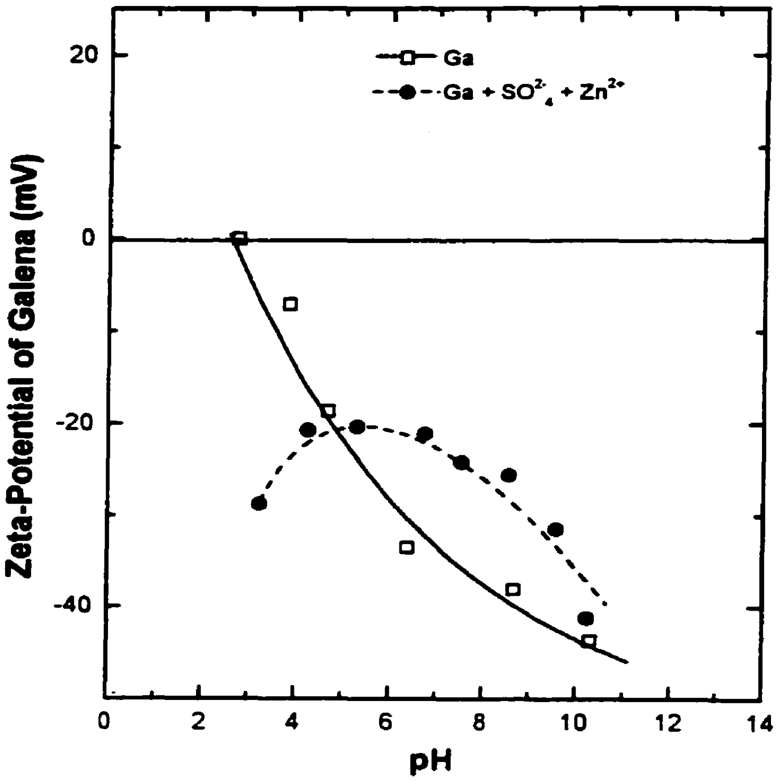

Figure 5.3b. Zeta-Potential of Galena vs pH: Alone, in the Presence of 4 ppm SO^{2-}_4 and 3 ppm Zn^{2+}.

Silica: Silica, after mixing with pyrite suffered little change in zeta-potential (Figure 5.4). This suggests that no significant quantities of ions were released or transferred.

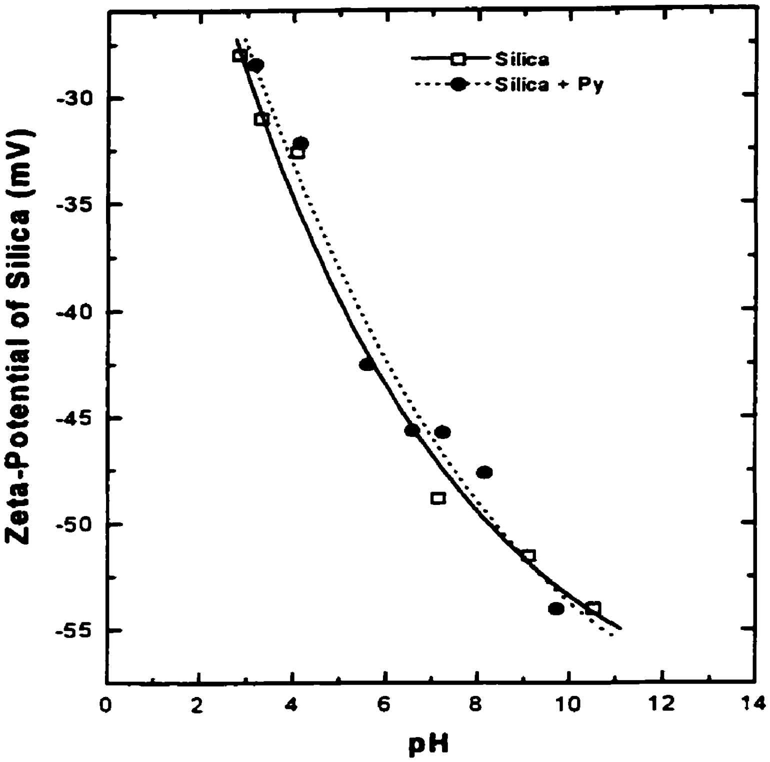

Figure 5.4. Zeta-Potential of Silica as a Function of pH: Alone, and after mixing with Pyrite.

The zeta-potential results demonstrate significant interactions can occur between sulphide minerals. One possible driving force for interaction is galvanic. The mixtures involving pyrite give the most clear evidence of this. Among the three sulphide minerals studied here, pyrite has the highest rest potential. Therefore, when pyrite is in contact with sphalerite and galena, it acts as a cathode drawing electrons from the second mineral. The second mineral is oxidized, forming various ionic metal and sulphur-oxygen species. These oxidation products may be mobile, either transferring directly on contact between mineral surfaces or going via the solution. The galvanic couple is completed by oxygen reduction to OH^- ions on the surface of pyrite. This introduces the possibility of iron oxyhydroxy species being formed, which may also be mobile. The end result of transfer of any of these species is a possible change in the zeta-potential of the contacted minerals, as observed in Figures 5.1, 5.2 and 5.3.

The changes in zeta-potential can be linked to specific species. In the case of the pyrite-sphalerite couple, cationic zinc species appear to dominate at alkaline pH, transferring from sphalerite to pyrite. In neutral and acidic environments, the pyrite zeta-potential was not affected by contact with sphalerite. This should not be taken to mean that galvanic effects are negligible over this pH range, but rather it could reflect that between pH 6 and 8 pyrite is only weakly negatively charged and attraction for cationic species is correspondingly weak. Also around neutral pH, cations are in the strongly hydrated ionic Zn^{2+} form which is bulky and not so readily adsorbed compared to the less strongly hydrated monohydroxy species ($Zn(OH)^+$) formed at alkaline pH [7]. Both factors will hinder adsorption of cationic species which may explain why the zeta-potential remained unchanged over this pH region.

Below pH 6, pyrite carries a positive surface charge. Any decrease in zeta-potential would suggest adsorption of anionic sulphoxy species released as a result of interaction with sphalerite. No decrease was observed, suggesting that the anionic species are either less mobile or insufficient number were produced to affect the zeta-potential of pyrite. With sufficient SO_4^{2-}, the zeta-potential does decrease in the acidic pH range (Figure 5.1b). For sphalerite below pH 8.5, cationic species dominate as the zeta-potential increased. This could mean that zinc oxidation species either preferentially remain on the surface compared to sulphoxy species or are re-adsorbed preferentially. Alternatively, iron species derived from the pyrite may be responsible.

The pyrite-galena couple has many similarities to the pyrite-sphalerite couple. Cationic lead species appear to dominate at alkaline pH, transferring from galena to pyrite, resulting in an increase in zeta-potential of pyrite. However, the zeta-potential of galena also increased, whereas for sphalerite it decreased perhaps because Zn^{2+} migrated from the sphalerite to pyrite resulting in a metal deficient sphalerite surface.

Below pH 5 there is a decrease in zeta-potential of galena, attributed to the presence of sulphoxy species resulting from galena oxidation (Figure 5.3b). Above this pH, cationic lead species appear to dominate and increase the zeta-potential (Figures 5.3a & 5.3b) [8].

In the case of the galena-sphalerite couple, anionic sulphoxy species appear to dominate below pH 5 on both minerals (Figures 5.2a and 5.3a). In this pH range, galena may have a lower rest potential than sphalerite [9], and could be the source of the sulphoxy species. With sufficient SO_4^{2-} ions in solution, the zeta-potential decreased at pH <5 (Figures 5.2b & 5.3b). At pH>5 sphalerite may be the source of oxidation products. Between pH 5 and 8.5, cationic zinc species dominate resulting in an increase in zeta-potential (Figures 5.2a & 5.3a). Above pH 8.5 these cationic species appear to transfer from sphalerite to galena, resulting in an increase in zeta-potential of galena and a corresponding decrease in zeta-potential of sphalerite (Figures 5.2a & 5.3a).

The results generally support a galvanic interaction model, particularly in the mixtures involving pyrite. In those cases the second mineral (sphalerite or galena) is significantly affected, showing the presence of sulphoxy and metallic species depending on the pH.

Indirect support for the significance of galvanic effects is the lack of effect when they are absent. The zeta-potential of silica was not affected by the presence of pyrite (Figure 5.4), suggesting simple contact is not enough but that a driving force for ionic species production is required. Likewise the lack of effect of galena supernatant on pyrite (Figure 5.1a) implies actual contact is required to produce sufficient ions to have an effect.

The fact that sulphide mineral interactions affect the electrokinetics of the minerals has an impact on predicting conditions for homo- and heterocoagulation. The present work has demonstrated that the zeta-potential measurement technique developed here provides a technique to detect interactions between minerals in a mixed system. Zeta-potential measurements on mixed sulphide mineral systems should provide a better indication of the coagulation/dispersion conditions than measurements on single minerals.

5.2 Correlation of Zeta-Potential of Mixed Minerals with Settling Data.

The extent of particle agglomeration can be judged by the settling rate - the more agglomerated the sample the higher the rate. The settling data of Vergouw et al. [10,11], was used for the comparison. The zeta-potential of the minerals singly and after mixing was compared with the settling velocity of the mixture.

5.2.1 Pyrite and Galena

The settling results indicate agglomeration occurs over the pH range 4-7 (Figure 5.5). Up to pH ca. 6 the minerals have opposite charge, suggesting a heterocoagulation mechanism, while above this pH both minerals are negatively charged whether the mixed or single mineral data are considered. The mixed mineral results however, suggest the zeta potential for both minerals is close to zero in the pH range 5-7 (ca. -10 mV) which suggests homocoagulation could be the coagulation mechanism. If this is the case both homo- and heterocoagulation are promoted at the same time and the settling data are better interpreted by the mixed mineral zeta-potential results.

Outside the pH range 4-7 the conditions are (relatively) dispersing. At the higher end of the pH range this corresponds to both minerals becoming strongly negatively charged (whether the single or mixed results are considered).

Based on the evidence, therefore, a zeta potential approaching zero appears to be the more significant of the two agglomeration mechanism. One interpretation may be that while for two particles of opposite charge to come together is quite straightforward, subsequent particles must arrange themselves to accommodate the repulsion of the like-charged particles already present in the agglomerate. Various morphologies could be contemplated (e.g., chains of alternately charged particles) but it does pose an obstacle. Agglomeration due to particles having a charge close to zero - regardless of the actual mineral type - suffers no such barrier. The agglomerates, in principle, can grow as large as the hydrodynamic conditions in the vessel allow. The barrier is lessened if the particles are very different in size. The heterocoagulation of fine particles of one charge on large particles of opposite charge (i.e., slime coating) is well known. Presumably the fine like charged particles can distribute over the surface of the larger oppositely charged particle and retain a significant inter-particle distance.

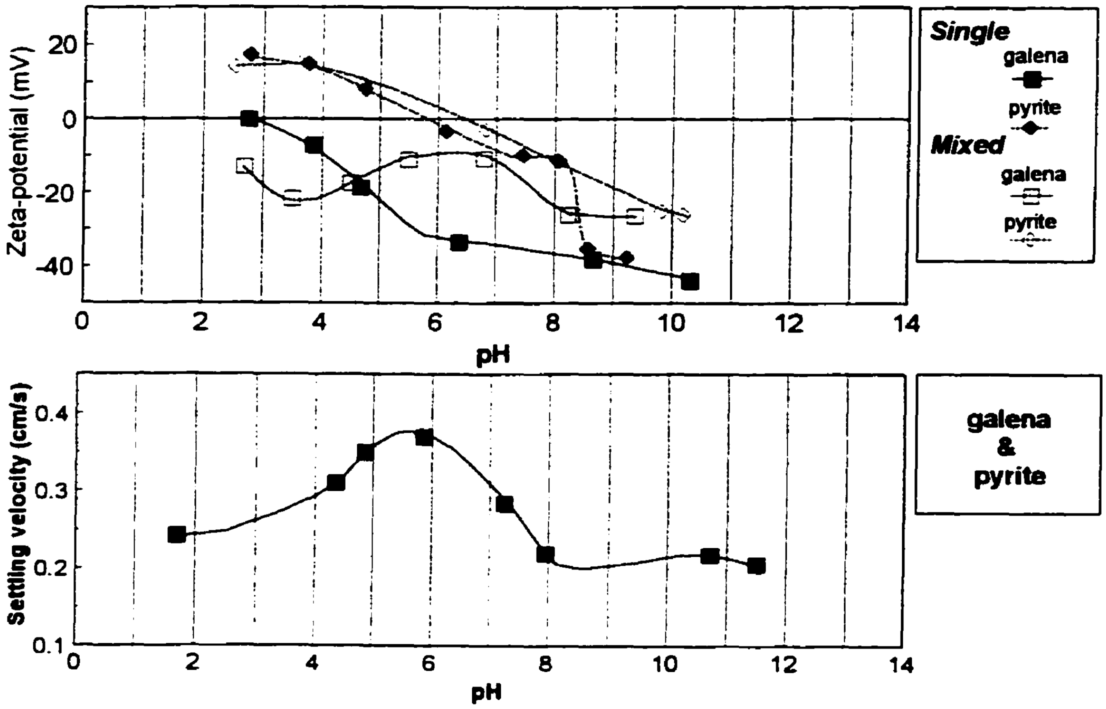

Figure 5.5. Comparison between Zeta-Potential and Settling Velocity of Galena and Pyrite as a Function of pH in the Absence of Metal Ions.

5.2.2 Sphalerite and Pyrite

The settling results (Figure 5.6) showed agglomeration was maximum around pH 5-6. This corresponds to a zeta-potential close to zero for of both minerals measured in the mixed mineral case.

Certainly the settling data do not correlate well with a heterocoagulation model based on the single mineral zeta-potential results, which imply maximum agglomeration should occur in the pH range 3-6 whereas there is strong dispersion at pH 3. The strong repulsion evident above pH 9 is predicted by both the single and mixed mineral zeta-potential data.

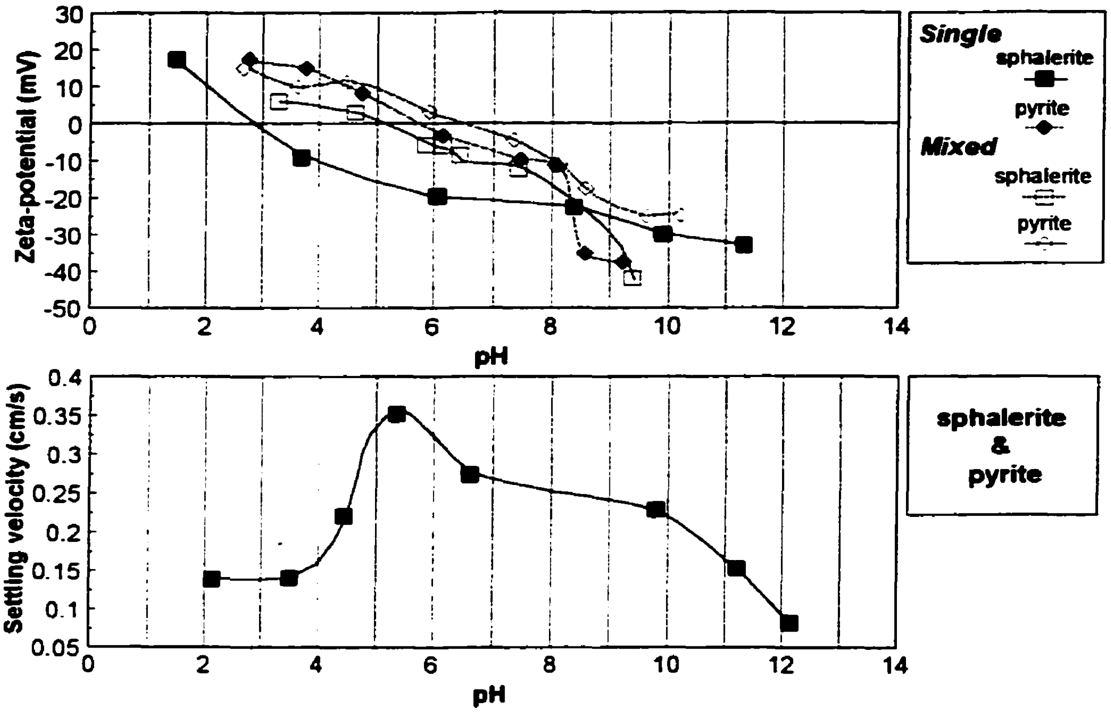

Figure 5.6. Comparison between Zeta-Potential and Settling Velocity of Sphalerite and Pyrite as a Function of pH in the Absence of Metal Ions

5.2.3 Sphalerite and Galena

The settling results (Figure 5.7) show agglomeration was maximum at approximately pH 2-3. The zeta-potential for both minerals in this pH range is around -10 mV according to the mixed case and about 0 for single minerals. This suggests that coagulation is due to the charge being close to zero, i.e., both homo- and heterocoagulation was occurring. This is consistent with the observations for pyrite-galena and sphalerite-pyrite. The system does not become strongly dispersed till above ca. pH 9 when the zeta-potential of both minerals (measured either way) is ca. -30 mV.

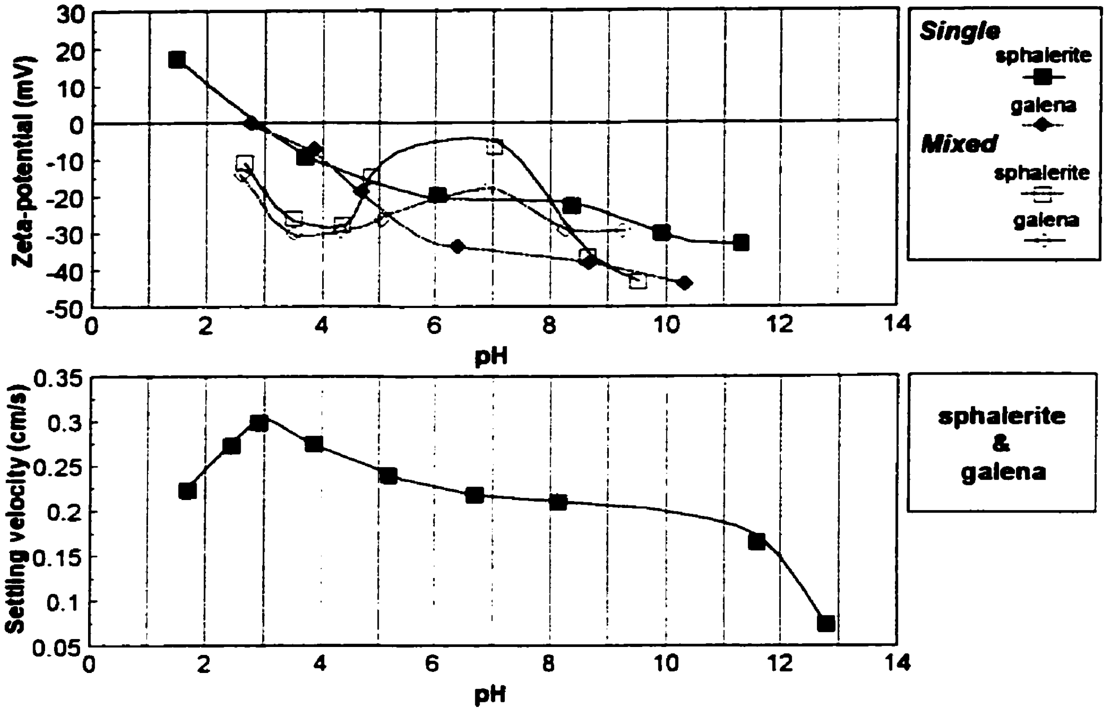

Figure 5.7. Comparison between Zeta-Potential and Settling Velocity of a Mixture of Sphalerite and Galena as a Function of pH in the Absence of Metal Ions.

5.3 Significance to Flotation

Galena is usually floated from pyrite (and other minerals) under moderately alkaline conditions. In the absence of metal ions, the evidence from this study shows that at this pH range the mineral particles are dispersing. Only if the minerals become exposed to near neutral environments is agglomeration a factor. Thus any conditioning or aeration stages ahead of flotation may want to consider this.

An observation which may play a role in flotation is that, at least for similar sized particles (as here), having opposite charge is not as significant as having a charge close to zero for promoting agglomeration. Conditions which lead to this, including the effect minerals have on each other and the effect of contaminant ions, may be detrimental to flotation.

5.4 Conclusions

5.4.1 Electrokinetic Study of Mixed Mineral Systems

The changes in zeta-potential were attributed to the relative affinity for the metallic and sulphoxy species released through galvanic interaction. When galvanic effects were absent, no changes in zeta-potential were found.

Mixtures of sulphide minerals cross contaminate each other, resulting in significant effects on the zeta-potential.

Pyrite was not strongly affected by galena and sphalerite, but the zeta-potential did tend to increase above pH 8.

Galena and sphalerite were significantly affected by the presence of a second sulphide showing evidence of sulphoxy (anionic) species and metallic (cationic) species at neutral and alkaline pH.

5.4.2 Correlation of Zeta-Potential of Mixed Minerals with Settling Data

Surface charge (zeta potential) and agglomeration (settling rate) were generally correlated for the galena-pyrite, sphalerite-galena and sphalerite-pyrite systems; agglomeration was promoted when the zeta-potential on both minerals in the pair was close to zero. Agglomeration was not promoted when the minerals were oppositely charged.

The pH giving maximum agglomeration in the mixture of galena and pyrite corresponded to both minerals having a zeta-potential close to zero. At low pH the minerals were oppositely charged but agglomeration was not promoted.

For sphalerite/pyrite and sphalerite/galena, the maximum in agglomeration occurred near the pH where both minerals were close to zero zeta-potential. This reinforces the same conclusion reached for the galena/pyrite system.

5.5 References

1. Fuerstenau, M. C., Kuhn, M. C., and Elgillani, D., Role of Dixanthogen in Xanthate Flotation of Pyrite, Transactions of the American Institute of Mining Engineers, 241, 1968, pp148-156.
2. Gaudin, A. M., and Sun, S. C., Correlation between Mineral Behaviour in Cataphoresis and in Flotation, Transactions of the American Institute of Mining Engineers, 169, 1946, pp347-367.
3. Fornasiero, D., Li, F., Ralston, J., and Smart, R. St. C., Oxidation of Galena Surfaces, Journal of Colloid and Interface Science, 164, 1994, pp333-344.
4. Zhang, Q., Xu, Z., and Finch, J. A., Surface Ionization and Complexation at the Sphalerite/Water Interface, Journal of Colloid and Interface Science, 169, 1995, pp414-421.
5. Bull, H. A., Ellefson, B. S., and Taylor, N. W., Electrokinetic Potentials and Mineral Flotation, The Journal of Physical Chemistry, 38, 1934, pp401-406.
6. Neville, P. C., and Hunter, R. J., The Control of Slime Coatings in Mineral Processing, Paper presented to 4th RACI Electrochemistry Conference, Adelaide, Australia, 1976.
7. Pugh, R. J., Surface Chemical Studies on Sulphide Suspensions, XVI International Mineral Congress, 1988, pp751-762.
8. Sui, C. C., Brienne, S. H. R., Rao, S. R., Xu, Z., and Finch, J. A., Metal Ion Production and Transfer between Sulphide Minerals, Minerals Engineering, 8(12), 1995, pp1523-1539.
9. Majima, H., How Oxidation Affects Selective Flotation of Complex Sulphide Ores, Canadian Metallurgical Quarterly, 8(3), 1969, pp269-273.
10. Vergouw, J. M., DiFeo, A., Xu, Z., and Finch, J. A., An Agglomeration Study of Sulphide Minerals using Zeta-Potential and Settling Rate. Part I: Pyrite and Galena, Minerals Engineering, 11(2), 1998, pp159-169.
11. Vergouw, J. M., DiFeo, A., Xu, Z., and Finch, J. A., An Agglomeration Study of Sulphide Minerals using Zeta-Potential and Settling Rate. Part II: Sphalerite/Pyrite and Sphalerite/Galena, Minerals Engineering, 11(7), 1998, pp605-614.

CHAPTER 6

INTERACTIONS IN THE SPHALERITE/SILICA SYSTEM

6.1 Introduction

Silica and silicate mineral impurities in zinc concentrates are a concern in the metallurgical processing by the roast-leach-electrowin process. During roasting, silicate minerals can be thermally altered to become partially soluble in the subsequent leaching step. If soluble silica exceeds 2.5 g/l in the acid leach solution, settling and filtering rates are affected and zinc loss to residue increases. Concentrates containing between 2 and 4 % silica can be subject to penalty charges. Therefore, reducing the silica impurities in these concentrates is important [1]. One possible source of contamination is through formation of sphalerite/silica agglomerates. This chapter examines sphalerite/silica interactions.

6.2 Correlation of Zeta-Potential of Sphalerite and Silica with Settling Data

6.2.1 No Metal Ions

6.2.1.1 *Sphalerite*

Figure 6.1 shows the zeta-potential and settling velocity results for sphalerite (in the absence of any added ions). There is homocoagulation of sphalerite at ca. pH 2 to 8.5 and dispersion above ca. pH 8.5. Homocoagulation of sphalerite, expected at ca. pH 3 as this is close to the i.e.p., is instead maximum at ca. pH 8.5 where the surface charge is strongly negative. Vergouw et al. [2] also found that the settling velocity increased with pH reaching a maximum at ca. pH 10 which did not correlate with the charge. Since agglomeration is not inferred by the surface charge, it suggests a hydrophobic force may exist. Subrahmanyam et al. [3] studying a natural sphalerite sample found contact angles from 75 to 90^0, indicating hydrophobicity which was attributed to a metal deficient sulfide (or sulfur-rich) surfaces. However, Subrahmanyan et al. [3] did not mention the pH at which the contact angle measurements were performed.

The surface chemistry of sphalerite remains a subject of debate. Muster and Prestidge [4] from a rheological study found that the maximum Bingham yield value (maximum agglomeration) occurred at the i.e.p (pH 7) of sphalerite. Muster et al. [5] performed a rheological study and surface force measurements (using atomic force microscopy) on synthetic sphalerite. They also observed that the greatest agglomeration (indicated by the highest shear stress) occurred at the iso-electric point ($pH_{i.e.p.}$ 7). (While the pH of maximum agglomeration correlates with the i.e.p in these cases, the i.e.p is high suggesting a well oxidised surface.) At pH 4 the shear stress was lower relative to pH 6 to 8, therefore, indicating the suspension was dispersed. However, at pH 4 atomic force microscopy indicated an attractive hydrophobic force. They attributed this lack of correlation to the difference in sample volume fraction between the two experimental techniques. In atomic force microscopy, the volume fraction is lower, therefore, oxidation of sphalerite will be higher leading to different surface properties.

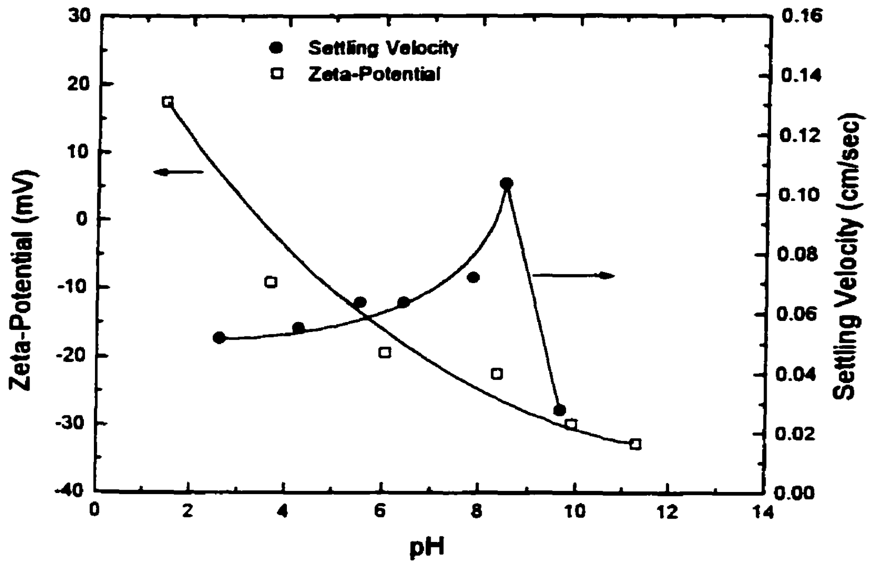

Figure 6.1. Comparison between Zeta-Potential and Settling Velocity of Sphalerite as a Function of pH in the Absence of Metal Ions.

6.2.1.2 *Silica*

Figure 6.2 illustrates the zeta-potential and settling velocity results for silica. Settling is virtually zero (i.e., system remains dispersed) over the whole pH range tested which corresponds to the strong negative charge over most of this range (> pH 4) causing electrostatic repulsion. In addition, silica is strongly hydrated which provides a further repulsive force. (The hydration forces accounts for the lack of agglomeration even at the i.e.p of silica [6]).

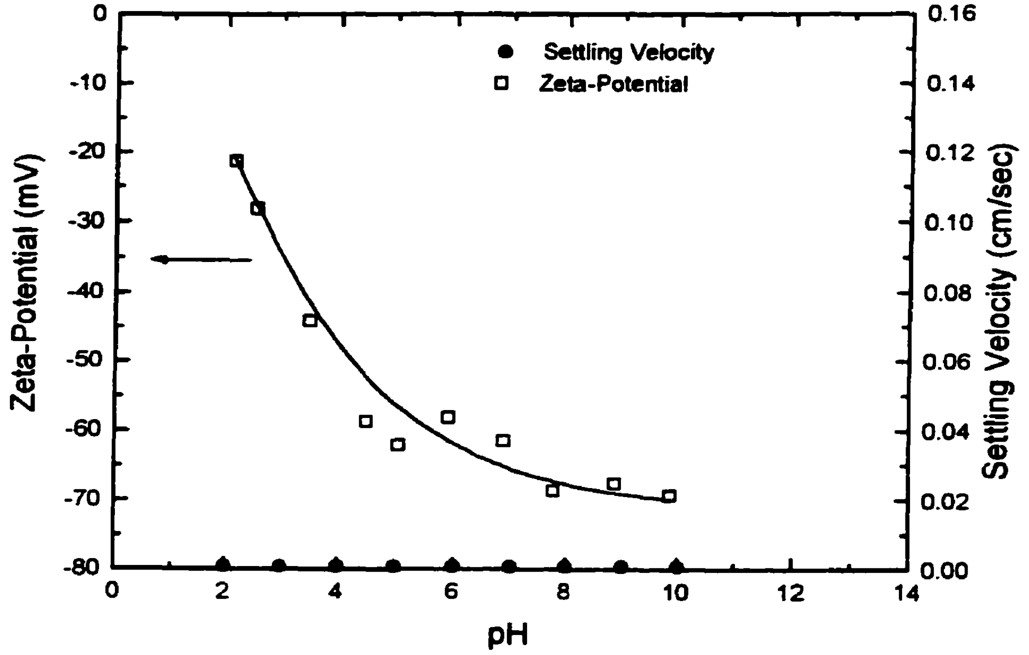

Figure 6.2. Comparison between Zeta-Potential and Settling Velocity of Silica as a Function of pH in the Absence of Metal Ions.

6.3 Correlation of Zeta-Potential of Sphalerite/Silica with Settling Data

6.3.1 No Metal Ions

Fine silica was conditioned with coarse sphalerite and the zeta-potential was measured as a function of pH (Figure 6.3). The zeta-potential is similar to the zeta-potential of silica conditioned alone, similar to the finding for silica and pyrite (Chapter 5).

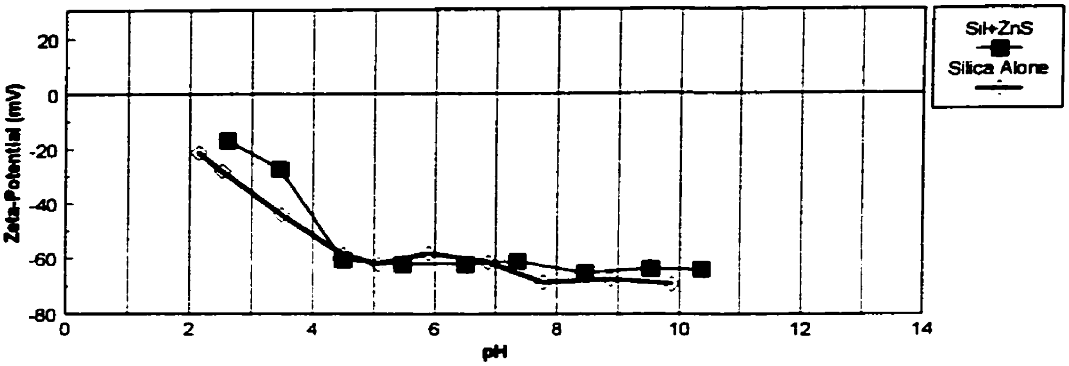

Figure 6.3. Zeta-Potential of Silica as a Function of pH: Alone and After Mixing with Sphalerite.

Figure 6.4 shows the zeta-potential and settling velocity results for the mixed minerals. At ca. pH 2 sphalerite settled and some silica remained in suspension signifying that sphalerite homocoagulated but did not heterocoagulate with silica. This is also supported by Figure 6.5 where a colour gradation down the cylinder is evident.

At ca. pH 3, there is some heterocoagulation (determined visually). The zeta-potential of sphalerite is almost zero at this pH so there may be a only weak repulsive force between sphalerite and silica (Figure 6.4).

From ca. pH 5.5 to 7.5 there is a high degree of heterocoagulation even though the zeta-potential of both silica and sphalerite is negative, and, therefore, electrostatic repulsion would be expected. To test if hydrophobic "contaminating" species were being transferred between the two minerals promoting heterocoagulation, XPS was performed on silica conditioned with sphalerite. No zinc or sulphur species were found on the silica surface indicating no transfer of contaminants. A combination of high charge on one mineral and a large difference in charge between the minerals could be responsible for heterocoagulation. Over the pH range 5.5 to 7.5, the zeta-potential of silica is highly negative. This can lead to a high quantity of positively charged ions in the diffuse layer. At the same time the difference in zeta-potential between silica and sphalerite is high, approximately 45 mV. (This is pursued further in Chapter 8.)

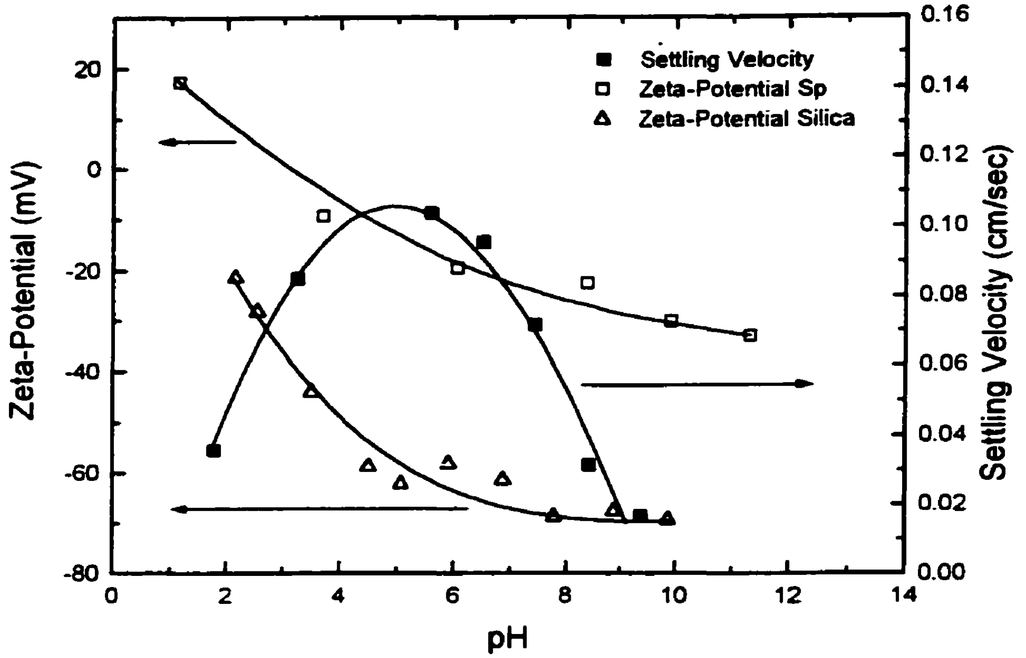

Figure 6.4. Comparison between Zeta-Potential and Settling Velocity of Sphalerite and Silica as a Function of pH in the Absence of Metal Ions.

At ca. pH 8.5, sphalerite settled while some silica remained in suspension, i.e., the sphalerite homocoagulated. Figure 6.5 shows a colour gradation down the cylinder signifying that some segregation of the phases has occurred.

At > ca. pH 9.5, sphalerite and silica are in a state of electrostatic repulsion and the settling velocity is correspondingly low. Figure 6.6 shows that there is no change in colour intensity vs distance from the top of the settling cylinder, which means that the system is dispersed and no phase separation occurs. At this pH, the dispersion corresponds to the result for sphalerite and silica alone (Figures 6.1 & 6.2).

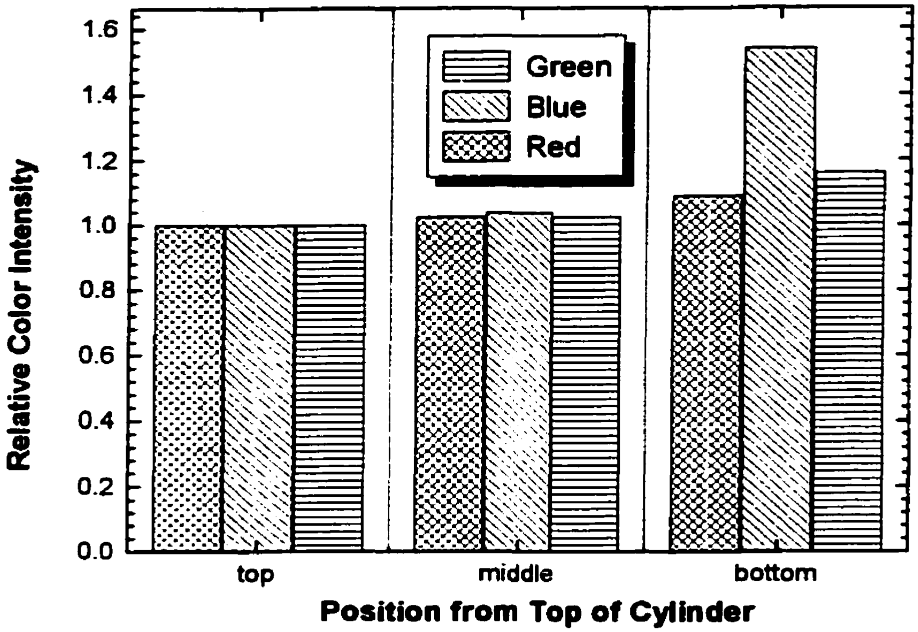

Figure 6.5. Sphalerite/Silica Mixture at ca. pH 8.5. Color Intensity is Relative to the Top Position of Settling Cylinder.

Muster and Prestidge [4] have performed a rheological study on a sphalerite/silica slurry. Prior to the measurements, sphalerite was conditioned for 2 hours at pH 10. They found the i.e.p. of sphalerite to be ca. pH 7 (implying an oxidized surface). The highest Bingham yield values (maximum heterocoagulation) occurred from ca. pH 4.5 to 7, and at pH 10 the slurry was dispersed. The rheology results are similar to the settling data presented here, but the surface properties (i.e.p.) appear to be quite different. Muster and Prestidge [4] found the i.e.p. and agglomeration data correlated which is not the case here. Either the interaction mechanism leading to agglomeration is different in the two cases (which seems unlikely) or the simple electrostatic model indicated in the Muster and Prestidge [4] work is not the true mechanism.

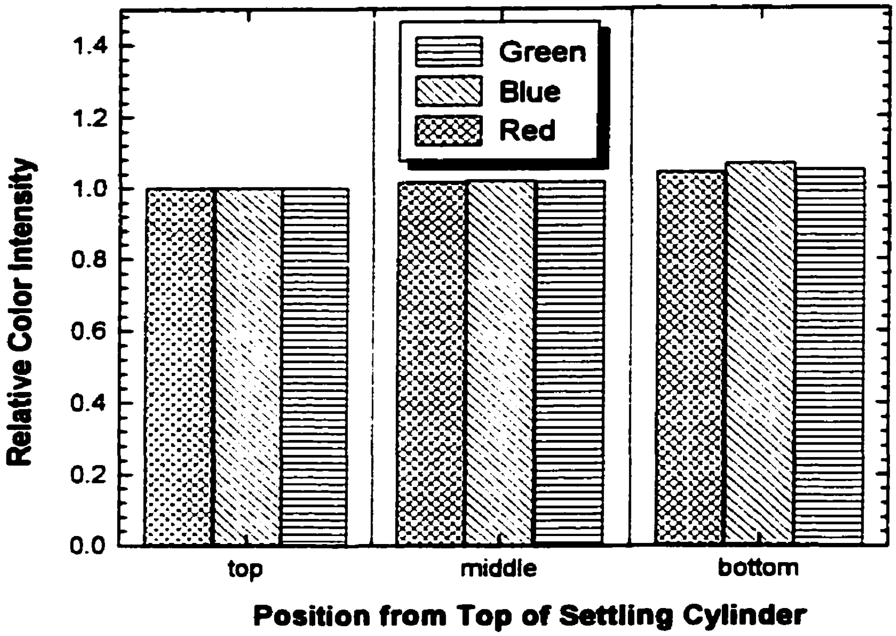

Figure 6.6. Sphalerite/Silica Mixture at ca. pH 9.5. Color Intensity is Relative to the Top Position of Settling Cylinder.

The relative conductivity (conductivity at time t/conductivity at time 0) can be used as an indication of whether the slurry was heterocoagulated, dispersed or had one component left in suspension (Figure 6.7). The curve at pH 9.3 represents the slurry in a state of dispersion because the relative conductivity remains close to one. The curve at pH 6.4 represents the slurry when heterocoagulated; at about 150 seconds, the relative conductivity of the system was equal to that for water alone indicating all solids have settled. The curve at pH 8.7 represents the slurry where sphalerite homocoagulated and some silica remained in suspension. This curve lies in between that for pH 6.4 and 9.3 thus indicating the relative conductivity is between that of water and of the dispersion, therefore, implying a component (or part of a component at least) is left in suspension.

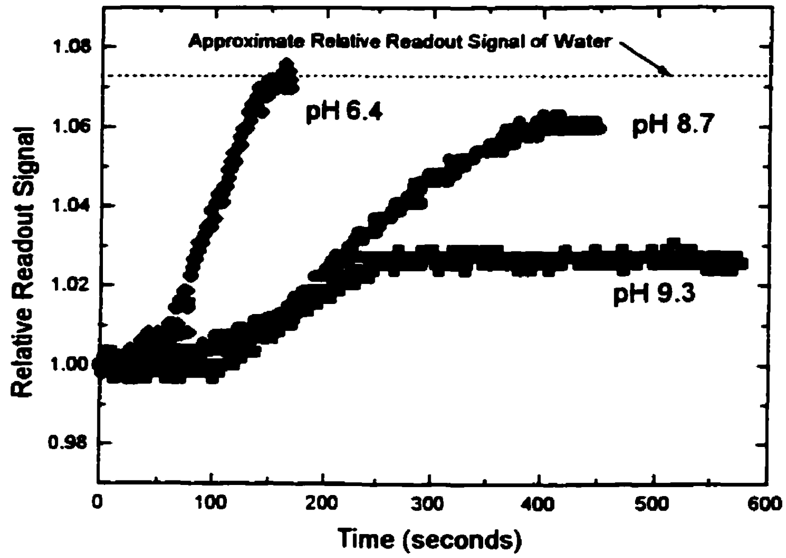

Figure 6.7. Relative Readout Signal vs Time for pH 6.4, 8.7 and 9.3.

6.3.2 Presence of Ca Ions.

6.3.2.1 *Sphalerite*

Sphalerite showed some tendency to coagulate over the full pH range but this became particularly evident above ca. pH 9 (Figure 6.8). Above ca. pH 10 up to ca. pH 13, the dominant species is $CaOH^+$ [7] which may be responsible for the increased zeta-potential and higher settling velocity. Figure 6.8 shows that Ca^{2+} gives a zeta-potential ca. -10 to -20 mV over the entire pH range tested, values conducive to coagulation.

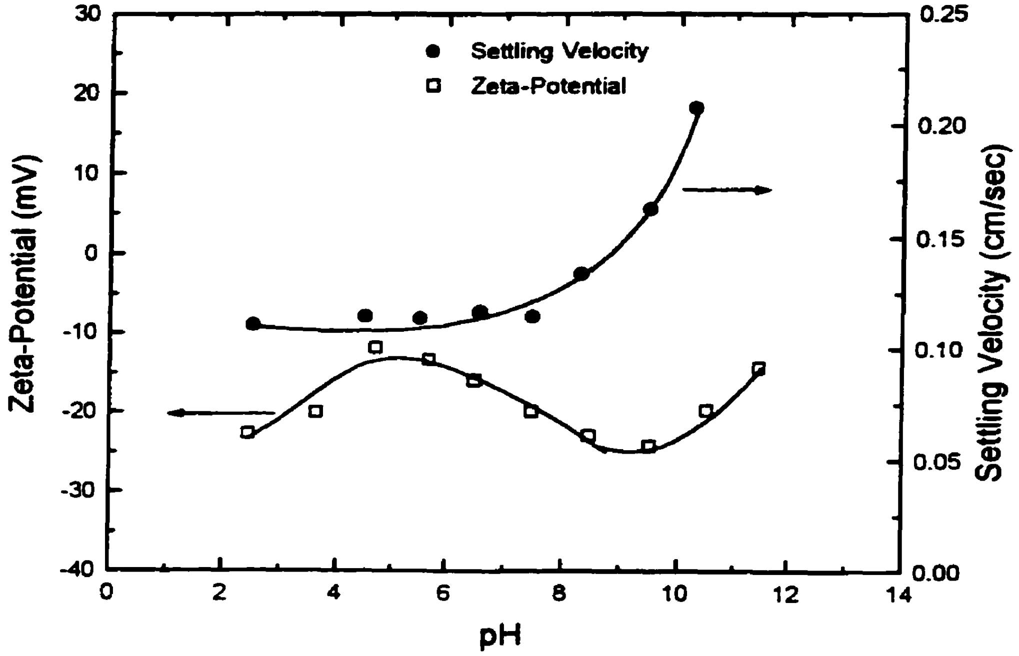

Figure 6.8. Comparison between Zeta-Potential and Settling Velocity of Sphalerite as a Function of pH in the Presence of Calcium Ions.

6.3.2.2 *Silica*

Silica was dispersed below ca. pH 6.5 (Figure 6.9) while above this pH settling velocity increased rapidly. The correlation with zeta-potential is not exact, but zeta-potential is increasing above pH 9 reaching close to zero at pH 11.5.

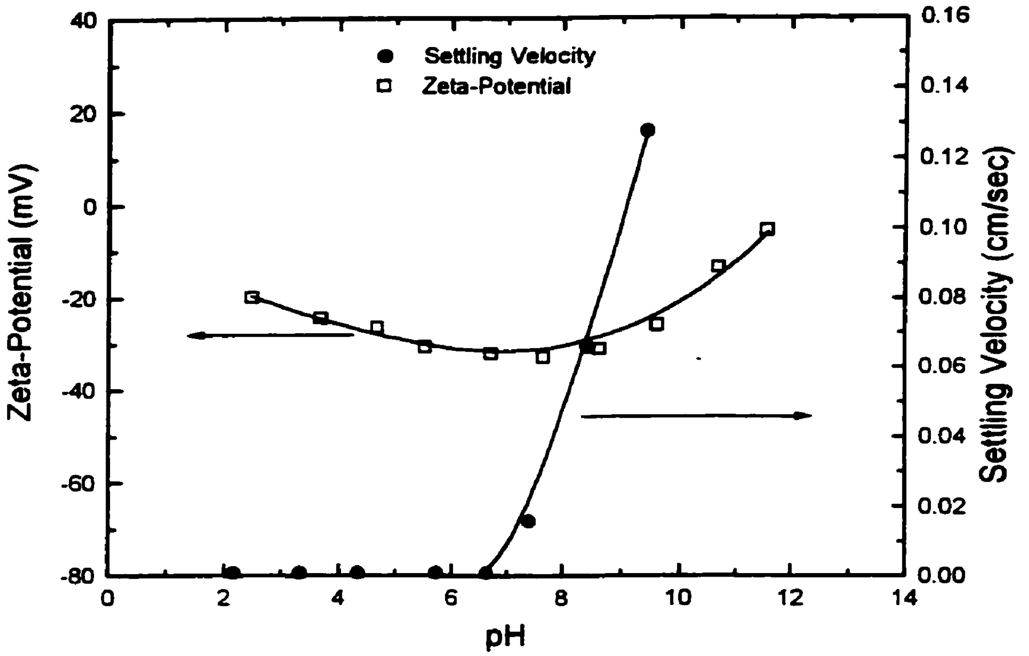

Figure 6.9. Comparison between Zeta-Potential and Settling Velocity of Silica as a Function of pH in the Presence of Calcium Ions.

Adsorption of $CaOH^-$ seems to be responsible for the increase in zeta-potential and settling rate.

6.3.2.3 *Sphalerite/Silica*

Sphalerite homocoagulated and silica was left in suspension in the acidic to neutral range (ca. pH 2 to 7). This is confirmed by the colour gradation at a pH representative of this range (Figure 6.11). Above pH 7 sphalerite and silica heterocoagulated.

The results appear to correspond to the single mineral results. Up to ca. pH 7 the sphalerite shows some tendency to homocoagulate (Figure 6.8) and the silica is strongly dispersed (Figure 6.9). The settling rate observed in Figure 6.10 is that of agglomerated sphalerite in a background of dispersed silica. Above pH 7 both sphalerite (Figure 6.8) and silica (Figure 6.9) agglomerate and this tendency is retained by the mixture (Figure 6.10). Unlike in the absence of Ca, the mixed mineral system behaves more as the single results would suggest.

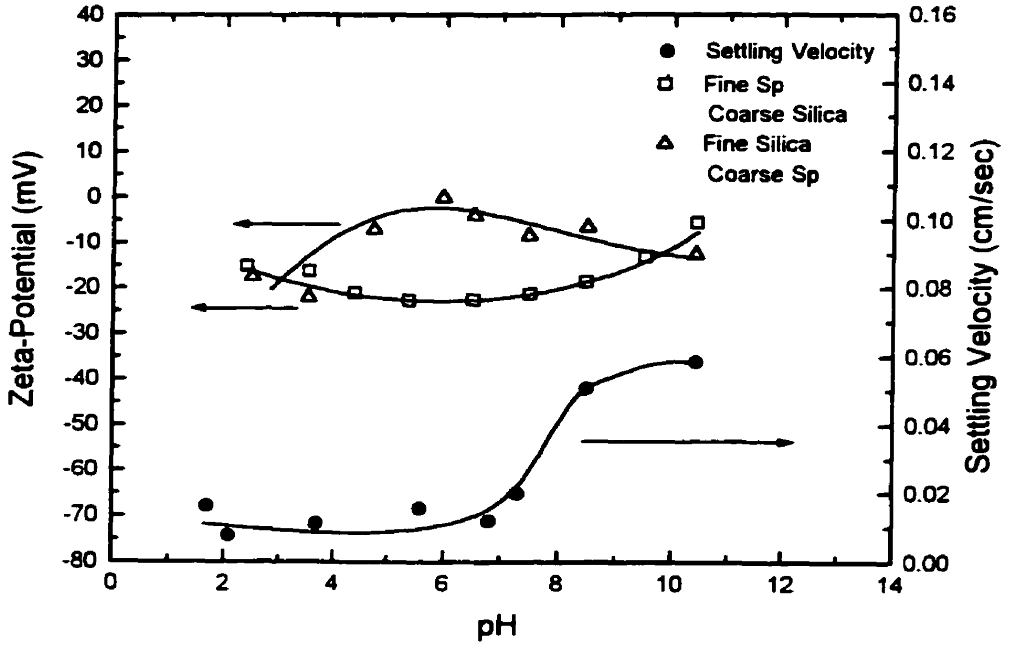

Figure 6.10. Comparison between Zeta-Potential and Settling Velocity of Sphalerite and Silica as a Function of pH in the Presence of Calcium Ions.

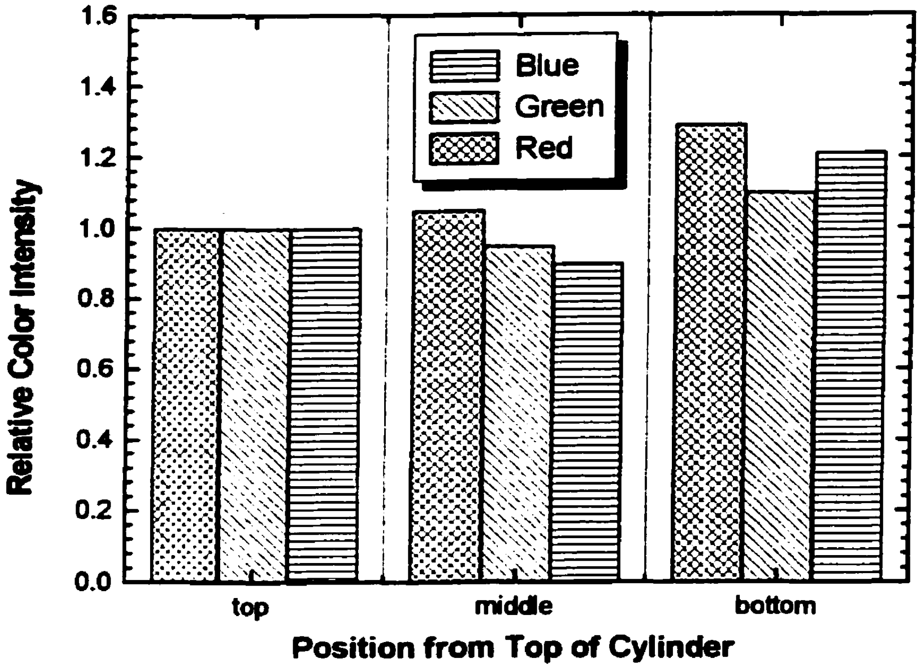

Figure 6.11. Sphalerite/Silica Mixture in the Presence of Ca^{2+} at ca. pH 4.5. Color Intensity is Relative to the Top Position of settling Cylinder.

6.4 Significance to Flotation

This research was undertaken in part to determine if settling studies, which are conveniently performed using the apparatus described here, provide insight into the state of agglomeration of sphalerite and silica which may influence selective flotation. The conditions studied thus far are too far from the real system to be of immediate application but can be used to illustrate how the results may eventually be interpreted.

Sphalerite is usually floated at moderately alkaline pH (8-11) the one notable exception being Cominco's Red Dog operation where flotation pH is close to 6. Consider this exception first. In the absence of contaminant ions, sphalerite and silica are expected to heterocoagulate around pH 6 which may degrade selectivity. In the presence of calcium, sphalerite and silica are dispersed perhaps promoting selectivity.

Next consider the range pH 8 to 11. In the contaminant-free case sphalerite selectively agglomerates at the low end of the range and silica is well dispersed. This may have a positive effect on flotation: the larger sphalerite particles will float more readily and selectively from the silica; or a negative effect: the sphalerite agglomerates may entrap silica. In the situation where calcium is present the results suggest sphalerite heterocoagulates with silica. Given that the presence of Ca (and other cationic contaminants) is more realistic, heterocoagulation may be the rule rather than the exception.

Misplacement of minerals in flotation related to agglomeration effects has long been suspected. Diagnosis of this phenomenon is far from a developed science. The approach described here based on an automated settling test procedure offers a convenient means of investigation.

6.5 Conclusions

6.5.1 Sphalerite

No calcium ions

There was partial homocoagulation of sphalerite from ca. pH 2 to 8 and complete homocoagulation at pH 8.5. At pH 8.5 this attraction was not expected as the zeta-potential of sphalerite is negative and suggests the presence of an attractive hydrophobic force may be the cause of homocoagulation. Above pH 9.5, the sphalerite was completely dispersed, as expected since the zeta-potential of sphalerite becomes strongly negative.

With calcium ions

Sphalerite showed some tendency to coagulate over the full pH range tested, becoming particularly evident above ca. pH 9. This is due to Ca^{2-} and $CaOH^{-}$ (at pH 10 to 13) adsorbing in the sphalerite double layer, lowering the zeta-potential and the associated electrostatic repulsion force, thus promoting agglomeration.

6.5.2 Silica

No calcium ions

The silica was dispersed over the pH range tested (2 to 10). This repulsion results from both electrostatic and hydration forces.

With calcium ions

Silica was dispersed below ca. pH 6.5 while above this pH the settling velocity increased rapidly, indicating homocoagulation. Below pH 6.5, repulsion occurred because the zeta-potential remained strongly negative. Above ca. pH 6.5 agglomeration occurred due to Ca^{2+} and $CaOH^{+}$ adsorbing in the silica double layer, lowering the absolute zeta-potential and the electrostatic repulsion force.

6.5.3 Sphalerite/Silica

No calcium ions

Heterocoagulation of sphalerite and silica occurred from ca. pH 3 to 7.5. From ca. pH 3 to 4 the zeta-potential of sphalerite is between 0 and -10 mV so electrostatic repulsion is low enough not to retard agglomeration. From ca. pH 4 to 7.5, the heterocoagulation cannot be explained by the zeta-potential measurements. Zeta-potential and XPS results do not show any "contaminating ions" are transferred between the minerals.

Homocoagulation of sphalerite and dispersion of silica occurred at ca. pH 2 and 8.5. The results at ca. pH 2 cannot be explained using zeta-potential measurements. At ca. pH 8.5 both materials are negatively charged so repulsion was expected. Also at this pH, sphalerite on its own homocoagulated (section 6.5.1).

Above pH 9.5, the suspension was dispersed, as expected because the zeta-potential of both materials is negative.

With calcium ions

Homocoagulation of sphalerite and dispersion of silica occurred from ca. pH 2 to 7. From ca. pH 2 to 4 the zeta-potential of both materials is negative, therefore, the two minerals do not heterocoagulate.

Heterocoagulation of sphalerite and silica occurred above ca. pH 7. This can be explained by surface charge because the zeta-potential of silica and sphalerite was significantly reduced.

6.6 References

1. Fairweather, M., Cominco Research, Trail, B. C., private communication 1999.
2. Vergouw, J. M., DiFeo, A., Xu, Z., and Finch, J. A., An Agglomeration Study of Sulphide minerals using Zeta-Potential and Settling Rate. Part II: Sphalerite/Pyrite and Sphalerite/ Galena, Minerals Engineering, 11(7), 1998, pp605-614.
3. Subrahmanyam, T. V., Prestidge, C. A., and Ralston, J., Contact Angle and Surface Analysis Studies of Sphalerite Particles, Minerals Engineering, 9(7), 1996, pp727-741.
4. Muster, T. H., and Prestidge, C. A., Rheological Investigations of Sulphide Mineral Slurries, Minerals Engineering, 8(12), 1998, pp1541-1555.
5. Muster, T. H., Toikka, G., Hayes, R. A., Prestidge, C. A., and Ralston, J., Interactions between Zinc Sulphide Particles under Flotation-Related Conditions, Colloids and Surfaces A: Physicochemical and Engineering Aspects, 106, 1996, pp203-211.
6. Hunter, R. J., Foundations of Colloid Science, Volume 1, 1987, p420.
7. Fuerstenau, M. C., and Palma, B. R., Anionic Flotation of Oxides and Silicates in Flotation, Memorial Volume I, (editor, Fuerstenau, D. W.), America Institute of Mining Engineers, New York, 1976, pp148-196.

CHAPTER 7

ATOMIC FORCE MICROSCOPY

7.1 Force Measurements between Silicon Nitride Tip and Mica.

7.1.1 Verification

To verify that the parts and equipment used in the atomic force microscope were adequately cleaned, standard force measurements between a silicon nitride tip and mica were performed and compared to results obtained by Butt [1].

Figure 7.1 illustrates the deflection versus separation results at ca. pH 6 for various KCl concentrations. These results are in accordance with those obtained by Butt [1] (Figure 7.2). As the KCl concentration increased, the repulsive force between the tip and mica was reduced. This phenomenon can be explained by the double layer being compressed when the KCl concentration increased.

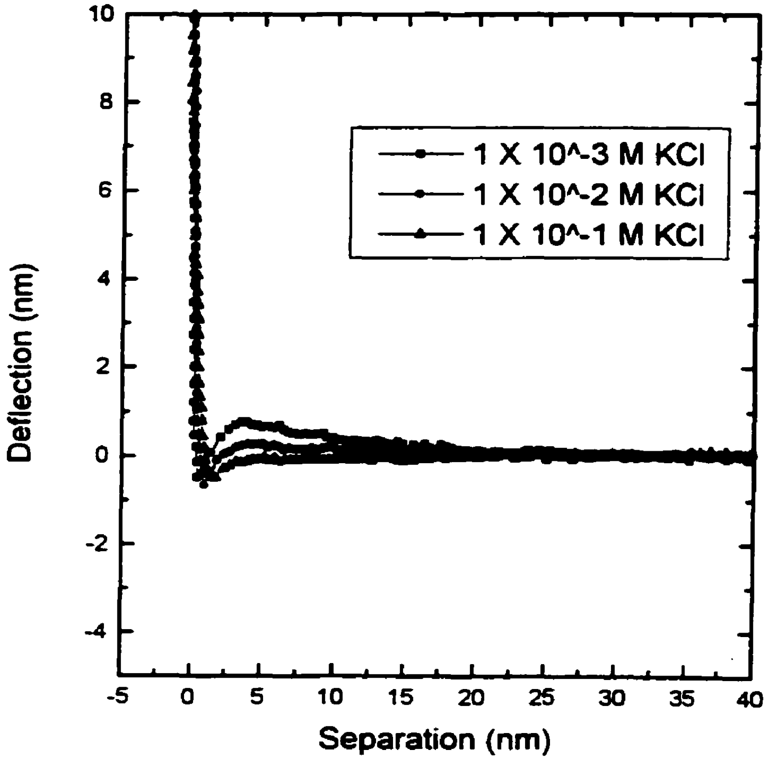

Figure 7.1. Deflection versus Separation between Silicon Nitride Tip and Mica in 10^{-3}, 10^{-2} and 10^{-1} M KCl at ca. pH 6.

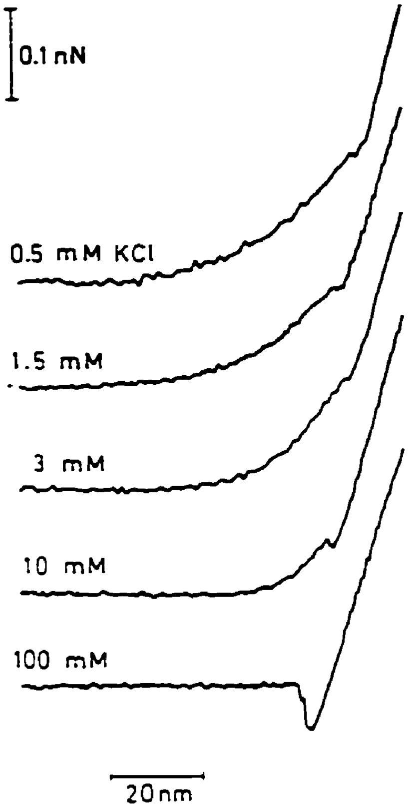

Figure 7.2. Force versus Distance for System in Figure 7.1 reported by Butt [1].

7.1.2 Results as a Function of pH

Figure 7.3 shows the deflection versus separation results of tip and mica at ca. pH 8 for various KCl concentrations. A similar effect was observed as at pH 6: when KCl concentration increased, the repulsive force decreased due to double layer compression. Figure 7.4 shows the deflection versus separation results for various KCl concentrations at pH 10. Similar results to pH 6 and 8 were observed.

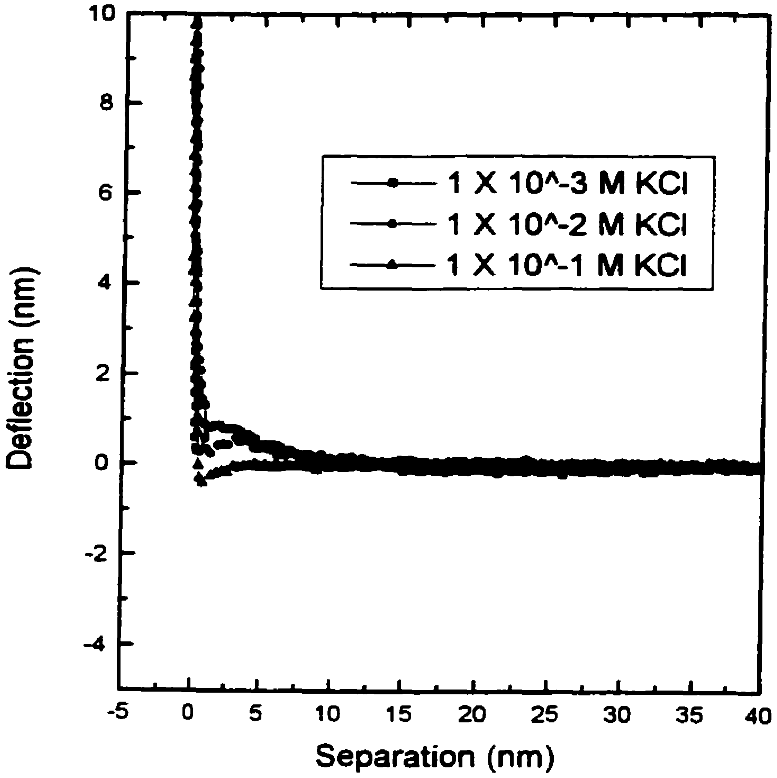

Figure 7.3. Deflection versus Separation between Silicon Nitride Tip and Mica in 10^{-3}, 10^{-2} and 10^{-1} M KCl at ca. pH 8.

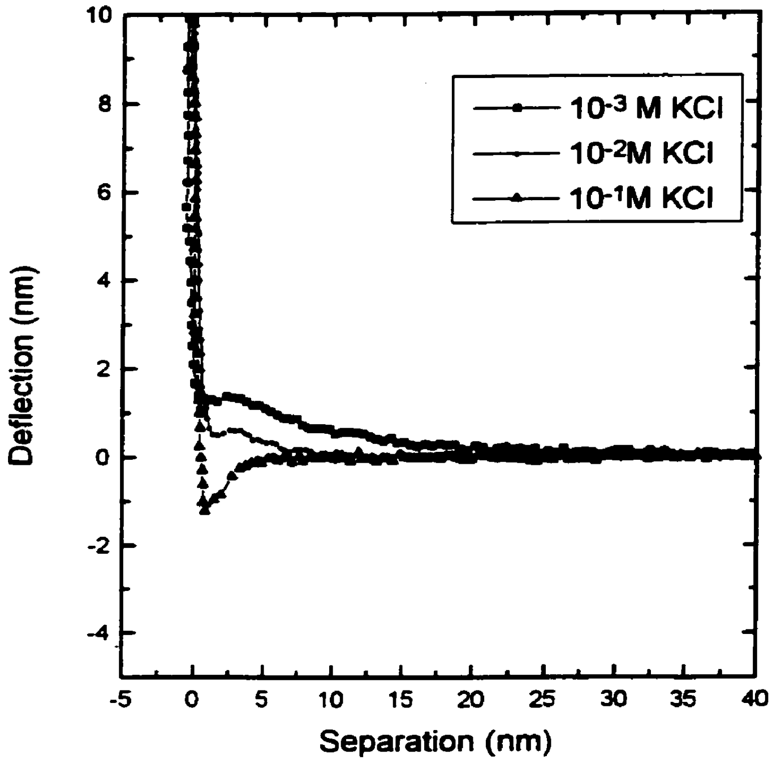

Figure 7.4. Deflection versus Separation between Silicon Nitride Tip and Mica in 10^{-3} M, 10^{-2} M and 10^{-1} M KCl at ca. pH 10.

Figure 7.5 shows the results of the deflection versus separation for the silicon nitride tip and mica at three pH in a background electrolyte of 10^{-3} M KCl. When the pH increased the deflection of the tip also increased due to an increasing repulsive force between the two components. A similar trend was observed for KCl concentrations of 10^{-2} M and 10^{-1} M (Figures 7.6 and 7.7, respectively).

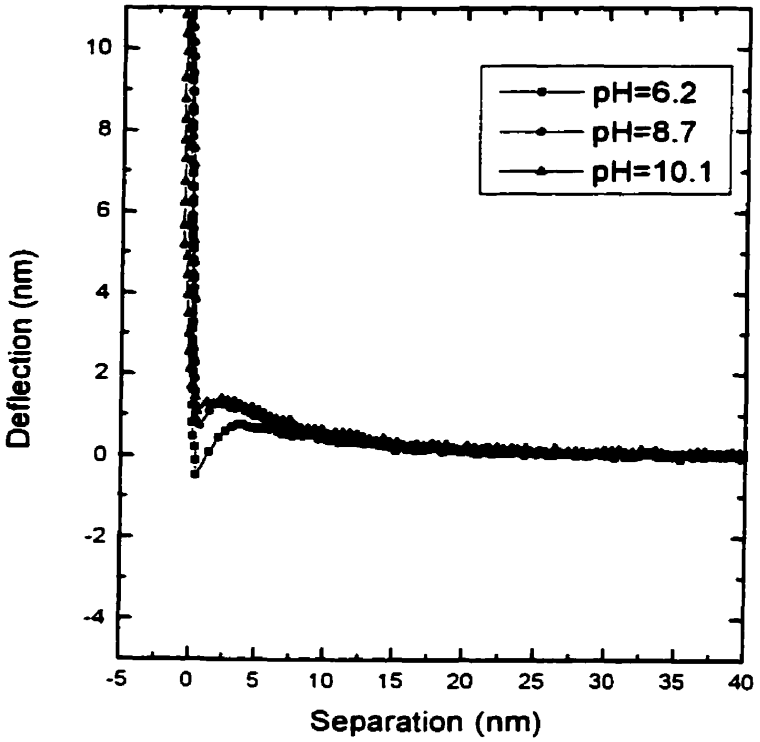

Figure 7.5. Deflection versus Separation between Silicon Nitride Tip and Mica in 10^{-3} M KCl at pH 6.2, 8.7 and 10.1.

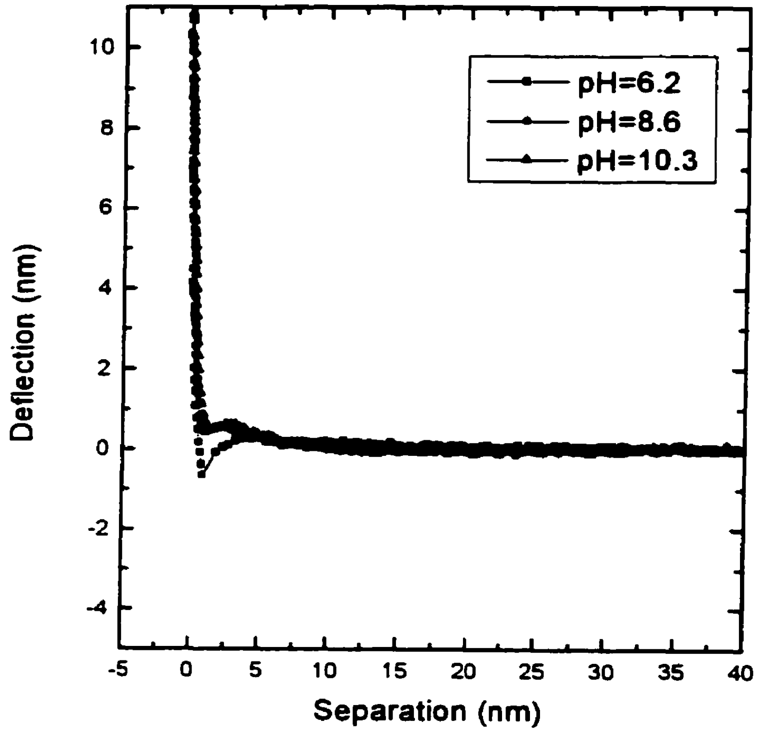

Figure 7.6. Deflection versus Separation between Silicon Nitride Tip and Mica in 10^{-2} M KCl at pH 6.2, 8.6 and 10.3.

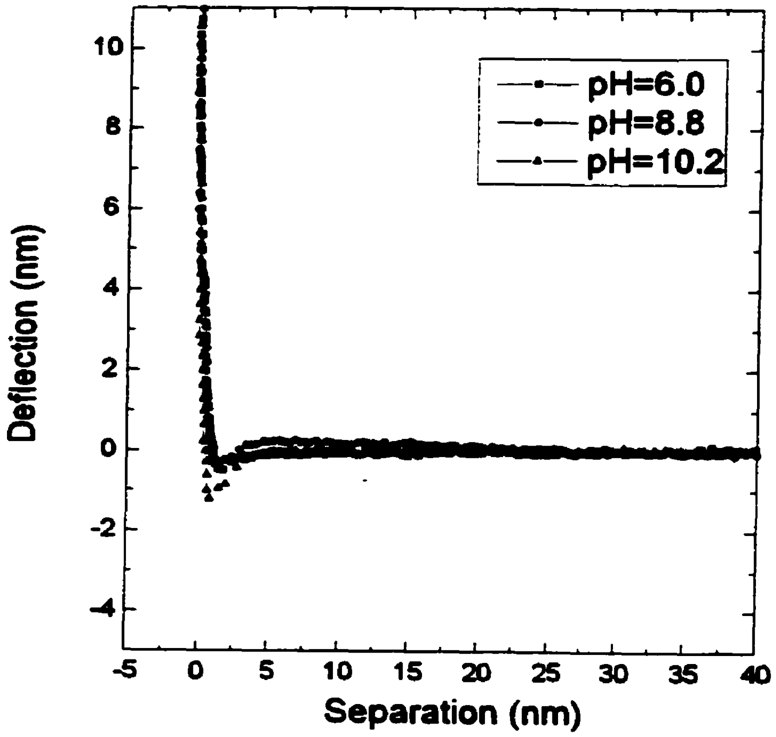

Figure 7.7. Deflection versus Separation between Silicon Nitride Tip and Mica in 10^{-1} M KCl at pH 6.0, 8.8 and 10.2.

7.2 Force Measurements between Silica Surfaces in Aqueous Solutions

The force/separation results for a silica sphere and a flat silica surface as a function of KCl concentration are shown in Figure 7.8. These data are similar to previous measurements reported by Ducker et al. [2] (Figure 7.9).

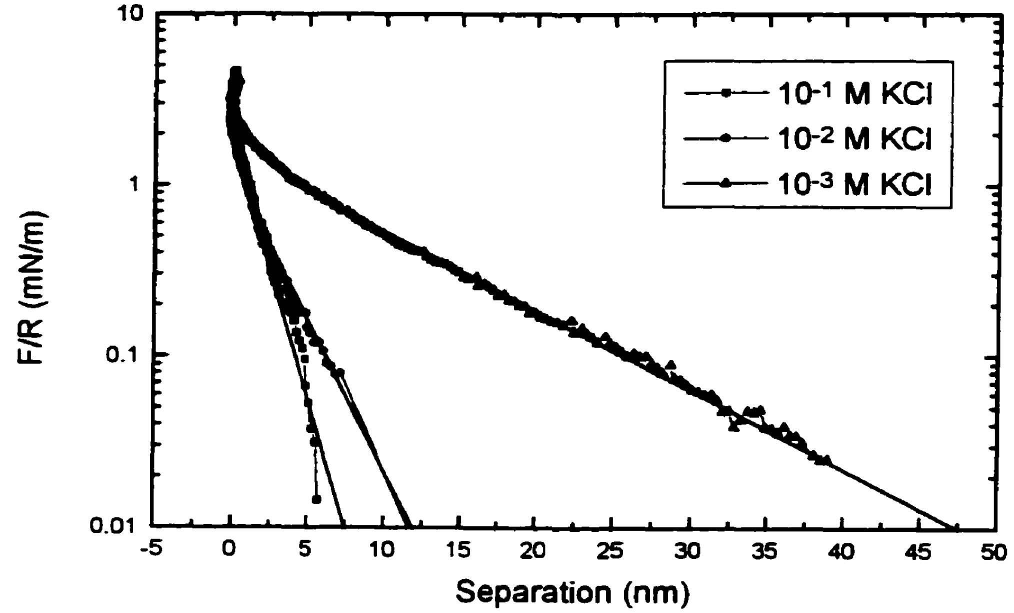

Figure 7.8 Force between Silica Particle and Flat Silica Substrate at 25 °C and ca pH 6. The Relevant Parameters are as Follows: At 1 X 10^{-3} M KCl, κ^{-1}=9.2 nm, ψ_o= -57 mV: 1 X 10^{-2} M KCl, κ^{-1}=2.5 nm, ψ_o= -31 mV; 1 X 10^{-1} M KCl, κ^{-1}=1.3 nm, ψ_o= -27 mV.

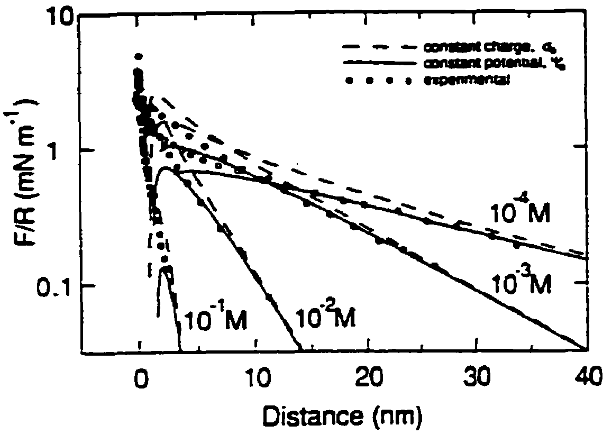

Figure 7.9 Force on a Silica Particle in Aqueous Solution in a Variety of NaCl Solutions at 25 ^{0}C and pH 5.7 taken from Ducker et al [2].

The measured forces decay exponentially with distance and both decay length and potential decrease with KCl concentration. These phenomena occur because the high concentration of KCl compresses the double layer [2].

Figure 7.10 shows the force between a silica sphere and flat silica as a function of pH. These measurements were performed in a background of 10^{-3} M KCl and the pH was changed with the addition of dilute NaOH. As pH increases the negative zeta-potential of silica increases (Figure 6.2), therefore, the repulsive force should increase with pH as shown in Figure 7.10.

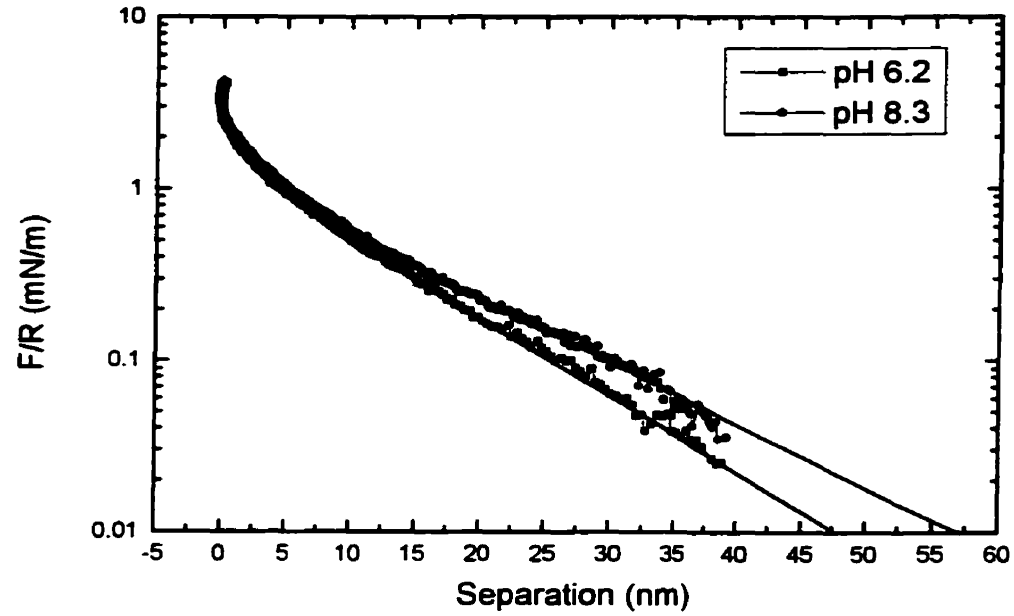

Figure 7.10. Forces between Silica Particle and Flat Silica Substrate as a Function of pH at 25 ^{0}C with no Ions in Solution. The Relevant Parameters are as Follows: 1 X 10^{-3} M KCl, pH 6.2, κ^{-1}=9.2 nm, ψ_o=-57.3 mV; pH 8.3, κ^{-1}=10.9 nm, ψ_o=-65 mV.

When calcium was added, the repulsive force decreased with increasing pH until an attractive force was observed as shown in Figures 7.11 and 7.12. These results are in accordance with zeta-potential and settling velocity results (Figure 6.9): as pH increased the negative zeta-potential decreased due to adsorption of cationic Ca species and, therefore, the repulsive force decreased.

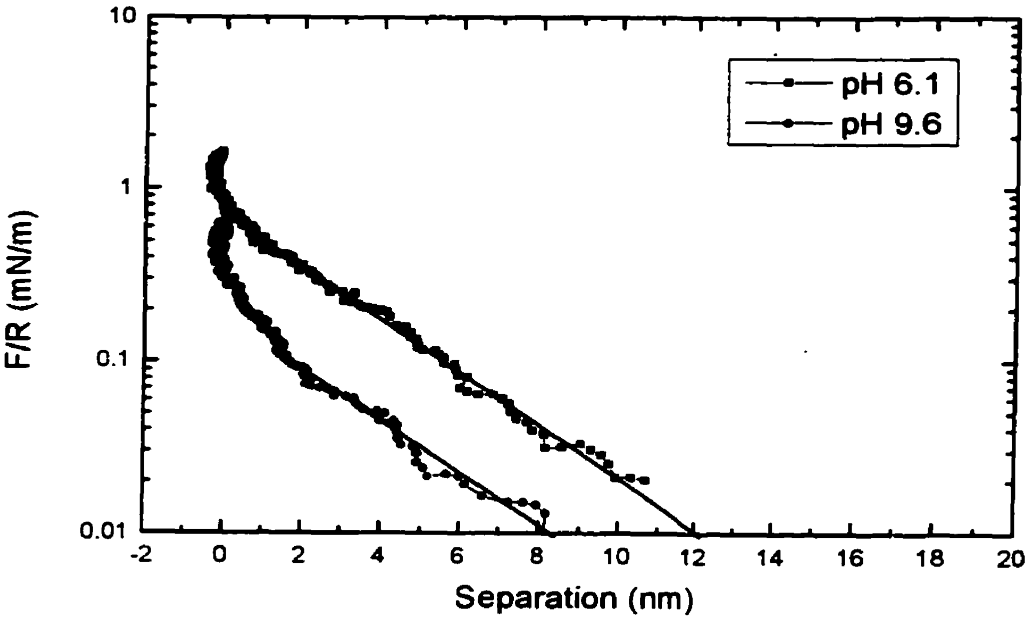

Figure 7.11. Forces between Silica Particle and Flat Silica Substrate at 25 °C and ca. pH 6.1 with 130 ppm Ca^{2+} in Solution. The Relevant Parameters are as Follows: 1 X 10^{-3} M KCl, pH 6.1, κ^{-1}=3.4 nm, ψ_o=-49.7 mV; pH 9.6, κ^{-1}=3.1 nm, ψ_o=-36.8 mV.

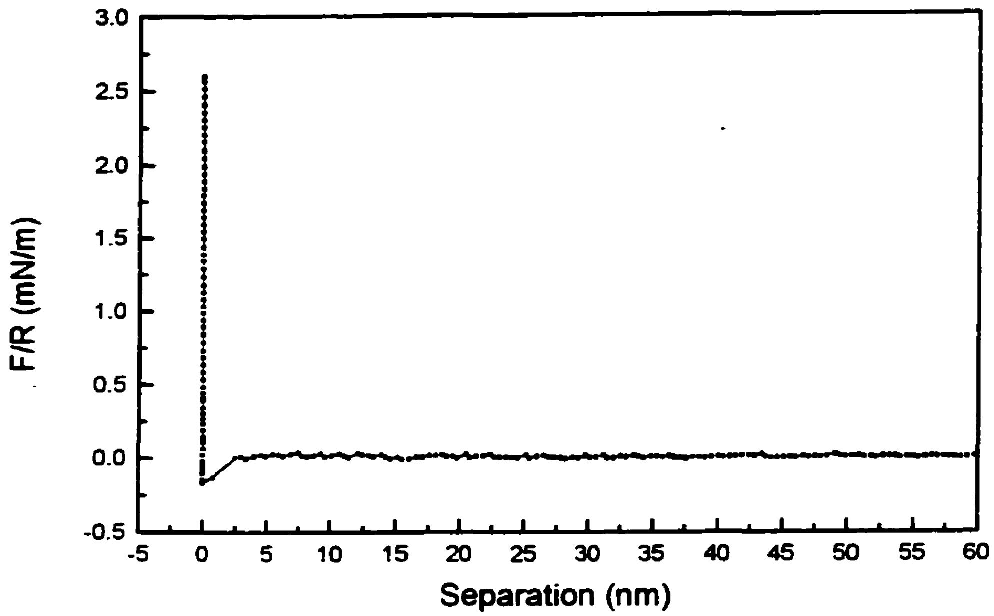

Figure 7.12 Attractive Force between Silica Particle and Silica Substrate in a Background Electrolyte of 1 X 10^{-3} M KCl and 130 ppm Ca^{2-} at pH 11.4.

7.3 Correlation of Silica/Silica Surface Forces and Settling Rate.

There was generally good correlation between the settling velocity results (Figure 6.2) and the AFM results: the surface potential of silica was negative (Figure 7.10) and the zeta-potential of silica was also negative (Figure 6.2). Around the i.e.p. of silica, coagulation did not occur due to the hydration effect. (This effect was confirmed by Ducker et al. [2] using atomic force microscopy.)

When calcium ions were added, there was also good correlation between the settling velocity and AFM results. As pH increased the zeta-potential decreased thus the repulsive force between silica was reduced and agglomeration occurred (Figure 6.9). This corresponded to the trend observed with atomic force microscopy; as pH increased the repulsive force decreased and eventually the interaction between silica was attractive (Figures 7.11 and 7.12).

7.4 Force Measurements between Silica and Sphalerite in Aqueous Solutions.

The surface force between sphalerite and silica, measured over the pH range 7.2-10.6 is shown in Figures 7.13-7.16. In all cases, except at pH 9.6, a repulsive force resulted as both mineral surface potentials were negative. Further, the surface potential became more negative and decay length increased with increasing pH. However, at pH 9.6 (Figure 7.15) a hydrophobic force was observed even though electrostatic repulsion would be expected because of the surface charge.

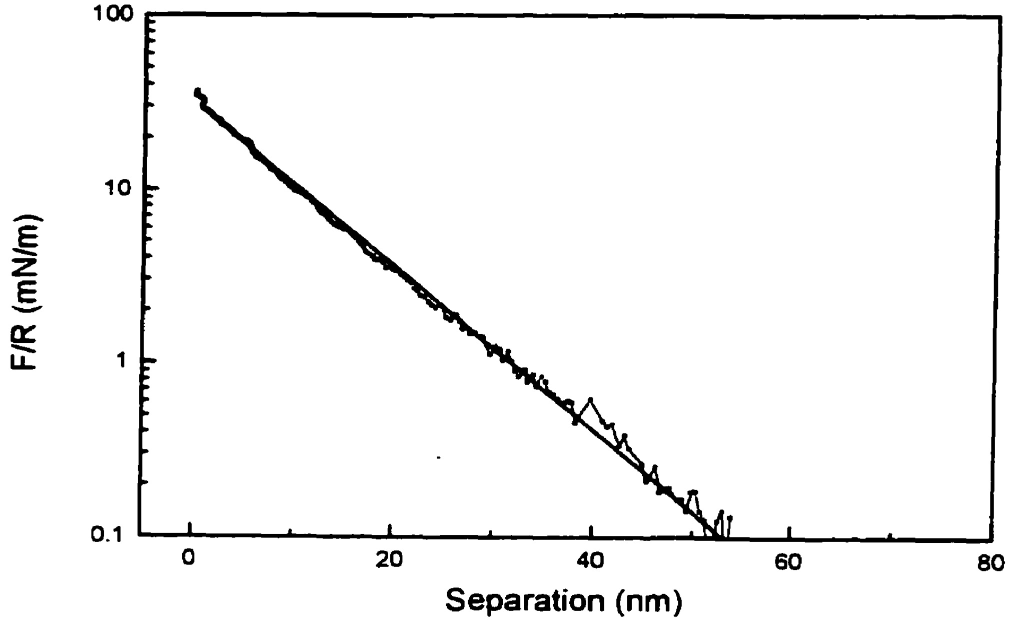

Figure 7.13. Force between Silica Particle and Sphalerite at pH 7.2. The relevant Parameters are as Follows: κ^{-1}=9.6 nm and ψ_{silica}=-60 mV and $\psi_{sphalerite}$=-51 mV.

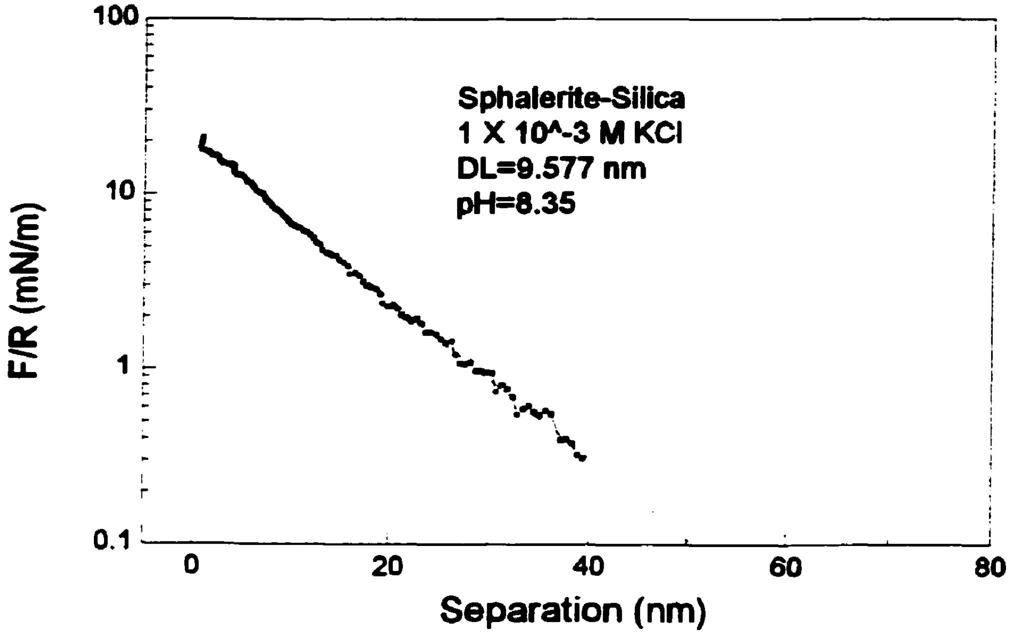

Figure 7.14. Force between Silica Particle and Sphalerite at ca. pH 8.4. The Relevant Parameters are as Follows: κ^{-1}=9.6 nm, ψ_{silica}=-63 mV, and $\psi_{sphalerite}$=-40 mV.

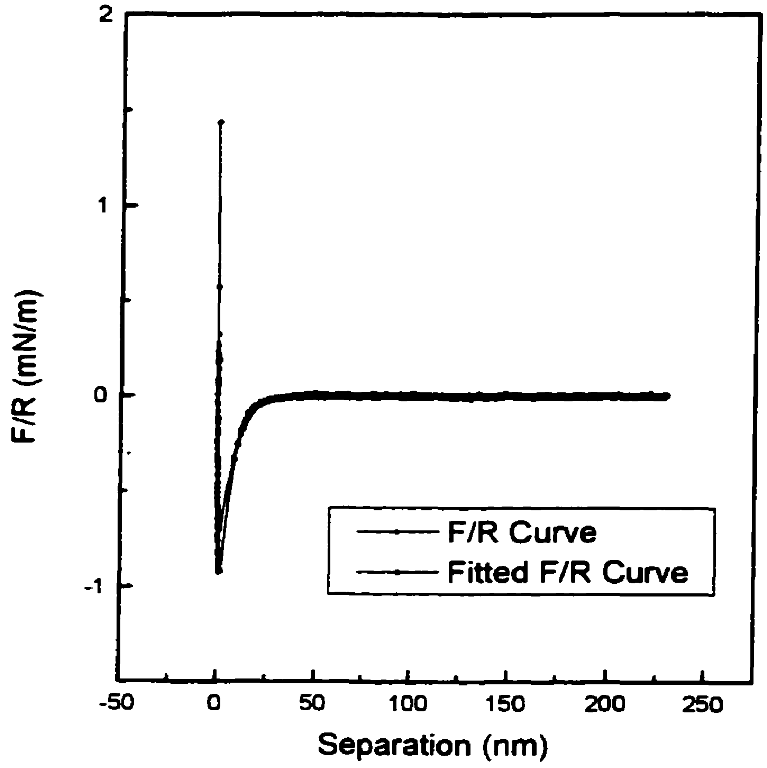

Figure 7.15. Force between Silica Particle and Sphalerite at ca pH 9.6. The relevant Parameters are as follows: C_1= -1.221, D_1= 6.402, C_2=0.833 and D_2= 0.490.

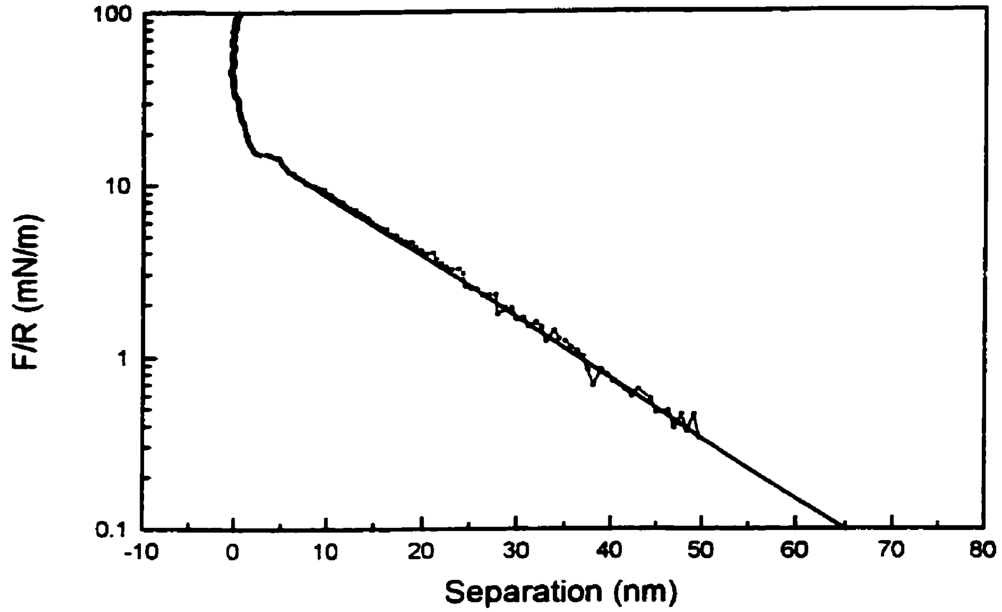

Figure 7.16. Force between Silica and Sphalerite at ca pH 10.6. The Relevant Parameters are as Follows: κ^{-1}=12.2 nm, ψ_{silica}=-70 mV and $\psi_{sphalerite}$=-60 mV.

7.5 Correlation of Sphalerite-Silica Surface Forces and Settling Velocity Results

At ca. pH 7.2, the settling results showed evidence of agglomeration (section 6.4, Figure 6.4). However, the AFM results (Figure 7.13) showed that the interaction was repulsive. At ca. pH 8.5, the settling results showed that the sphalerite homocoagulated and some silica remained in suspension (section 6.4, Figure 6.5), thus the interaction was repulsive (partially at least). At this pH the AFM results (Figure 7.14) corresponded with the settling results. At pH 9.6, AFM results showed that there was attraction (Figure 7.15) but settling results showed that the system was dispersed (section 6.4, Figure 6.6). Therefore, the AFM results are not in accordance with the settling experiments for ca. pH 9.6. At ca. pH 10.6, the AFM results show that the interaction was repulsive, this was in accordance with the settling velocity results and the fact that the zeta-potential of both minerals is strongly negative.

There seem be three possible explanations for this limited agreement between settling and AFM results. The elemental analysis (Chapter 4) shows that the sphalerites used in the settling and AFM experiments were different thus perhaps causing the disagreement. Muster et al. [3] attributed their lack of correlation between rheology and surface force measurements to the different volume fractions used in the two techniques. They found sphalerite slurry to be dispersed at pH 4, but observed an attractive force. The atomic force microscopy measurements being carried out at very low volume fractions may induce sphalerite oxidation compared to the higher pulp density of the rheology and settling experiments. They considered that under acidic pH conditions, zinc hydroxide phases are present on the partially oxidised zinc sulphide surface which dissolve [3]:

$$(ZnS)_n\ yZn(OH)_2 + 2yH^+ \rightarrow nZnS + 2yH_2O + yZn^{2+} \qquad (7.1)$$

with the exposed zinc sulphide surface becoming sulphur-rich:

$$(ZnS)_n \rightarrow Zn_{n-x}S_n + xZn^{2+} + 2xe^- \qquad (7.2)$$

resulting in a hydrophobic surface. The surface cleaning process (reactions (7.1) and (7.2)) is kinetically controlled, the rate being strongly dependent on the pH, pulp potential, dispersion volume fraction and hydrodynamic conditions. With the relatively high particle volume fractions used in the rheological studies compared with AFM, reactions (7.1) and (7.2) may be limited over the timescale of the experiment [3].

At pH 7.2, there may be a zinc depleted sphalerite surface (due to higher oxidation rates in AFM) and Zn^{2-} ions in solution which can readsorb on the mineral surfaces. These factors can change the surface properties resulting in a repulsive rather than attractive (settling experiments) interaction. The higher oxidation rates (leaving a zinc depleted sphalerite surface) may be the explanation for the lower (more negative) zeta-potential of sphalerite (atomic force microscopy experiments) compared to the settling experiments.

After every force measurement at a given pH, the fluid cell of the AFM was flushed with 10^{-3} M KCl at the pH of the following experiment. Therefore, all of the oxidation products in solution and perhaps on the mineral surfaces were washed out of the fluid cell. In the subsequent experiments (pH 8.4, 9.6 and 10.6), the sphalerite may have had a metal deficient surface ($Zn_{n-x}S_n$) according to reactions 7.1 and 7.2. The metal deficient surface and sulphoxy species (from sphalerite oxidation) may adsorb on silica and cause the hydrophobic attraction at pH 9.6.

Interestingly, in both techniques (AFM and settling), an attractive force was observed in the sphalerite/silica system although it occurred at a different pH. Thus the AFM does confirm that a force of attraction can exist even though the zeta-potential of both minerals is negative.

7.6 Conclusions

The interaction force for silica-silica was repulsive at pH 6.2 and 8.3. This was expected as the zeta-potential of silica at both pH is strongly negative (section 6.3.1). There was good correlation between the settling and AFM experiments.

The repulsive silica-silica interaction force with Ca^{2+} in solution decreased with increasing pH and eventually above pH 11 the force became attractive. This occurred because the zeta-potential of silica decreased with increasing pH (section 6.5.2) due to increasing adsorption of Ca^{2+} and $CaOH^{+}$. There was good correlation between the settling and AFM experiments.

Surface forces for sphalerite-silica interactions (no ions in solution) were repulsive at ca pH 7.2, 8.4 and 10.6. There was an attractive force at pH 9.6. There was poor correlation between the settling and AFM results which is tentatively attributed to different degrees of oxidation between the two techniques.

7.7 References

1. Butt, H., Measuring Electrostatic, van der Waals and Hydration Forces in Electrolyte Solutions with Atomic Force Microscope, Biophysical Journal, 60, 1991, pp1438-1444.

2. Ducker, W. A., Senden, T. J., and Pashley, R. M., Measurement of Forces in Liquids Using a Force Microscope, Langmuir, 8, 1992, pp1831-1836.

3. Muster, T. H., Toikka, G., Hayes, R. A., Prestidge, C. A., and Ralston, J., Interactions between Zinc Sulphide Particles under Flotation-Related Conditions, Colloids and Surface A: Physicochemical and Engineering Aspects, 106, 1996, pp203-211.

CHAPTER 8

CONCLUSIONS, CONTRIBUTIONS, AND FUTURE WORK

8.1 Conclusions

8.1.1 Electrokinetic and Settling Study of Mixed Sulphide Minerals

1. Mixtures of oxidised sulphide minerals cross contaminate each other with metal ions. This can result in significant effects on the zeta-potential.
2. Galena and sphalerite were significantly affected by the presence of a second sulphide showing evidence of (anionic) sulphoxy species and (cationic) metallic species at neutral and alkaline pH, respectively.
3. Pyrite was not strongly affected by galena and sphalerite, but the zeta-potential did tend to increase above pH 8.
4. The changes in zeta-potential were attributed to the relative affinity for metallic and sulphoxy species released through galvanic interaction. When galvanic effects were absent, no changes in zeta-potential were found.
5. In the mixed sulphide systems, sphalerite/pyrite, sphalerite/galena and galena/pyrite, the maximum in agglomeration occurred near the pH where both minerals are close to zero zeta-

potential.

8.1.2 Sphalerite/Silica Interactions

8.1.2.1 *Sphalerite*

Absence of calcium ions

1. The maximum settling velocity (highest homocoagulation) occurred at pH 8.5 and is attributed to an attractive hydrophobic force.
2. Above pH 9.5, sphalerite was dispersed, corresponding to the high negative zeta-potential of sphalerite promoting a repulsive interaction.

With calcium ions

1. Highest settling velocity occurred above pH 9, caused by Ca^{2+} and $CaOH^{-}$ (> ca. pH 10 to 13) ions adsorbing in the double layer, thus reducing the zeta-potential and electrostatic repulsive force.

8.1.2.2 *Silica*

Absence of calcium ions

1. Silica was dispersed from pH 2 to 10, as expected because the zeta-potential is strongly negative.

With calcium ions

1. Silica was dispersed below ca. pH 6.5, and coagulated above this pH. Coagulation was caused by the reduction of the zeta-potential due to the adsorption of Ca^{2+} and $CaOH^{-}$ (> ca. pH 10 to 13) ions in the silica double layer.

8.1.2.3 *Sphalerite/Silica*

Absence of calcium ions

1. Heterocoagulation occurred from ca. pH 3-7. Over the range pH 4 to 7 heterocoagulation may be caused by the same attractive hydrophobic force suggested for sphalerite alone.

Around pH 3-4, the zeta-potential of sphalerite is between 0 to -10 mV, so the electrostatic repulsive force is low enough not to retard agglomeration.

2. At pH 2, the sphalerite homocoagulated while some silica remained dispersed. The minerals have opposite charge and heterocoagulation is expected. For two particles of opposite charge to come together is straightforward, however, subsequent particles must arrange themselves to accommodate the repulsion of like-charged particles already present in the agglomerate.
3. At pH 8.5, the sphalerite homocoagulated while some silica remained dispersed. The sphalerite/silica repulsion was expected (at pH 8.5) corresponding to the zeta-potential of both minerals being negative.
4. Above pH 9.5, the slurry was dispersed corresponding to the zeta-potential of both minerals being negative.

With calcium ions

1. Heterocoagulation occurred above pH 7. The zeta-potential and hence the electrostatic repulsive force was lowered due to the adsorption of Ca^{2+} and $CaOH^{+}$ (> ca. pH 10 to 13) ions in the double layer, thus promoting agglomeration.
2. Below pH 7, sphalerite homocoagulated and some silica was dispersed. The dispersion of silica was expected as the zeta-potential of both minerals is negative but the homocoagulation of sphalerite was not expected, but agreed with the observation on sphalerite alone (section 9.1.2.1).

8.1.3 Atomic Force Microscopy

1. The surface forces measured between silicon nitride tip and mica are in agreement with those reported by Butt.
2. The surface forces measured between a silica sphere and a silica substrate are in agreement with those reported by Ducker et al.
3. The agreement with other researchers confirms the preparation procedure is adequate.

4. There was good correlation between the silica settling rate and atomic force microscopy measurements. In the absence of calcium ions, the interaction was repulsive at all the pH tested. In the presence of calcium ions, as the pH increased, the repulsive force decreased and eventually was eliminated and the interaction was attractive.
5. There was poor correlation between sphalerite-silica settling rate and atomic force microscopy measurements at pH 7.2 and 9.6. A possible cause is the different volume fractions used in the two techniques and different chemical composition of the sphalerite samples. In atomic force microscopy, the volume fraction is low leading to higher oxidation rates of sphalerite which affect the surface properties and interaction between the two minerals.
6. At pH 7.2, 8.4 and 10.6 an electrostatic repulsive force was observed, however, at pH 9.6, there was an attractive (hydrophobic) force.
7. Atomic force microscopy confirmed that a force of attraction can exist between sphalerite and silica, however, the pH at which it occurs is different from that suggested by the settling experiments.

8.2 Contributions to Knowledge

1. The effect of the presence of a sulphide mineral on the zeta-potential of one another was described and interpreted.
2. From the correlation of the electrokinetic study and settling experiments of mixed sulphide minerals, it was found that the maximum agglomeration corresponded to the zeta-potential of the two minerals approaching zero, i.e. a "homocoagulation" condition.
3. The effect of pH and calcium ions on sphalerite-silica interactions was determined through electrokinetic, settling rate and atomic force microscopy measurements.
4. Colour intensity gradation and relative conductivity measurements were used to confirm phase separation in the sphalerite-silica system.
5. Surface force measurements on sphalerite-silica interaction was studied as a function of pH.

8.3 Recommendations for Future Work

1. Use a narrower size range than <38 µm, because it will be easier to interpret settling measurements.
2. Use mixtures of radically different size for interaction studies.
3. The zeta-potential distribution of sulphide and silica minerals, should be measured to further facilitate correlation of zeta-potential with settling velocity experiments.
4. Sphalerite-silica experiments should be performed in the presence of Cu^{2+}, X^-, Pb^{2+}, Fe^{2+} and SO^{2-}_4 as these ions are present in flotation practice.
5. The minerals used in this work were specimen samples. Similar work on plant-derived samples should be performed to try to generalize the findings.
6. Perform flotation experiments on the sphalerite/silica system to investigate how agglomeration affects flotation.
7. Rheology tests should be done and correlated with settling experiments. In rheology measurements a shear stress is applied to the slurry, whereas, in the settling tests the slurry is more static. The impact of shear and the relevance to flotation need consideration.
8. Attempts should be made to "see" the agglomerates to analyse morphology and perhaps provide insight into the agglomeration mechanism.
9. In practice, oxidation of sulphide mineral surfaces is unavoidable. The impact of controlled oxidation on sphalerite/silica interaction should be examined. The difference between settling rate and AFM data may then be resolved.

APPENDIX A

Table A1 - Size Distribution for Sphalerite (<38 µm)

Size (µm)	Percent Distribution	Percent Cumulative Passing
38	8	92
30	9	91
25	5	86
20	15	71
15	15	56
10	16	40
5	20	20
0	20	0

Table A2 - Size Distribution for Silica (<30 µm)

Size (µm)	Percent Distribution	Percent Cumulative Passing
30	1	99
25	4	95
20	7	88
15	16	72
10	19	53
5	21	32
0	32	0

Table A3 - Assays for Sphalerite in Overflow and Underflow

pH	Ions in Solution	Location	Percent Sphalerite
1.50	None	Underflow	75.7
1.50	None	Overflow	<0.02
8.43	None	Underflow	73.6
8.43	None	Overflow	48.7
8.75	None	Overflow	11.2
8.75	None	Underflow	64.7
3.40	Calcium	Underflow	67.1
3.40	Calcium	Overflow	<0.02